

Spring 2003

Residual Compressive Strength Prediction of Carbon/Epoxy Laminates Subjected to Low Velocity Impact Damage

Christopher D. Hess

Embry-Riddle Aeronautical University - Daytona Beach

Follow this and additional works at: <https://commons.erau.edu/db-theses>



Part of the [Aerospace Engineering Commons](#)

Scholarly Commons Citation

Hess, Christopher D., "Residual Compressive Strength Prediction of Carbon/Epoxy Laminates Subjected to Low Velocity Impact Damage" (2003). *Theses - Daytona Beach*. 277.

<https://commons.erau.edu/db-theses/277>

This thesis is brought to you for free and open access by Embry-Riddle Aeronautical University – Daytona Beach at ERAU Scholarly Commons. It has been accepted for inclusion in the Theses - Daytona Beach collection by an authorized administrator of ERAU Scholarly Commons. For more information, please contact commons@erau.edu.

**RESIDUAL COMPRESSIVE STRENGTH PREDICTION OF CARBON/EPOXY
LAMINATES SUBJECTED TO LOW VELOCITY IMPACT DAMAGE**

by

Christopher D. Hess

A Thesis Submitted to the Graduate Studies Office in
Partial Fulfillment of the Requirements for the Degree of
Master of Science in Aerospace Engineering

Embry-Riddle Aeronautical University
Daytona Beach, Florida
Spring 2003

UMI Number: EP32078

INFORMATION TO USERS

The quality of this reproduction is dependent upon the quality of the copy submitted. Broken or indistinct print, colored or poor quality illustrations and photographs, print bleed-through, substandard margins, and improper alignment can adversely affect reproduction.

In the unlikely event that the author did not send a complete manuscript and there are missing pages, these will be noted. Also, if unauthorized copyright material had to be removed, a note will indicate the deletion.

UMI[®]

UMI Microform EP32078
Copyright 2011 by ProQuest LLC
All rights reserved. This microform edition is protected against
unauthorized copying under Title 17, United States Code.

ProQuest LLC
789 East Eisenhower Parkway
P.O. Box 1346
Ann Arbor, MI 48106-1346

**RESIDUAL COMPRESSIVE STRENGTH PREDICTION OF CARBON/EPOXY
LAMINATES SUBJECTED TO LOW VELOCITY IMPACT DAMAGE**

by

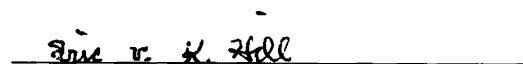
Christopher D. Hess

This thesis was prepared under the direction of the candidate's thesis committee chairmen, Dr. Yi Zhao and Dr. Eric Hill, Department of Aerospace Engineering, and has been approved by the members of his thesis committee. It was submitted to the School of Graduate Studies and Research and was accepted in partial fulfillment of the requirements for the degree of Master of Science in Aerospace Engineering

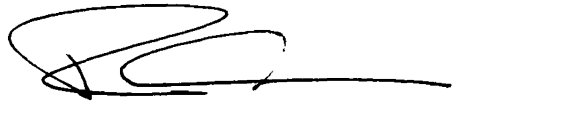
THESIS COMMITTEE:



Dr. Yi Zhao
Chairman



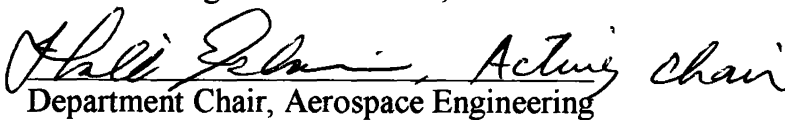
Dr. Eric v. K. Hill
Chairman



Dr. Richard P. Anderson
Member



Graduate Program Coordinator, MSAE



Department Chair, Aerospace Engineering

6/23/03
Date

ACKNOWLEDGMENTS

As a result of this study, there have been too many failures and headaches; however, the gratification of completing this research and the earned character values pertaining to tenacity and perseverance will be remembered for a lifetime. I would like to thank my friends and colleagues Siddharth David and Daewon Kim for spending their time and labor during material creation and testing. Special thanks go to Levavie Indieka for his MATLAB comprehension and dedication. I would like to thank my thesis committee, Drs. Yi Zhao, Eric v. K. Hill, and Richard P. Anderson for their advice and criticism. A very big thank you goes to my advisors, Dr. Zhao and Dr. Hill, for financially supporting me through graduate school by means of teaching and research assistantships. Not only was graduate school financed, but also the many subtle points in engineering enrichment were learned through these positions. In warm appreciation for Dr. Hill, what I have learned on the cross country trails and in the classroom regarding integrity, dedication, and professionalism will long be remembered. Another special thanks to Dr. Zhao, whose interest in the subject has led to the acquisition of incredible equipment that has made this research possible. Finally, I thank my parents who have always supported and encouraged me throughout life and especially college. I would also like to thank the Mangold family, who have provided a home away from home; the 5% of my week spent in their household has been a very gratifying comfort. Last but not least, I would like to thank Him who has blessed me with unimaginable talents and circumstances; let me never forget Your glorification.

ABSTRACT

Author: Christopher D. Hess
Title: Residual Compressive Strength Prediction of Carbon/Epoxy Laminates
Subjected to Low Velocity Impact Damage
Institution: Embry-Riddle Aeronautical University
Degree: Master of Science in Aerospace Engineering
Year: 2003

Low energy impact damage to a composite structure is difficult to detect and can have profound effects on compressive strengths. Low energy impact damage is sometimes termed as barely visible impact damage (BVID). Detecting BVID is only possible by implementing nondestructive testing (NDT) techniques. Depending upon the support conditions, material system, laminate thickness, lay-up orientation, and impactor geometry, velocity, and hardness, the types of damage associated with BVID include delaminations, longitudinal and transverse matrix cracks, and in some cases, fiber breaks. Material properties such as the strengths of the matrix, fibers, fiber/matrix interface, and more important for BVID, ply interface properties in a multi-ply laminate, are all parameters that determine impact resistance. After the composite structure experiences BVID, the depletion of the structural strength is determined as result of compression after impact (CAI) material testing.

The primary emphasis of this research is to predict structural compressive strength after low energy/low velocity impact using neural networks. After the composite structure absorbs BVID, it is common to determine structural strength depletion based on impact energy. Because impact energy is seldom known in real world applications, it is more reasonable to determine ultimate strength based on amount of damage present. The technique used in this research to assess the damage and predict ultimate strength includes ultrasonic testing (UT), to generate an image representing the damage, and neural networks to predict future performance.

Using the pixel data from the ultrasonic C-scan image of the impact damage, in conjunction with CAI testing, and analyzing it with a backpropagation neural network,

correlations on ultimate compressive strength can be made. This analysis demonstrates the ability of a neural network to predict the ultimate compressive strengths of impact damaged composite structures using UT data.

TABLE OF CONTENTS

Signature Page	ii
Acknowledgments.....	iii
Abstract.....	iv
Table of Contents.....	vi
List of Figures.....	viii
List of Tables	x
CHAPTER 1 INTRODUCTION.....	1
1.1 Overview.....	1
1.2 Testing Parameters.....	2
1.2.1 Impact Support Conditions	3
1.2.2 Material System	3
1.2.3 Impact Velocity.....	3
1.2.4 Laminate Thickness	4
1.2.5 Laminate Lay-Up Orientation.....	5
1.2.6 Impactor Shape	6
1.3 Previous Research.....	6
1.4 Present Research	6
CHAPTER 2 BACKGROUND	8
2.1 Material System	8
2.2 Ultrasonic Testing.....	8
2.3 Acoustic Emission	15
2.3.1 Acoustic Emission Theory.....	16
2.3.2 Previous Acoustic Emission Research.....	20
2.4 Neural Networks	22
2.5 MATLAB.....	24
CHAPTER 3 PROCEDURE.....	27
3.1 Carbon/Epoxy Laminates.....	27
3.2 Impact Testing	27

3.3 Ultrasonic C-scan Testing.....	30
3.4 Acoustic Emission and Compression Testing.....	32
3.5 Neural Networks	34
CHAPTER 4 RESULTS	35
4.1 Impact and Compression Testing.....	35
4.2 Neural Network Applications	43
CHAPTER 5 CONCLUSIONS AND RECOMMENDATIONS	52
5.1 Conclusions.....	52
5.2 Recommendations.....	53
REFERENCES	55
BIBLIOGRAPHY	57
APPENDIX	
A AS4/3501-5A Product Data Sheet	58
B MATLAB Image Assessing M-file.....	61
C MATLAB Image Assessment	63
D Acoustic Emission Amplitude Distribution	76
E Neural Network Input Data for Batches A, C, CH, and D	83

LIST OF FIGURES

Figure 1.1.1 (a) Delaminations and orientations throughout a laminate and (b) actual delaminations in E-glass	2
Figure 1.1.2 Crack propagation in (a) thick laminates and (b) thin laminates.....	5
Figure 2.2.1 A-trace display of the pulse echo technique.....	9
Figure 2.2.2 C-scan travel path (a) and C-scan image of a discontinuity (b)	10
Figure 2.2.3 Ultrasonic transducer cutaway	11
Figure 2.2.4 Typical pulse echo UT system	11
Figure 2.2.5 Illustration of transducer in (a) 2-D and (b) 3-D showing near field along the acoustic axis	14
Figure 2.3.1 Acoustic emission stress wave reflection.....	16
Figure 2.3.2 Acoustic emission broadband transducer cutaway.....	18
Figure 2.3.3 Acoustic emission system.....	18
Figure 2.3.4 Acoustic emission time based waveform parameters.....	19
Figure 2.3.5 Acoustic emission amplitude distribution	22
Figure 2.4.1 Neuron processing element	23
Figure 2.4.2 Backpropagation neural network architecture.....	24
Figure 2.5.1 Sixteen color C-scan image (top) and image matrix represented by MATLAB (bottom).....	25
Figure 2.5.2 C-scan image (top) and MATLAB assessment (bottom).....	26
Figure 3.2.1 Instron Dynatup 9250	28
Figure 3.2.2 Pneumatic clamping fixture.....	29
Figure 3.3.1 UltraPAC II C-scan imaging system	30
Figure 3.3.2 Hardware setup parameters	31
Figure 3.4.1 Compression after impact (CAI) fixture with AE transducers.....	33
Figure 3.4.2 Data acquisition setup for compression testing.....	34
Figure 4.1.1 Impact energy vs. peak impact load according to specimen batch.....	37
Figure 4.1.2 Impact energy vs. peak impact load according to ply thickness	37
Figure 4.1.3 Front surface (a) and back surface (b) impact damage.....	38
Figure 4.1.4 Specimen failure as a result of compression loading	38

Figure 4.1.5 Compressive load vs. impact energy	39
Figure 4.1.6 (a) Free-edge compression failure location (b) ply separation failure	41
Figure 4.1.7 Compressive load versus impact energy (including batch D)	42
Figure 4.2.1 Network input parameters for batch CH	45
Figure 4.2.2 Network input parameters for batch A	46
Figure 4.2.3 Network input parameters for batch C	47
Figure 4.2.4 Network input parameters for batch D	48

LIST OF TABLES

Table 2.3.1	AE parameters describing failure mechanisms of fiberglass/epoxy FWPV .	20
Table 2.3.2	AE Parameters describing failure mechanisms of graphite/epoxy tensile test specimens	21
Table 4.1.1	Specimen laminates and corresponding impact and compression loads	35
Table 4.2.1	Neural network prediction results for batch CH.....	45
Table 4.2.2	Neural network prediction results for batch A.....	46
Table 4.2.3	Neural network prediction results for batch C.....	47
Table 4.2.4	Neural network prediction results for batch D.....	48
Table 4.2.5	Neural network output from three different networks for all 16 ply data.....	49

CHAPTER 1

INTRODUCTION

1.1 OVERVIEW

In the aircraft industry today the use of composite materials is increasingly desirable due to their high strength to weight ratio. One restrictive design criteria, however, for a composite structure is impact tolerance. Of the types of damage a composite structure may experience, low energy impact damage can be dangerous because the damage oftentimes goes undetected and can subsequently grow under load. This barely visible impact damage (BVID) can have adverse effects on the material's structural strength. The results of the compression tests show BVID caused strength reductions of 60 percent in graphite composite structures [2].

When exploring material properties that result from impact damage, there are many parameters of the test that affect the material reaction. The failure modes associated with BVID consist primarily of matrix cracks, delaminations, and occasionally fiber breaks. Delaminations are the most critical failure mode of BVID when a structure is loaded in compression. Delaminations are susceptible to occur at interfacing plies that are orientated in different fiber directions. This is generally true for material systems that have a brittle matrix supporting the ply interface stresses, such as carbon/epoxy materials. The size of the delamination area depends on many parameters that are described later, while the orientation of the delamination can be correlated to the fiber orientation of the lamina. Shown in Figure 1.1.1(a) is a schematic of the delamination orientation within the laminate, and an actual image of the delaminations within an E-glass laminate is shown in Figure 1.1.1(b). It should be noted that delamination shapes often are quite irregular and difficult to ascertain [1]. Delamination initiates after a certain damage threshold has been reached and then propagates linearly with impact energy [1]. In addition to material properties, i.e., elastic constants and strengths, the delamination area in an impacted composite plate is also dependent on external effects such as the type of loading, shape of the impactor, impacting velocity, and boundary conditions of the specimen [4].

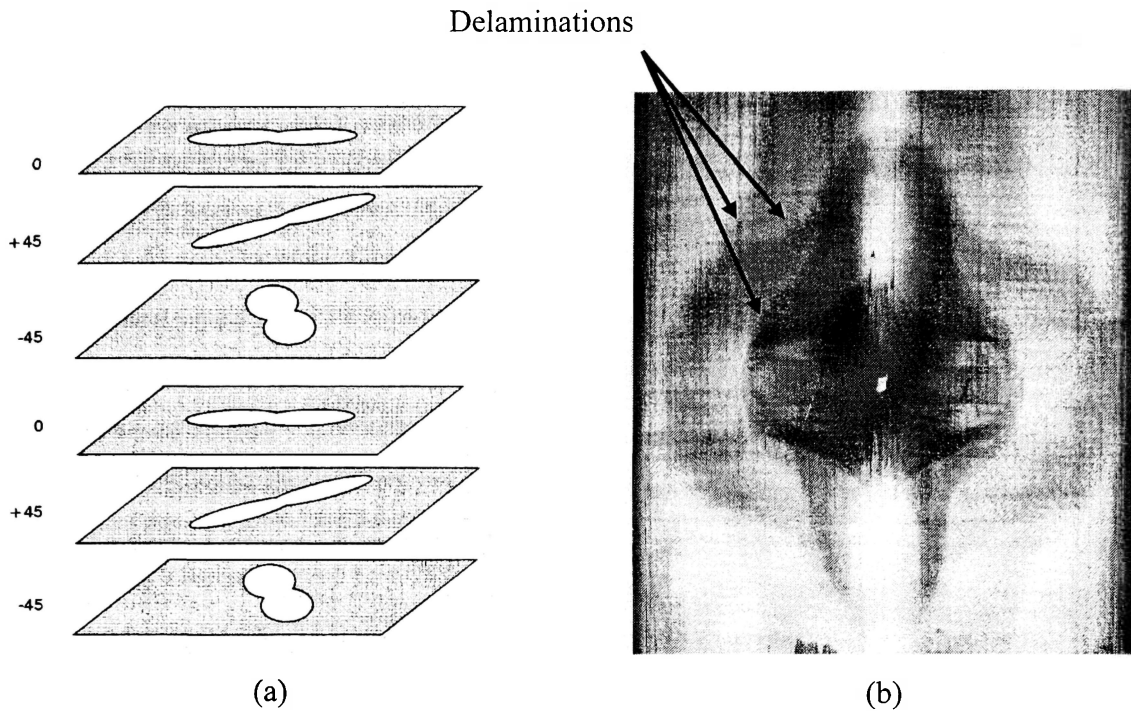


Figure 1.1.1 (a) Delaminations and orientations throughout a laminate and (b) actual delaminations in E-glass

1.2 TESTING PARAMETERS

Below is a list of testing parameters that must be considered when researching impact resistance. Following the list is a short explanation of each parameter. Keep in mind that these impact constraints are intended to simulate conditions that the material might experience in use.

- Impact support boundary conditions
- Material system
- Impact velocity
- Laminate thickness
- Laminate lay-up orientation
- Impactor shape
- Impactor stiffness

1.2.1 Impact Support Conditions

The three most common types of support conditions are clamped edges, simply supported edges, and back-face supports. The last condition is representative of a sub-structure or stiffener supporting and preventing deformation of a laminate that is absorbing impact damage. Here, the failure mode is primarily matrix shattering as a result of the highly localized contact stresses.

1.2.2 Material System

This research focuses on continuous fiber/epoxy systems. Due to the complexity of the dynamic impact, previous research has many theories correlating damage phenomenon with failure modes. This is mainly due to the various types of materials available. However, during low velocity impact on continuous fiber/epoxy systems, damage initiation is started from small matrix cracks that develop as a result of excessive transverse shear stress or bending stress. It is postulated that when the matrix cracks propagate through the material normal to the surface and reach an interface between lamina of different fiber orientation, delaminations develop. Material properties E_1 , E_2 , G_{12} , and ν_{12} , along with the laminate scheme, define the overall rigidities of the impacted plate. These properties greatly influence the contact force history, thus having a distinct effect on impact resistance. Since a majority of the low velocity impact damage resistance is defined by the matrix properties, new matrix materials have been developed such as PEEK thermoplastics and rubber modified epoxy resins. Compression tests have shown that PEEK laminates are superior to epoxy laminates [1] in impact resistance.

1.2.3 Impact Velocity

The energy associated with impact testing comes primarily from kinetic energy. To determine precisely the amount of energy the structure absorbs becomes increasingly complicated with precision; however, the generic equation for kinetic energy is given in Equation 1.

$$E = \frac{1}{2}mV^2 \quad (1)$$

If energy is held constant during impact, but velocity and mass are altered respectively, the amount of damage a material absorbs could change. For example, if mass is increased and velocity decreased during impact, the actual impact energy is the same as a high velocity low mass impact, but the amount of damage could be considerably different. Moreover, materials are strain rate sensitive. That is, if a material absorbs the same energy but within a shorter impulse, there could possibly be more damage. NASA CP 2321 [3] postulates that the compression wave associated with a high velocity/low mass projectile impact, causes the plate to translate much faster than that required for the overall response of the plate structure. This highly localized deformation gradient cause's large transverse shear and normal stresses which can cause failure within the laminate. In the NASA CP 2321 research, many material systems were used to compare high velocity/low mass and low velocity/high mass impact conditions, of which the high velocity/low mass conditions had greater damage size and decreased compression after impact strength.

1.2.4 Laminate Thickness

When an impact event occurs, the material response can be significantly different depending upon the thickness. In thick laminates, the response to a certain impact energy results in matrix cracking at the first layer because of the highly localized contact stresses associated with the impacting projectile. The damage progresses downward through the laminate layers creating delaminations and transverse shear cracks and resulting in a “pine tree” pattern as shown in Figure 1.1.2(a). Thin laminates respond to impact energy just the opposite of thick laminates, as shown in Figure 1.1.2(b). Due to the high bending stresses on the back face of the thin laminates, matrix cracks are introduced in the lowest layer and propagate upward creating delaminations and shear cracks in a reverse pine tree pattern.

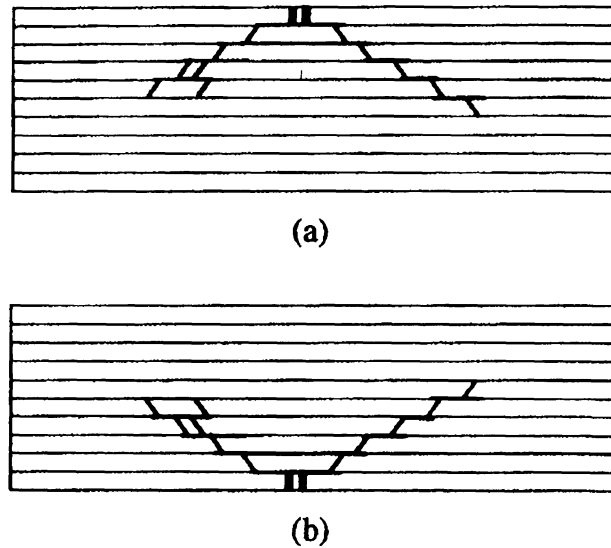


Figure 1.1.2 Crack propagation in (a) thick laminates and (b) thin laminates

1.2.5 Laminate Lay-Up Orientation

In industry, many continuous fiber system laminates are made of layers oriented in multiple directions. This allows the structure to be stiffer in many directions and thus capable of supporting multi-directional loads. As a result of anisotropy in composites, many new, complicated, and different failure modes can develop when compared to homogeneous materials such as metals. It is difficult to determine which failure mode will predominate as a composite structurally fails. However, previous research has shown that as a result of impact damage, delaminations and matrix cracks are the most prevalent failure mechanisms.

There are many models that have been proposed to explain why delaminations occur as a result of highly localized stresses. Most models are built around the fact that a laminate is made up of many lamina oriented in different directions. If two adjacent plies have the same fiber orientation, no delamination will occur at the interface between them [1]. These material property mismatches cause nonuniform stress distributions in the composite laminate when it is subjected to load [4]. Thus, each layer will respond and deform in a particular way, while the laminate is experiencing a global load. As these layers deform and respond differently to a global load, interlaminar stresses are introduced. These interlaminar stresses are mainly supported by the fiber/matrix

interface between each lamina. If these stresses become too great under a concentrated load, delaminations will develop.

1.2.6 Impactor Shape

Impactor shape can define the extent of the localized damage. When mass and impact velocity are held constant, sharper projectiles will create more localized damage than blunt projectiles. Also, impactor stiffness is a consideration to be included.

Impactors that are less stiff will deform along with the structure during impact; thus, the amount of damage introduced is less. Because not all real world impacts are made with extremely stiff impactors, this constraint should not be ignored.

1.3 PREVIOUS RESEARCH

Presently, there are two common methods of impact testing in the industry. The compression after impact (CAI) standards come from Boeing (BSS-7260) and NASA (ST-1) [15]. Both standards require the specimens to be relatively large, ranging from 0.15 to 0.25 inches thick with a planar size of 6 x 4 inches (Boeing) and 12.5 x 7 inches (NASA) during impact and then trimmed to 5 x 3 inches (Boeing) and 5 x 5 inches (NASA) prior to compression testing. The quantity and cost required for the materials alone, if this research were to utilize either of these two standards, is too great. Also, the machinery required to load the specimen for compression testing after impact for these standards is between 35-50 kips for the Boeing standard and even more for the NASA standard. Currently Embry-Riddle Aeronautical University's capability is limited to a hydraulic 10 kip MTS machine or a mechanical screw-type Tinius Olsen machine capable of 30 kips. Therefore, specimen design was constrained by these limitations.

1.4 PRESENT RESEARCH

This research is effectively pursuing ultimate compressive strength prediction as a function of impact damage using a neural network to correlate ultrasonic test data. The ideal solution would be to predict ultimate strengths to a 5% error using UT data alone.

If this is not possible, the acoustic emission (AE) data gathered during compression after impact loading may offer more information for a more accurate neural network prediction.

The materials used in this research differed in lay-up orientation and thickness only. The laminates are much thinner than those called for in the Boeing or NASA CAI testing standard, with a maximum thickness of approximately 0.10 inches. The impact support conditions included clamped edges. The impact tup itself was extremely stiff and had a 5/8 inch hemispherical head. The impact energy used herein ranged from 0-20.0 ft-lb_f. All testing is done at room temperature without specimen preload during impact. After impacting the specimen, an ultrasonic image of the damaged region is taken and subsequently quantified using an algorithm in MATLAB. The compressed ultrasonic C-scan image data is then inputted into a backpropagation neural network to make predictions on ultimate compressive strength.

CHAPTER 2

BACKGROUND

2.1 MATERIAL SYSTEM

The material used in this research was Hexcel AS4/3501-5A, a carbon/epoxy system. Originally, this material was developed by Hercules, but Hexcel purchased the company in 1996. The cure cycle and material properties provided in Appendix A of this report come from Hercules. It should be concluded that this is an accurate, but outdated product information sheet. AS4/3501-5A is a carbon/epoxy prepreg tape that has unidirectional fibers and an amine-cured epoxy resin. The resin is virtually identical to the very common AS4/3501-6 system, differing only in cure cycle and certain material properties. Selection of this material was due to the following reasons. First, this carbon/epoxy is a very commonly used composite system in industry. Second, the imaging capabilities of carbon prepreg are easily ascertainable using the UltraPAC II ultrasonic C-scan imaging system. Finally, carbon/epoxy materials are very susceptible to delamination during low velocity impact due to large elastic moduli mismatch between the fibers and the matrix, which is of particular interest in this research.

2.2 ULTRASONIC TESTING

Ultrasonic testing (UT) is a nondestructive testing (NDT) technique that sends high frequency sound waves through a material to detect imperfections, discontinuities, and changes in material properties. Applications range from subterranean analysis to the detection of minute flaws in structural materials. A popular form of UT uses a pulse-echo transducer that pulses a sound wave through a material and receives an echo representing any discontinuities and/or the back face. Discontinuities or defects cause reflection of the sound waves, and the detection of the reflected or transmitted waves permits the defects to be located [5].

The echoes can be analyzed in a number of ways. One form of analysis is the pulse echo A-scan. This is accomplished using a single transducer capable of

transmitting and receiving a signal. The A-scan will visually show the input pulse and back wall echoes along with any inconsistencies or defect echoes within the material on an amplitude versus range (time) graph as shown in Figure 2.2.1.

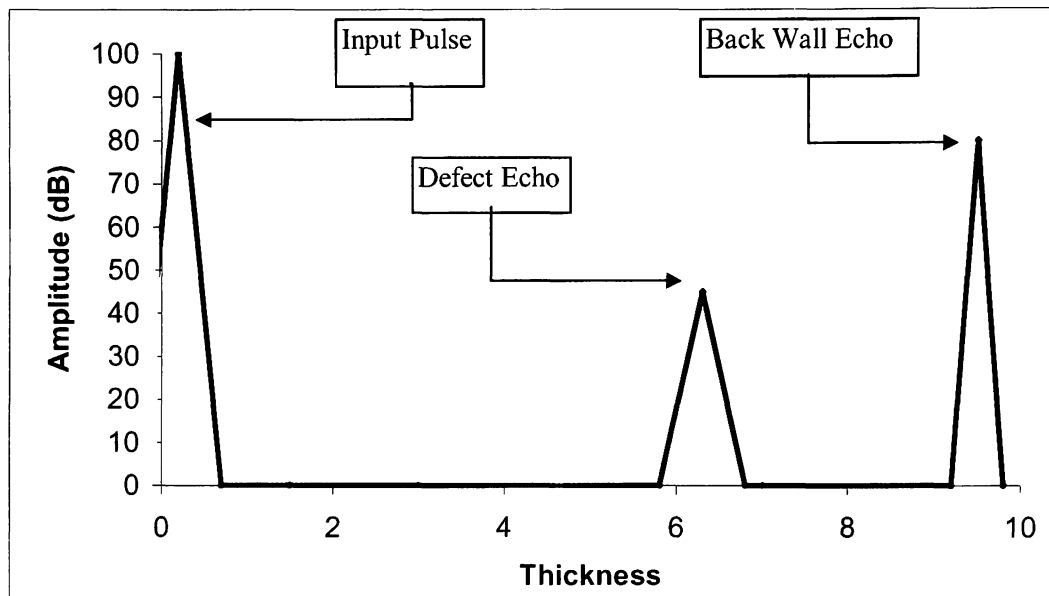


Figure 2.2.1 A-trace display of the pulse echo technique

An ultrasonic C-scan will give a 2-D planar image illustrating where and how large an inconsistency is by simply storing the data over a series of A-traces as shown in Figure 2.2.2(a). The C-scan uses gated A-scan information to create a 2-D image of the material and thus the dimensions of the flaw. The image that develops is a measure of amplitude changes of the defect in the A-trace over a fixed time interval or gate as shown in Figure 2.2.2(b). The amplitude of the defect echo provides a measure of the damage present: the greater the damage, the higher the amplitude (relative to the surrounding material) and the brighter the image, shown on Figure 2.2.2(b).

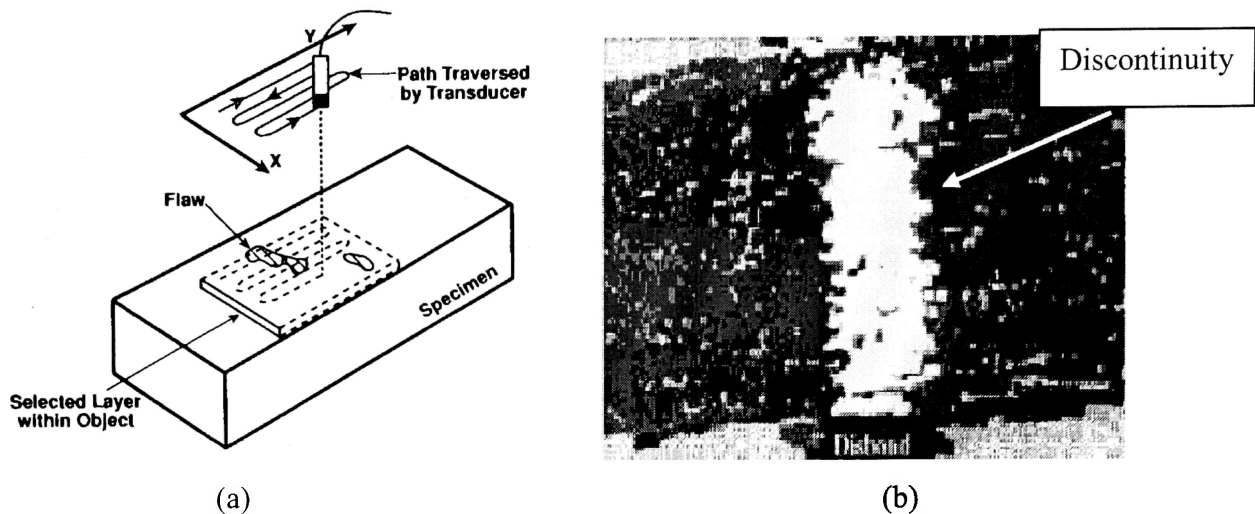


Figure 2.2.2 C-scan travel path (a) and C-scan image of a discontinuity (b)

Ultrasonic waves are generated by suitable transducers in which a single electrical “spike” of short rise time ($< 10\text{ns}$) is converted into high frequency mechanical vibrations of the solid [5]. The principal modern sources of ultrasound are created by specially cut crystals of materials such as quartz or ceramics such as barium titanate and lead zirconate. The application of an alternating electrical voltage across the opposite faces of a disc made of such materials produces an alternating expansion and contraction of the disc at the impressed frequency. This phenomenon is known as piezoelectricity. The transducers used in high frequency ultrasonic testing are usually made of an active element of piezoelectric crystal. In the case of pulse echo, a transducer will have two piezoelectric crystals, one for pulsing and one for receiving. Depending on the crystal material type, there will also be a backing material to help dampen and absorb the received ultrasonic energy. Finally, there is a wear plate or “shoe” that protects the piezoelectric crystal. Figure 2.2.3 shows a transducer made of a single piezoelectric crystal.

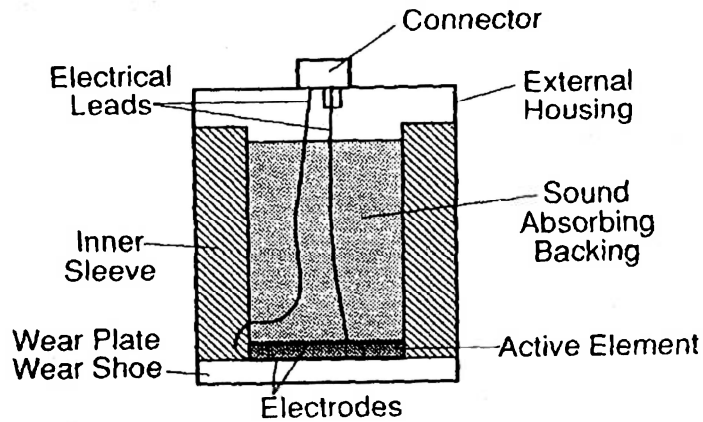


Figure 2.2.3 Ultrasonic transducer cutaway

The pulse echo method is used extensively for flaw characterization and assessment. When the ultrasonic transducer is coupled to the surface by an appropriate couplant, it sends high frequency sound waves through the medium. The pulse is reflected either by a discontinuity or the back face and is detected by the same transducer. The pulses are emitted at a constant rate, and an oscilloscope can determine which pulse is outgoing and which is reflected or incoming. The time required for the pulse wave to travel through the medium and echo back to the same transducer can easily be displayed on an oscilloscope. A typical ultrasonic pulse echo system is shown in Figure 2.2.4.

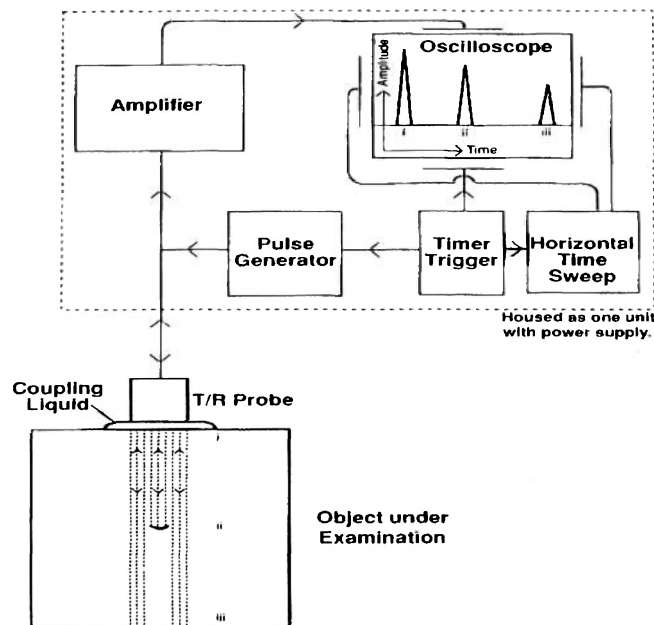


Figure 2.2.4 Typical pulse echo UT system

Unless a low frequency ultrasonic transmission system is used, couplants must be applied between the inspection material surface and the transducer surface. The couplant provides a suitable sound path for the ultrasonic energy to transmit through. Without the couplant, the amount of transmitting energy would be very low due to the very low specific acoustical impedance of air. The amount of transmitted energy at the boundary of the material is proportional to the specific acoustical impedances of the couplant and the material given in accordance with Equation 2:

$$T_E = 1 - R_E = \frac{4Z_1Z_2}{(Z_1 + Z_2)^2} \quad (2)$$

where

- T_E = transmitted energy
- R_E = reflected energy
- Z = specific acoustic impedance = ρV
- ρ = material density
- V = wave velocity.

For example, the percentage of reflected energy between steel and air is 100% and between steel and water is 88% [5]. Generally, couplants come in some form of liquid, gel, or oil. Important properties are to fill all surface irregularities, allow free movement of the transducer probe, prevent air pockets, and be easily applied and removed from the surface.

As the transducer generates pulses, the sound waves propagate through a medium at different frequencies. The pulse shape distorts with time and distance in any medium. The sound wave thus weakens as a result of scattering, dispersion, and by the frictional motion of the particles within the solid. This wave attenuation is more pronounced in composites due to their anisotropic condition. Depending on the conditions being tested or the flaw resolution that an NDT operator requires, attenuation can be a concern. The attenuation of sound waves increases with increases in frequency. Ultrasonic waves are dampened far more rapidly than those of audible sound. The frequency used by the operator dictates the level of resolution achieved during the test. The lower the frequency used, the more penetration achieved. The drawback is that the resolution is extremely low. Low frequency waves because of their large periods, cannot navigate cracks like

high frequency waves do. High frequency waves, on the other hand, attenuate much faster than low frequency waves and thus have less penetration power, but high frequency waves generate better resolution of the flaw site.

The ultrasonic sound beam is not uniform in intensity in length or cross section and is susceptible to diffraction effects as a result of the finite size of the source. There are extensive beam intensity fluctuations near the source, which is known as the near field or Fresnel zone. These high and low pressure areas are generated because the crystal is not a point source of sound pressure. The high and low pressure waves are joined into a uniform front at the end of the Fresnel zone that is a certain distance (N) from the piezoelectric crystal. Because of acoustic variations within the near field, it can be extremely difficult to accurately evaluate flaws in materials near the surface when using a surface contact transducer. The UltraPAC II system used in this research has a three axis motor system; thus, the distance between the surface of the specimen and the transducer can be adjusted so that near field effects can be avoided. The couplant in this system is simply water. The ultrasonic beam is more uniform in the far field, or Fraunhofer zone, where the beam spreads out in a pattern originating from the center of the transducer. The transition between the Fresnel and Fraunhofer zones occurs at a distance, N , and is sometimes referred to as the "natural focus" of a flat or unfocused transducer. The near/far distance, N , is significant because amplitude variations that characterize the near field can make flaw evaluation difficult (see Figures 2.2.5(a) and 2.2.5(b)).

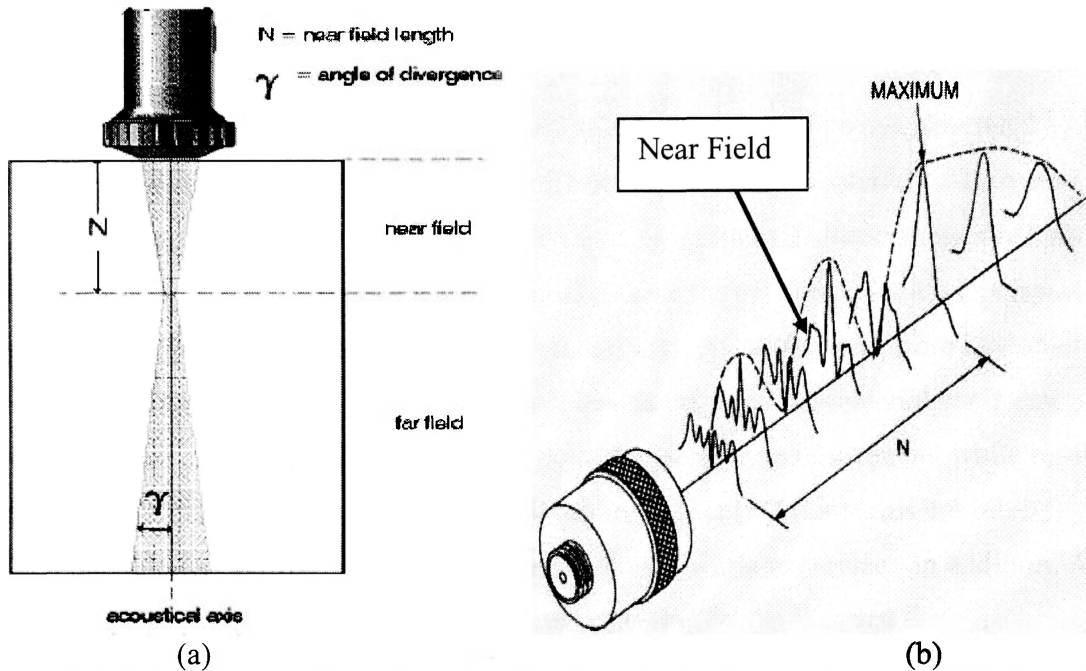


Figure 2.2.5 Illustration of transducer in (a) 2-D and (b) 3-D showing near field along the acoustic axis

The approximation of the location of the focal point (N) is a reasonably simple calculation for flat unfocused transducers. Given below in Equation 3 is a common relation used in ultrasonic testing.

$$N = \frac{D_{eff}^2 f}{4c} \quad (3)$$

where D_{eff} = 0.97 of the crystal diameter
 f = frequency
 c = material wave velocity.

A sample calculation using equation 3 is provided using parameters from this research.

Diameter of transducer crystal diameter = 0.25 inches
 Frequency of transducer = 5 MHz
 Average in plane wave velocity of AS4/3501-5A = 112,200 in/s

$$N = \frac{(0.25 \text{ in} * 0.97)^2 (5,000,000 \frac{\text{cycles}}{\text{s}})}{4 * 112,200 \frac{\text{in}}{\text{s}}} = 0.655 \text{ inches}$$

2.3 ACOUSTIC EMISSION

Acoustic emission (AE) can be defined as a transient elastic wave generated by a rapid release of energy as a result of a redistribution of stress in a material. AE studies have been incorporated from seismic monitoring of the earth to dislocation movements in stressed metals. When structures are stimulated by an external change in load, pressure, strain, or perhaps temperature, this induces AE activity. AE is different from any other form of NDT for two reasons. First, the signal has its origin in the material itself, not from any external sources [6]. Second, acoustic emission detects movement while most other methods detect existing geometrical discontinuities [6]. AE systems are often incorporated to monitor larger structures nonintrusively while in service. In addition, AE is further complicated in comparison to ultrasonic testing by the fact that the characteristics of the “input” or emitted signals are relatively unknown [7]. The characteristics of the received waveforms can be vastly different from one another throughout the AE test. This is because the AE source mechanism within the material produces considerably different waveform parameters. For example, in composites, the waveform associated with delaminations is quite different from the waveform corresponding to transverse matrix cracking. Also, due to the attenuation of the wave as it propagates through the material and specimen resonances, the received signal is significantly different from the emitted signal of the source. Typically, the global AE inspection is used to locate areas with structural problems, and other NDT methods are then used to identify more precisely the nature of the emitting defects [6]. Recent efforts and techniques have been implemented to estimate the residual strength or life of the structure, using AE amplitude distribution data. The present research effort will incorporate these techniques for material strength prediction using AE, and are discussed in greater detail later.

2.3.1 Acoustic Emission Theory

Since acoustic emission is a dynamic event that exists as a point source which emits energy in spherical wavefronts (Figure 2.3.1), wave propagation in a semi-infinite medium is extremely complicated. The width and height of the wave will vary greatly depending on the source mechanism. AE sources generate both longitudinal and shear waves. When these waves contact a surface or reflect they undergo mode conversions, which gives rise to surface waves that are detected as AE signals. Rayleigh (surface) waves can be filtered out of the data acquisition system. The timing parameters within the data acquisition system omit these waveforms because they propagate at much slower wave velocities when compared to longitudinal waves. Other wave types such as Lamb (plate) waves are dispersive or dependant on frequency. In a solid material, wave velocity depends on the density and the elastic properties. Additionally, the velocity is a function of propagation direction in anisotropic materials such as composites, because of the dependence of elastic properties on direction [7]. Another problem that may be encountered is receiving a signal a second time as a result of reflection. However, due to the material used in this research, the edge support conditions during testing, and the very high threshold setting, reflections should not be a problem.

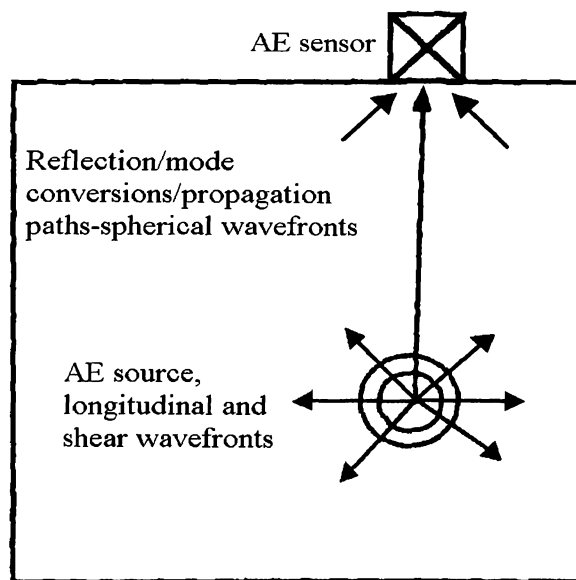


Figure 2.3.1 Acoustic emission stress wave

Wave attenuation can also have detrimental effects on AE monitoring. Previously discussed in the ultrasonic testing section, wave attenuation is the loss of acoustic wave amplitude with propagation distance. In AE, attenuation is typically frequency dependant, the higher the frequency, the faster the amplitude decay. When dealing with composites, the attenuation can be much faster due to anisotropy. When the wave propagates, the frictional motion of the particles will also cause the wave amplitude to degrade. As with ultrasonic testing, AE transducers must incorporate a couplant to transmit the AE signal from the material to the sensor. The couplant used in this research was hot-melt glue.

When a stress wave is emitted, it will propagate through the medium and be received by an acoustic emission transducer. Similar to an ultrasonic transducer, an AE transducer has a piezoelectric crystal which converts the mechanical energy of the waveform into an electrical signal. The piezoelectric crystal generates a very small voltage, and depending on the type of AE transducer, there is either an internal or external amplifier that magnifies the electrical signal by 40dB or 100 times. Later, the signal will be amplified again, usually by 20dB, within the data acquisition system. Since waveforms come in a wide variety of shapes and forms (as a result of attenuation or different source mechanisms) the amplitude scale is logarithmic. Shown below in Equation 4 is an expression for the amplitude of an AE signal:

$$Amplitude(dB) = 20 \log \frac{V_{sig}}{V_{ref}} \quad (4)$$

Here $V_{ref} = 1.0\mu V$.

The transducers used in this research are a narrow band resonating type. These transducers have a high sensitivity, resonating at 150 kHz. The preamplifiers include a band-pass filter of 100kHz-300 kHz which filters out any low frequency or high frequency noise. This frequency bandwidth is considerably higher than that of noise associated with structural vibrations; however, it is low enough to minimize electromagnetic interference (EMI) [7]. A majority of all usable AE data exist within these frequency ranges. If an AE operator wanted to study high fidelity signal analysis then a broadband transducer would be used. A drawback of this technique is that all

noise sources must be identified. A cutaway of a broadband transducer is shown in Figure 2.3.2. A broadband transducer will have the damping material as backing whereas a narrowband or resonant transducer does not. A typical AE data acquisition system is shown in Figure 2.3.3. Once the signal is received, it is amplified one more time, processed, and saved for future reference and analysis.

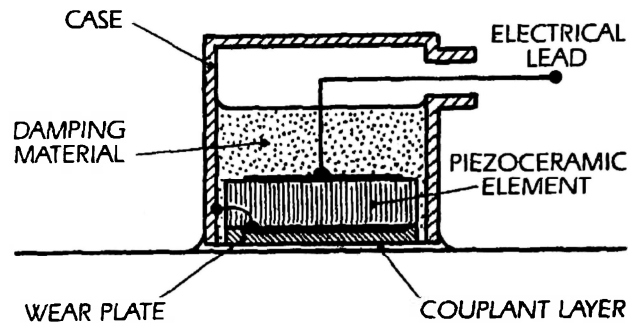


Figure 2.3.2 Acoustic emission broadband transducer cutaway

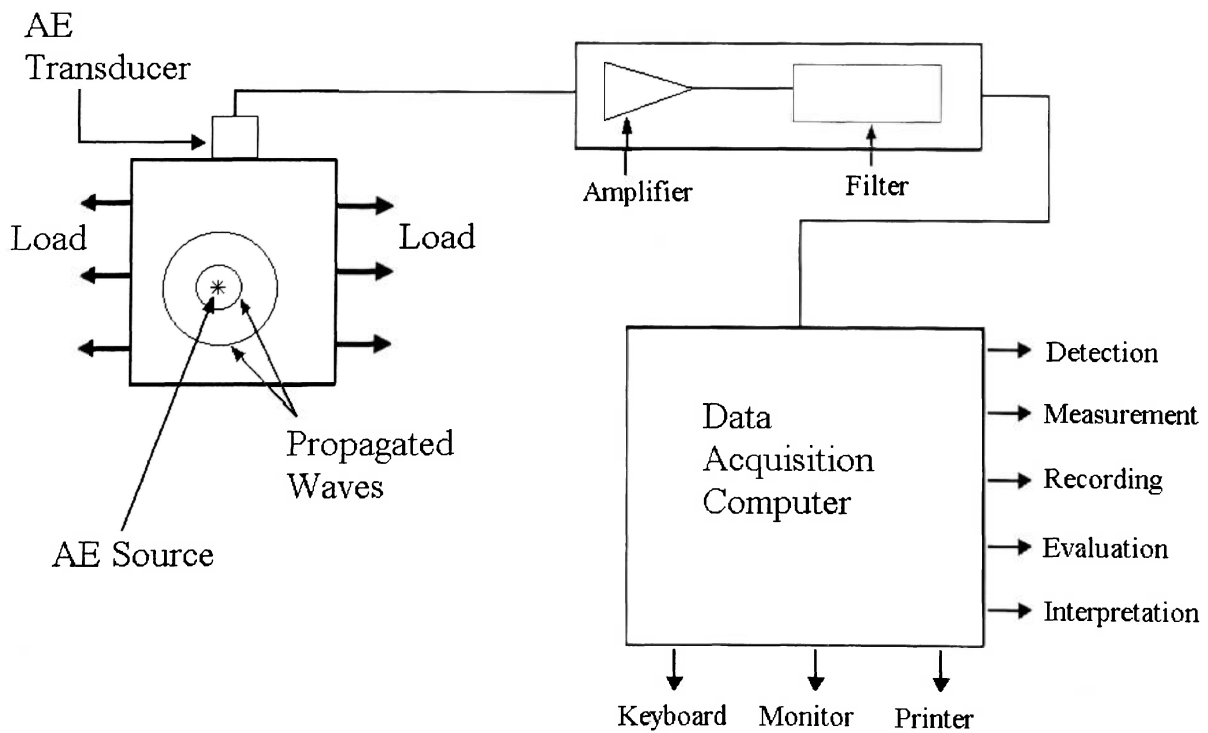


Figure 2.3.3 Acoustic emission system

The parameters commonly used in AE time based data analysis are given in Figure 2.3.4. The amplitude is the maximum peak of the waveform signal, and it is calculated according to Equation 4. The threshold is a setting within the data acquisition system that determines the minimum signal voltage recorded. Any signals that are received by the transducer that are below the threshold are disregarded. This parameter is used to omit system noise. The duration of the signal is the amount of time it takes for the signal waveform to drop below the threshold. The rise time is the amount of time required for the signal to reach the maximum amplitude after crossing the threshold. Counts are the number of times the signal crosses the threshold. MARSE is the mean area under the rectified signal envelope and is more commonly called AE energy. This is essentially the area of the absolute value of the signal.

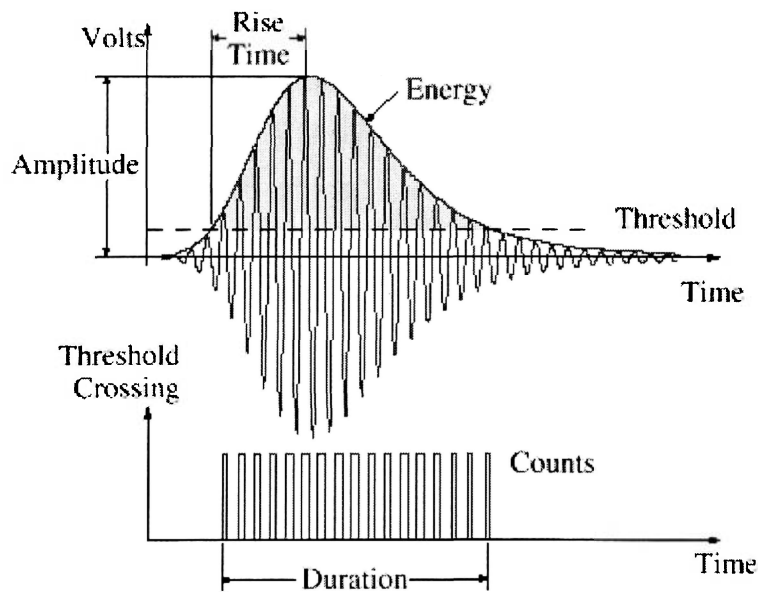


Figure 2.3.4 Acoustic emission time based waveform parameters

One difficult task in acoustic emission is to analyze a particular waveform signal and correlate it to a particular source mechanism. The difficulty in source identification arises from the significant changes that occur in the AE signals as they propagate [7]. The signals are further altered by the sensors and measurement instrumentation [7]. If the signals can be correlated to the source mechanisms, the value of AE data can be significant. However, when an AE test is performed, there are often thousands of

recorded AE signals, and it would be extremely difficult to sort this data and categorize it into the various source mechanisms. For example, a composite structure might have a five possible source mechanisms ranging from delaminations, fiber breaks, fiber pullouts, to transverse and longitudinal matrix cracking.

2.3.2 Previous Acoustic Emission Research

At Embry-Riddle Aeronautical University there have been numerous graduate theses topics that have attempted to either identify certain AE parameter ranges associated with a particular source mechanism or correlate AE parameters to a source mechanism without determining what that source mechanism is. These data have also been used to make ultimate strength predictions through multiple linear regression analysis or by inputting the data to a backpropagation neural network.

Fisher [8] used statistical analysis to group the failure mechanisms in a fiberglass/epoxy filament wound pressure vessel (FWPV) according to certain AE parameters, listed in Table 2.3.1. Ely [9] created special graphite/epoxy tensile test specimens to ensure that there was only one type of source mechanism emitted during tensile testing. After testing multiple specialized specimens, Ely generated AE parametric ranges to describe the three types of failure mechanisms presented in Table 2.3.2.

Table 2.3.1 AE parameters describing failure mechanisms of fiberglass/epoxy FWPV [8]

AE Parameters	Failure Mechanisms		
	Matrix Cracking	Delaminations	Fiber Breaks
Counts	Low	High	Low-Medium
Amplitude	Low	High	Very High
Energy	Low	High	Medium-High
Duration	Short	Long	Short-Medium

Table 2.3.2 AE Parameters describing failure mechanisms of graphite/epoxy tensile test specimens [9]

	Amplitude (dB)	Duration (μ s)	Risetime (μ s)	Counts	Energy
Matrix Cracking	37-49 [42]	0-60 [2]	0-60 [4]	0-10 [1]	1-6 [2]
Longitudinal Splitting	40-59 [49]	3-813 [124]	1-74 [30]	1-62 [16]	1-13 [4]
Fiber Breakage	60-84 [66]	11-714 [297]	25-75 [40]	18-113 [46]	5-186 [27]

As previously stated, some graduate research work has incorporated neural networks to classify the AE data and predict residual strength. Generally, the only AE data that has been applied to a neural network is the acoustic emission amplitude distribution histogram. Fatzinger [10] applied the acoustic emission amplitude distribution from 10 fiberglass/epoxy I-beams and was able to predict failure load on the remaining 4 beams with a worst case error of 9.5%. Fisher [8] used the AE amplitude distribution from fiberglass/epoxy pressure vessels that failed at varying temperatures, and was able to predict the burst pressure with a worst case error of 1.9%. Hill, Walker, and Rowell [11] used the AE amplitude distribution from 17 different graphite/epoxy pressure vessels made of three different resin types and were able to predict burst pressure with a worst case error of 3.89%. Lansing, Walker, and Russell [12] predicted burst pressures in 17 impact damaged graphite/epoxy and aramide/epoxy filament wound pressure vessels made from three different resins and produced an average 5% error between the predicted output and actual output.

The AE amplitude distribution curve contains a lot of data representing failure mechanisms. It has been determined that the “humps” that make up the distribution represent different failure mechanisms, as shown in the amplitude category in Tables 2.3.1-2.3.2. Shown in Figure 2.3.5 is the AE distribution with multiple “humps”. Defining what failure mechanism is represented by which hump is arguable; however, it appears that the neural network can predict ultimate strengths without this information.

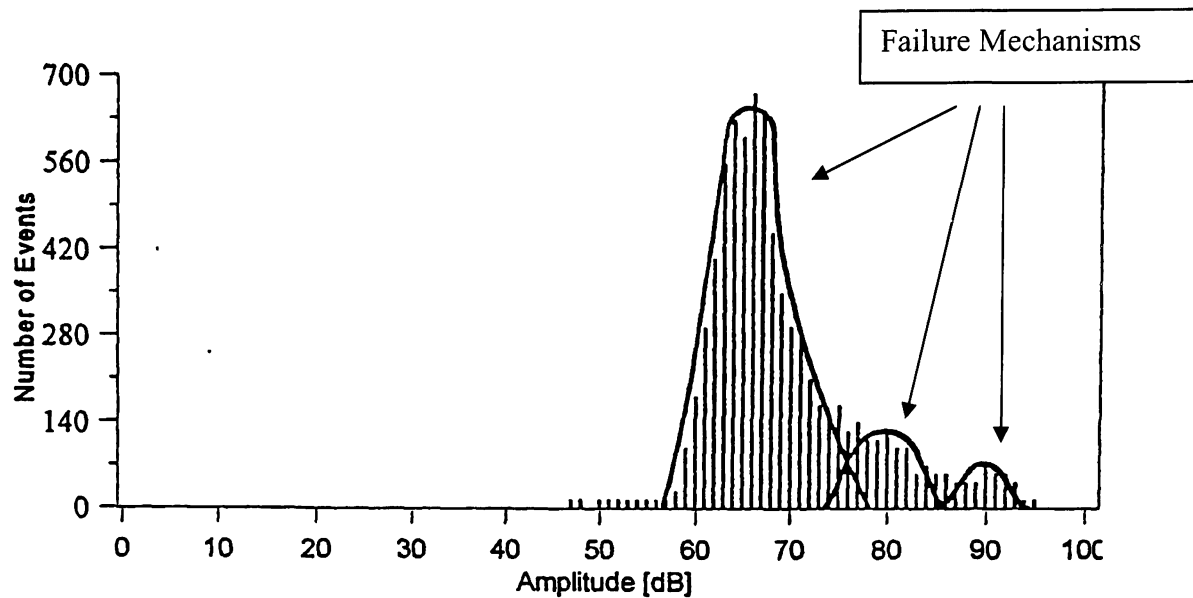


Figure 2.3.5 Acoustic emission amplitude distribution

2.4 NEURAL NETWORKS

A neural network is a mathematical processing tool that consists of a set of algorithms that can classify or predict on complex, highly nonlinear data. These networks are composed of interconnected parallel processing elements (PEs) or neurons that calculate a simple function. Each PE in a network has input vectors which are converted to a weighted output that feeds to other PEs. These interconnections allow for the exchange of data or information. On a global scale, neural networks are able to converge on imprecise or noisy data, of which the physical parameters are not understood or extremely complex. Artificial neural networks were inspired by the massively parallel computational process of the human brain. Parallel computation and error adjustment calculations are similar to multi-neuron processing and synaptic correction that occur within the brain.

A popular form of neural network is an unconstrained optimization backpropagation algorithm. This type of neural network consists of a feedforward network where each individual PE passes information onto the next PE in one direction. The PE first sums the weighted inputs then applies it to a transfer function and finally outputs a new weighted vector to the next layer of neurons as seen in Figure 2.4.1. This

type of network also has an architecture that exists in multiple layers, shown in Figure 2.4.2. The first layer in a backpropagation neural network (BPNN) is the input layer and the final layer is the output layer. Any layers in between are called hidden layers. Each layer can consist of any number of PEs, and there could be multiple hidden layers. The limits to the network are determined by computer processing speed. The network architecture depends upon the complexity of the problem that the network is applied to solving. A BPNN is a supervised network which requires the desired output to be known; thus the network can learn by example. The learning capability of the network is a result of weight adjustments between processing elements. Initially the weights are arbitrary, but once the network iterates, the solution of the network is compared with the known output and a mean-squared error is backpropagated into certain locations in the network to adjust the weights, and the cycle then repeats. This error adjustment calculation is repeated many times until the network converges to an acceptable error level.

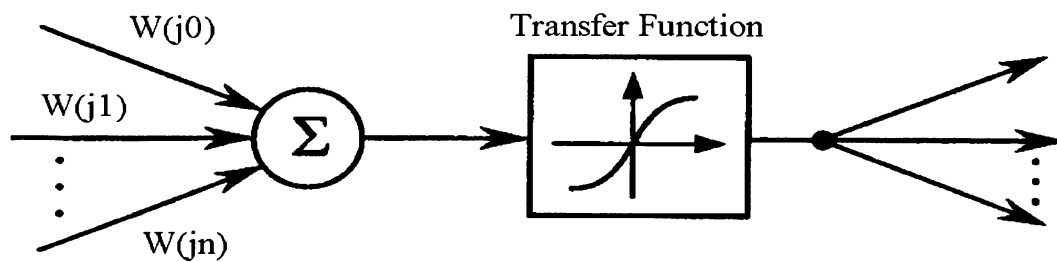


Figure 2.4.1 Neuron processing element

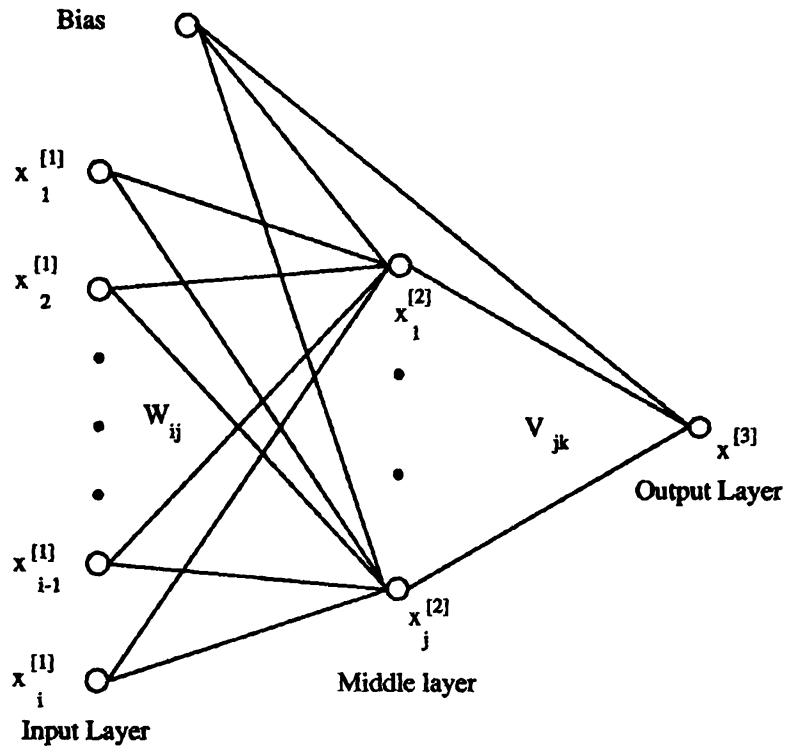
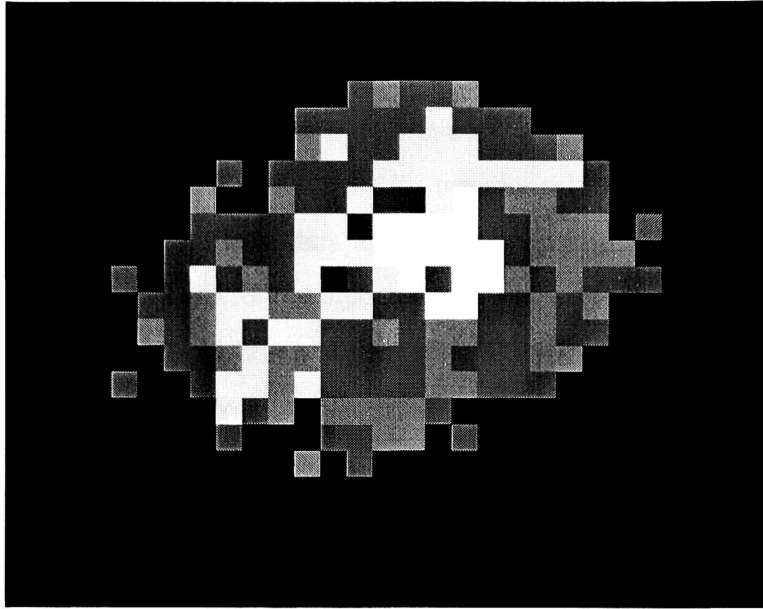


Figure 2.4.2 Backpropagation neural network architecture

2.5 MATLAB

MATLAB is a mathematical tool that was used to analyze the ultrasonic C-scan data. Within MATLAB, an M-file was created with an algorithm to assess the data. The M-file is shown in Appendix B of this report. Initially, the image files are stored in the UltraPac II C-scan system and retrieved in PCX format. Later, the images are transformed into 16 color bitmap image files. Each pixel in an image has a color and each color hue is represented by a number from 0-16 (in the 16 color format). In the color-number format, black is represented by the numerical value of 0, while white is 15; the lighter the color, the higher the numerical pixel value. MATLAB opens these image files as a matrix array, with the pixel location and color number representing the actual image. Shown in Figure 2.5.1 is an example of how MATLAB represents an image.



0	0	0	0	0	0	0	0	0	0	0	0	0	0	0	0	0	0	0	0	0	0	0	0	0
0	0	0	0	0	0	0	0	0	0	0	0	0	0	0	0	0	0	0	0	0	0	0	0	0
0	0	0	0	0	0	0	0	0	0	0	0	0	0	0	0	0	0	0	0	0	0	0	0	0
0	0	0	0	0	0	0	0	0	0	0	0	2	10	2	2	10	0	0	0	0	0	0	0	0
0	0	0	0	0	0	0	0	0	0	2	2	2	2	2	11	2	2	2	0	0	0	0	0	0
0	0	0	0	0	0	0	0	0	0	10	11	2	2	11	11	11	2	2	2	10	0	0	0	0
0	0	0	0	0	0	0	0	2	0	2	2	2	2	11	11	11	11	11	11	11	2	0	0	0
0	0	0	0	0	0	0	10	0	0	10	2	2	11	9	9	11	15	2	10	10	2	2	0	0
0	0	0	0	0	0	2	2	2	2	11	11	9	15	15	15	15	2	2	10	10	10	0	2	0
0	0	0	0	0	2	2	10	2	2	11	11	11	15	15	15	15	15	2	10	10	10	10	0	0
0	0	0	0	2	0	2	11	2	10	2	11	9	2	11	15	2	15	15	10	2	10	2	2	0
0	0	0	0	2	2	10	11	11	10	10	11	11	2	2	15	15	2	2	10	2	10	0	0	0
0	0	0	0	10	2	10	11	2	11	11	2	2	10	2	10	10	2	2	10	2	2	0	0	0
0	0	0	0	0	2	2	10	11	10	10	2	2	2	2	10	2	2	2	10	10	0	0	0	0
0	0	0	0	2	0	0	2	11	11	10	11	2	2	2	2	10	10	2	2	2	0	0	0	0
0	0	0	0	0	0	0	0	11	2	10	0	10	10	10	10	2	0	0	0	0	0	0	0	0
0	0	0	0	0	0	0	0	2	0	0	0	2	2	10	10	0	2	0	0	0	0	0	0	0
0	0	0	0	0	0	0	0	0	0	10	0	2	0	0	0	0	0	0	0	0	0	0	0	0
0	0	0	0	0	0	0	0	0	0	0	0	0	0	0	0	0	0	0	0	0	0	0	0	0
0	0	0	0	0	0	0	0	0	0	0	0	0	0	0	0	0	0	0	0	0	0	0	0	0
0	0	0	0	0	0	0	0	0	0	0	0	0	0	0	0	0	0	0	0	0	0	0	0	0
0	0	0	0	0	0	0	0	0	0	0	0	0	0	0	0	0	0	0	0	0	0	0	0	0
0	0	0	0	0	0	0	0	0	0	0	0	0	0	0	0	0	0	0	0	0	0	0	0	0
0	0	0	0	0	0	0	0	0	0	0	0	0	0	0	0	0	0	0	0	0	0	0	0	0
0	0	0	0	0	0	0	0	0	0	0	0	0	0	0	0	0	0	0	0	0	0	0	0	0
0	0	0	0	0	0	0	0	0	0	0	0	0	0	0	0	0	0	0	0	0	0	0	0	0

Figure 2.5.1 Sixteen color C-scan image (top) and image matrix represented by MATLAB (bottom)

The image shown at the top of Figure 2.5.1 is very small, hence the distortion as seen. The matrix size is 23 rows by 25 columns representing a total of 575 data points. The C-scan images used for this research were approximately a 400 by 200 matrix for a total of 80,000 data points. To assess this much data is impractical; hence, by manipulating the matrix and calculating certain parameters, the image is simplified prior to inputting it to a neural network. The MATLAB M-file algorithm is relatively simple, in that it sums the rows or columns of the image matrix and then normalizes these values. Because the flaws or discontinuities appear as high echo amplitudes in the ultrasonic C-scan image file, these pixels are light colored and have a high pixel numerical value. The columns or rows that have more light colored pixels have a higher summation and can be represented as peaks in a distribution. Shown in Figure 2.5.2 is an actual C-scan image file after MATLAB manipulation.

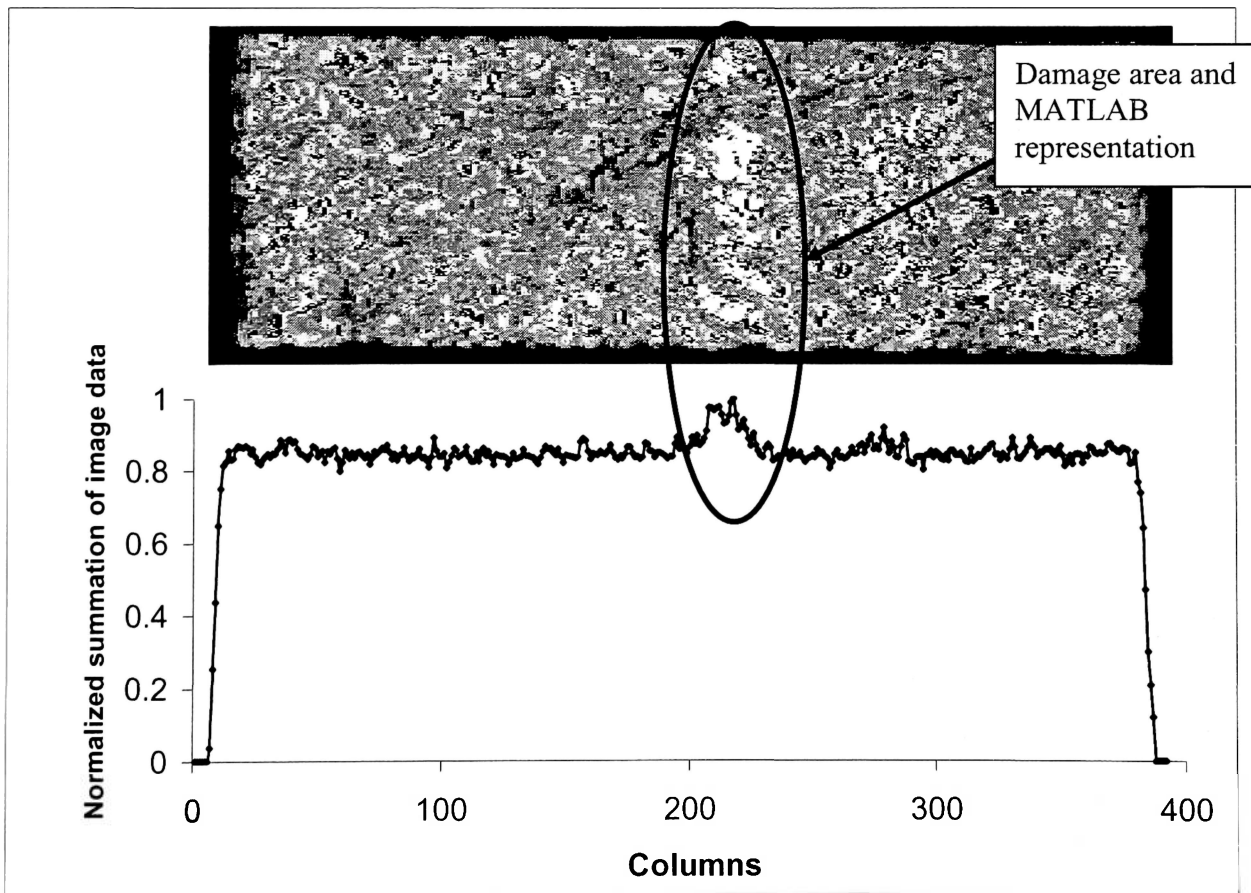


Figure 2.5.2 C-scan image (top) and MATLAB assessment (bottom)

CHAPTER 3 PROCEDURE

3.1 CARBON/EPOXY LAMINATES

The material used in this research was AS4/3501-5A. There were two lay-up configurations as follows:

- $[0, +/-90, 0]_{2S}$
- $[0, +/-90, 0]_S$

The reason for these laminate orientations is that there is a maximum propensity for delamination creation during impact as a result of lamina oriented at 90° angles. As previously stated, the interlaminar stresses associated with lamina mismatch angles are greatest at 90°. The laminates were cured according to the specification attached in Appendix A. They were created as 12 x 12 inch tiles and then cut to size using a wet-diamond-blade cutting tool. Using a wet-diamond-blade cutting tool prevents the laminate from growing artificial delaminations that can develop as a result of cutting stresses. The impact specimens for the duration of testing were cut from the tiles into 3.5 x 6 inch rectangles.

3.2 IMPACT TESTING

Once the laminates were manufactured and cut to size, they were impacted at a low energy level ranging from 2.5-20.0 ft-lb_f. The equipment used for impact testing was the Instron Dynatup 9250 shown in Figure 3.2.1. The data acquisition system was capable of recording up to four channels. Two channels were occupied, one for the impulse data coming from the tup, and a second channel for measuring the dynamic load of the impulse by connecting an accelerometer to the drop sled. However, for this research, only the data from the tup were analyzed. The remaining two channels were not used at this time.

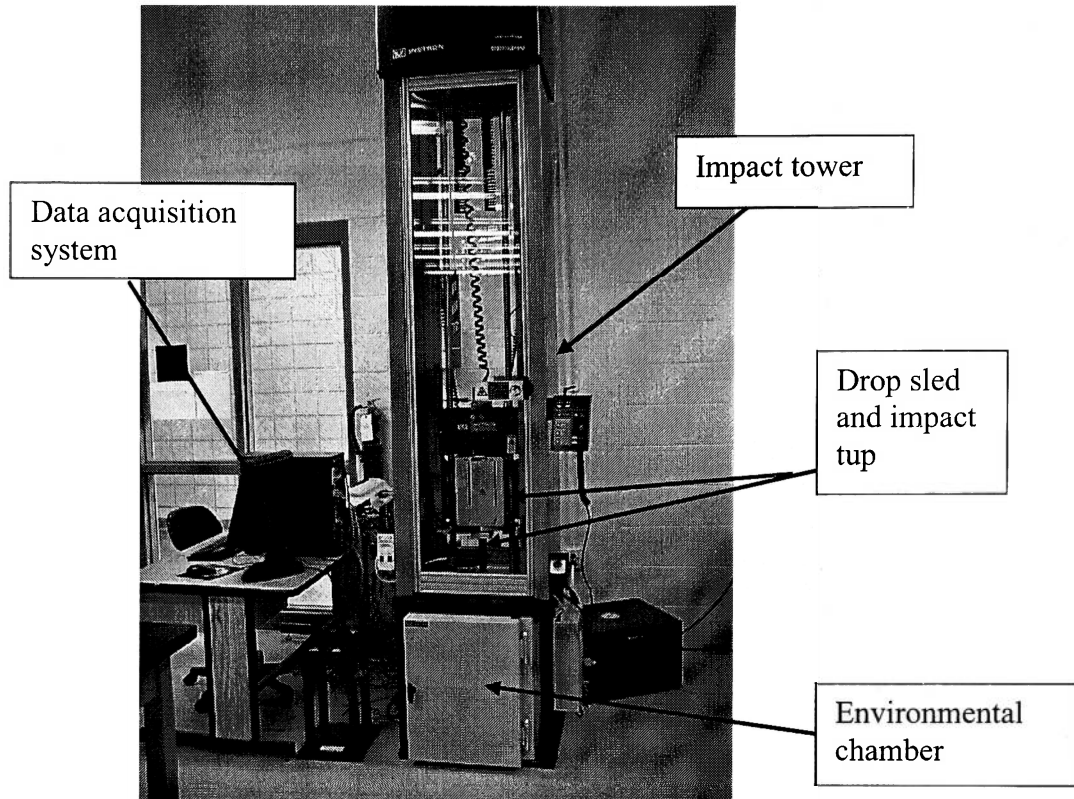


Figure 3.2.1 Instron Dynatup 9250

During impact, the Instron drop tower has pneumatic rebound stoppers. These stoppers deflect upward after impact to catch the drop sled and prevent it from impacting the specimen a second time. Thus all the data presented in the results section are from a single impact.

The clamping fixture for the Instron drop tower is pneumatic. Presently, this fixture is located in the environmental chamber. The clamping device creates a fixed support condition along the edges of the specimen as shown in Figure 3.2.2. Before actual impact, the top clamping plate pulls down as a result of the pneumatic cylinders and secures the specimen. It should be noted that prior to releasing the drop sled the pressure gauge for the pneumatic clamping device must be reading a desired pressure for the clamping fixture to be active. In this research, the pneumatic clamping pressure gauge read approximately 60-70 psi. If there is an error in the clamping fixture (thus no pressure and no clamped support condition), the system will impact the specimen regardless. Also before testing, it is recommended that the drop tower's frictional

coefficients and velocity measurement capability be tested and reconfigured. These tasks are easily completed within the software properties.

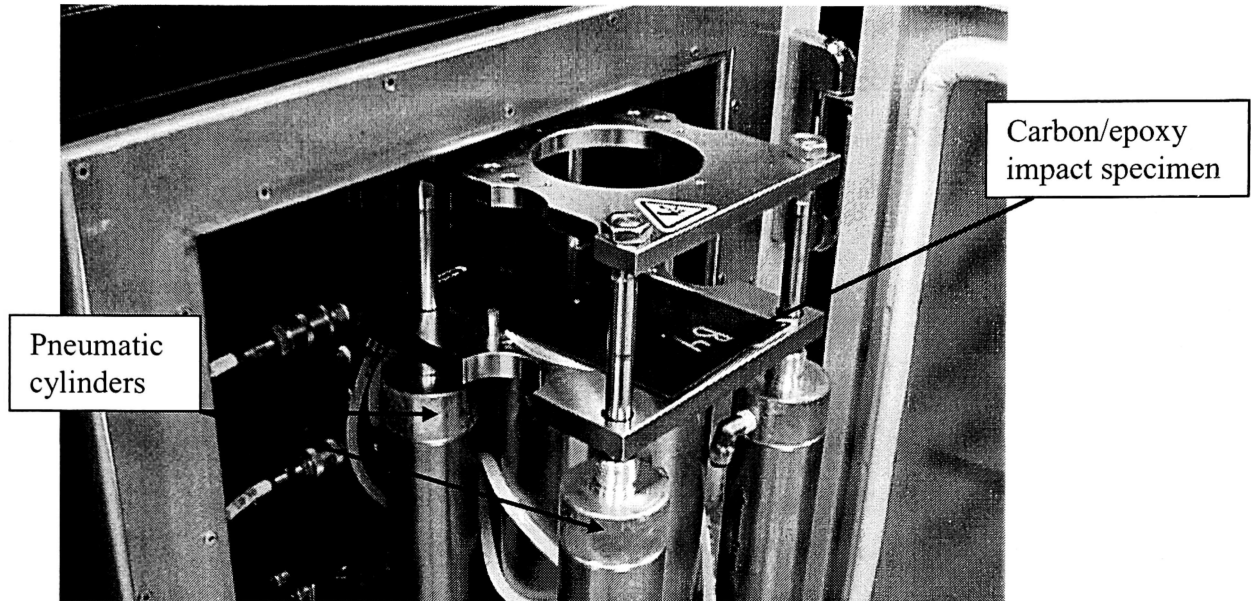


Figure 3.2.2 Pneumatic clamping fixture

One parameter that was used and stored within the system method was the 25 millisecond recording range. Recording impulse information over a 25ms range is arbitrary. It was determined that, depending on the velocity at impact, the start gate might be initiated prematurely; consequently, impulse data may stop recording in advance if this parameter is set too low. The actual impulses last approximately 5-10ms. However, the resolution was not compromised because within that 25ms there are approximately 8,000 data points. The data recorded during impact within this 25ms parameter are load, impact energy, velocity, and deflection versus time. This research utilized the peak load during the impulse and the maximum impact energy as seen in the results.

3.3 ULTRASONIC C-SCAN TESTING

After the laminates were impacted, they were ultrasonically C-scanned. The ultrasonic C-scan was accomplished using a Physical Acoustics Corporation UltraPAC II water immersion system. The ultrasonic transducer used for this research had an unfocused 0.25 inch diameter piezoelectric crystal that pulsed at 5 MHz. Shown in Figure 3.3.1 is the system used for damage assessment.

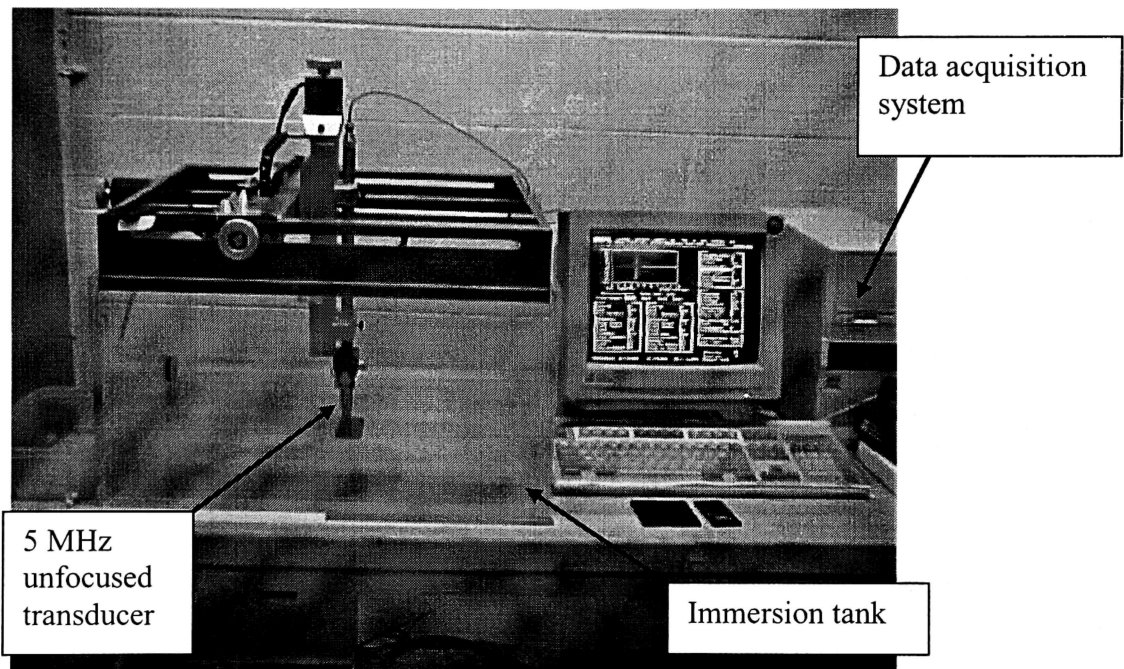


Figure 3.3.1 UltraPAC II C-scan imaging system

All scanning was done in the far field which is approximately 0.65 inches from the specimen surface (Equation 3). Shown in Figure 3.3.2 are the Hardware setup screen and the associated parameters that were used in this research. All of the images that were generated from the ultrasonic C-scan were to assess amplitude changes. The other options such as Time-of-Flight images were not used in this research. The gates shown in Figure 3.3.2 are represented by the small horizontal lines that are in the A-trace display. These gates record only information that passes through them along the horizontal range. The gates shown are essentially recording information at various depths within the laminate. The sample rate within the Sweep/Digitizer option was set

relatively low at 32MHz. This was due to the extraneous noise that often accompanies the higher sampling rate. All of the options shown will change considerably for different materials. It was found as a result of this research, that the parameters shown in Figure 3.3.2 produced the best results.

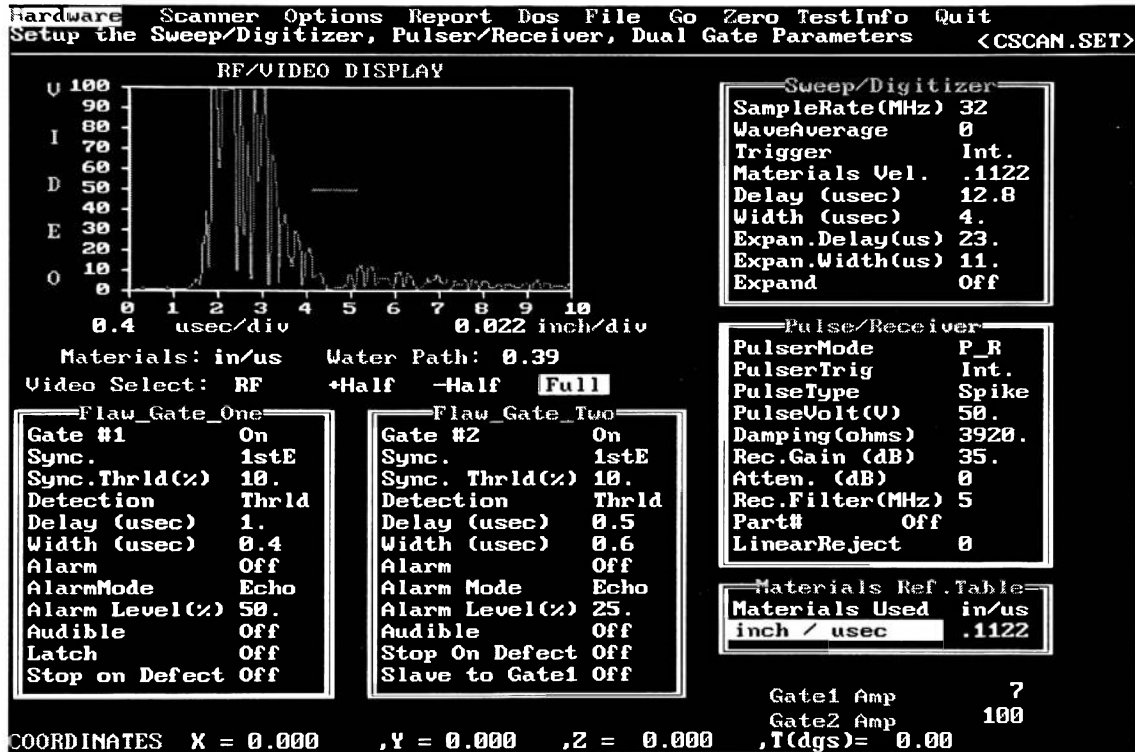


Figure 3.3.2 Hardware setup parameters

3.4 ACOUSTIC EMISSION AND COMPRESSION TESTING

After scanning the laminates ultrasonically, the test specimens were prepared for compression testing. Acoustic emission data were acquired during compression testing to determine the onset of failure. The acoustic emission data acquisition system used for this research was the Physical Acoustics Corporation AEwin software along with the DiSP data acquisition board that is capable of capturing up to 4 channels of data. The entire system is portable within a laptop computer. Important parameters configured within the AEwin software are as follows:

- Preamp Gain = 40 dB
- Threshold = 60 dB
- Peak detection time (PDT) = 50 μ s
- Hit definition Time (HDT) = 100 μ s
- Hit lockout time (HLT) = 300 μ s

The values for PDT, HDT, and HLT are those recommended in the DiSP user's manual for composite structures. The preamp gain is the amplification within the transducer. The threshold was set high because of the tendency of this material to be "noisy". When this value was set lower, there were too many AE hits recorded, thus making the data images blurred due to the overlap. The peak detection time (PDT) is the maximum amount of time allotted to determine the true peak of the waveform signal. Correct PDT ensures that the true risetime and peak are recorded. If set incorrectly, the peak maximum and the risetime recorded, could possibly be a local maximum of a waveform instead of a global maximum. Hit definition time (HDT) defines when one waveform signal is separated from another. HDT is the allotted time span spent after the waveform signal drops below the threshold, thus determining the end of a hit and closing out the measurement process. Hit lockout time (HLT) is set to inhibit reflected signals, from being measured and stored. The HLT starts precisely when the HDT ends. During this time, the system moves the measured waveform data into its buffers. The minimum time setting for the DiSP system is 300 μ s for this function.

Compression testing was accomplished using a Tinius Olsen machine. The compression jig was a Boeing BSS-7260 compression after impact (CAI) fixture. Shown in Figure 3.4.1 is the fixture with a compression specimen and acoustic emission transducers installed. The fixture has adjustable channels or grooves along the sides that allowed the specimen to slide into it. These channels or grooves prevent the specimen from buckling during loading. The AE hardware consisted of two PAC R15 transducers and one PAC R15I transducer from Physical Acoustics Corporation. The reason for the using the smaller R15 transducers was due to the limited space that was available to hot melt glue them to the surface of the laminate. The PAC 1220A external preamplifiers and filters for the R15 transducers along with the complete data acquisition system are shown in Figure 3.4.2. The larger R15I transducer was attached to the compression jig to monitor the AE data that propagated into the fixture.

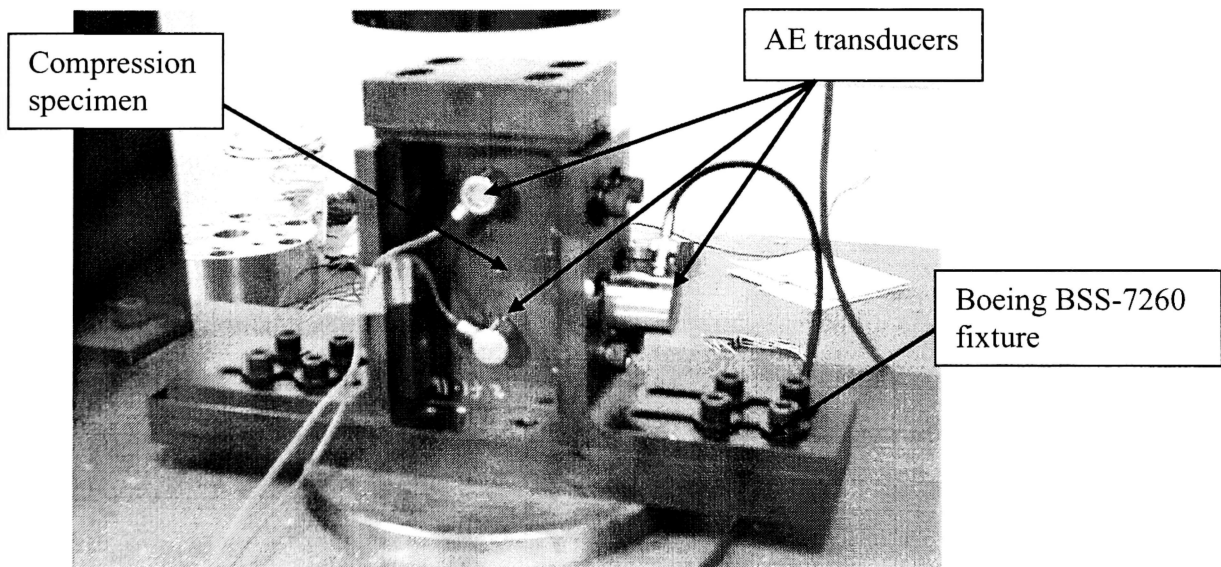


Figure 3.4.1 Compression after impact (CAI) fixture with AE transducers

Initially an attempt was made to locate the source of the failure mechanism by means of linear location between the two R15 transducers. However, due to the sides of the specimen in contact with the compression jig, much of the waveform energy attenuated out of the specimen, thus never reaching both transducers. It is important to

tape the Microdot-BNC cables down in order to prevent the transducers from popping off as a result of the large amount of energy released when the specimens failed.

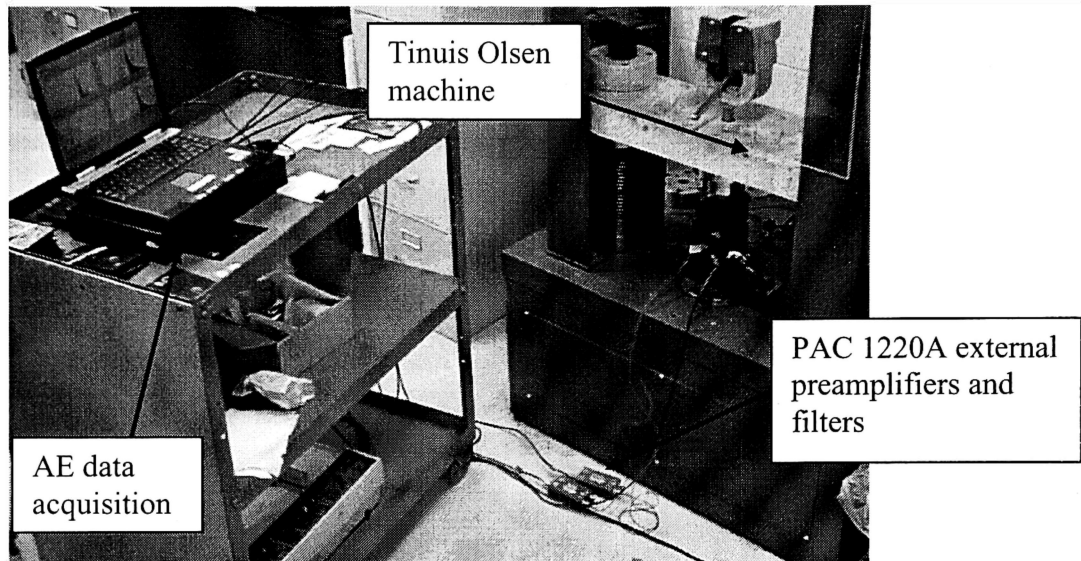


Figure 3.4.2 Data acquisition setup for compression testing

3.5 NEURAL NETWORKS

The neural network software used in this research was Neural Works Professional II/Plus by NeuralWare. When applying neural computing, sometimes it is difficult to determine what the network is converging on. This is because optimization techniques such as backpropagation algorithms are difficult to comprehend, especially after thousands of iterations. The Neural Works Professional II/Plus allows more user interface to adjust certain parameters, thus it helps the user understand some advantages to neural computing. A drawback to this software is the need to adjust all the parameters correctly to minimize error, which is typically a trial-and-error process.

CHAPTER 4 RESULTS

4.1 IMPACT AND COMPRESSION TESTING

As previously stated, the test samples includes 8 ply and 16 ply laminates. Shown in Table 4.1 are the specimens and their corresponding impact energies, compression after impact (CAI) failure loads, and boundary conditions.

Table 4.1.1 Specimen laminates and corresponding impact and compression loads

Ply #	Specimen #	Impact Energy [ft-lb _f]	CAI Load [lb _f]	Boundary Conditions
8 Ply	CDH1	4.97	1322.9	Clamped
	CDH2	5.34	1714.8	Clamped
	CDH3	8.24	1423.1	Clamped
	CDH4	7.15	1373.4	Clamped
	CDH5	3.15	964.46	Clamped
	CDH6	3.16	1025.3	Clamped
	B1	0	2402.5	Clamped
	B2	0	2295.1	Clamped
	B3	5.27	1750.0	Clamped
	B4	5.3	3057.1	Clamped
	B5	6.65	2502.0	Clamped
	B6	6.67	2997.2	Clamped
16 Ply	CH1	8.76	2969.7	Clamped
	CH2	8.82	2974.1	Clamped
	CH3*	8.47	---	Clamped
	CH4	15.54	2974.1	Clamped
	CH5	15.23	2941.6	Clamped
	CH6	15.25	2984.4	Clamped
	C1	3.26	1298.2	Clamped
	C2	3.4	2732.0	Clamped
	C3	10.59	2398.2	Clamped
	C4	10.3	2007.2	Clamped
	C5	16.42	3317.1	Clamped
	C6	16.35	2132.7	Clamped
	A1	0	4936.5	Clamped
	A2	0	2865.6	Clamped
	A3	2.23	6531.9	Clamped
	A4	20.2	3042.2	Clamped
	A5	21.43	3910.1	Clamped
	A6	20.75	4174.8	Clamped
	D1*	0	---	Unsupported
	D2	0	8367.5	Unsupported
	D3	1.7	5324.7	Unsupported
	D4	1.52	5987.2	Unsupported
	D5	7.24	6023.5	Unsupported
	D6	7.23	6292.0	Unsupported

*failure to record compression after impact load

Shown in Figure 4.1.1 and Figure 4.1.2 are the results from the actual impact testing. Overall, there were 36 samples, 12 eight ply laminates and 24 sixteen ply laminates. The Instron Dynatup data acquisition system gives a wide variety of information concerning the impulse. Peak impact load, total impact energy, plate deflection, impact velocity, and impact time are determined for each impact test. Figure 4.1.1 plots two of the impulse data parameters, peak impact energy versus peak impact load for each batch. The peak impact load is the maximum load absorbed during the impulse. During impact, the variation in peak impact load can help determine material quality and stiffness. Figure 4.1.2 organizes the same data as in Figure 4.1.1 according to ply thickness. Trendlines were added to show not only the trend but also to show the variability in the data. As can be seen in Figures 4.1.1 and 4.1.2, the 8 ply laminates had very little variation in the trend when compared to the 16 ply laminates. Prior to impact testing, it was determined that the specimens in batch A and C were made of poor quality, i.e. many manufacturing discontinuities. Shown in Figure 4.1.1, the best fit coefficient of determination (R^2) is lower for batch A and C when compared to the other 16 ply laminates. The trends shown in Figure 4.1.2 are a better representation of the data, because the curves do not enter an impossible region located below the peak impact load axis as shown in the trends in Figure 4.1.1.

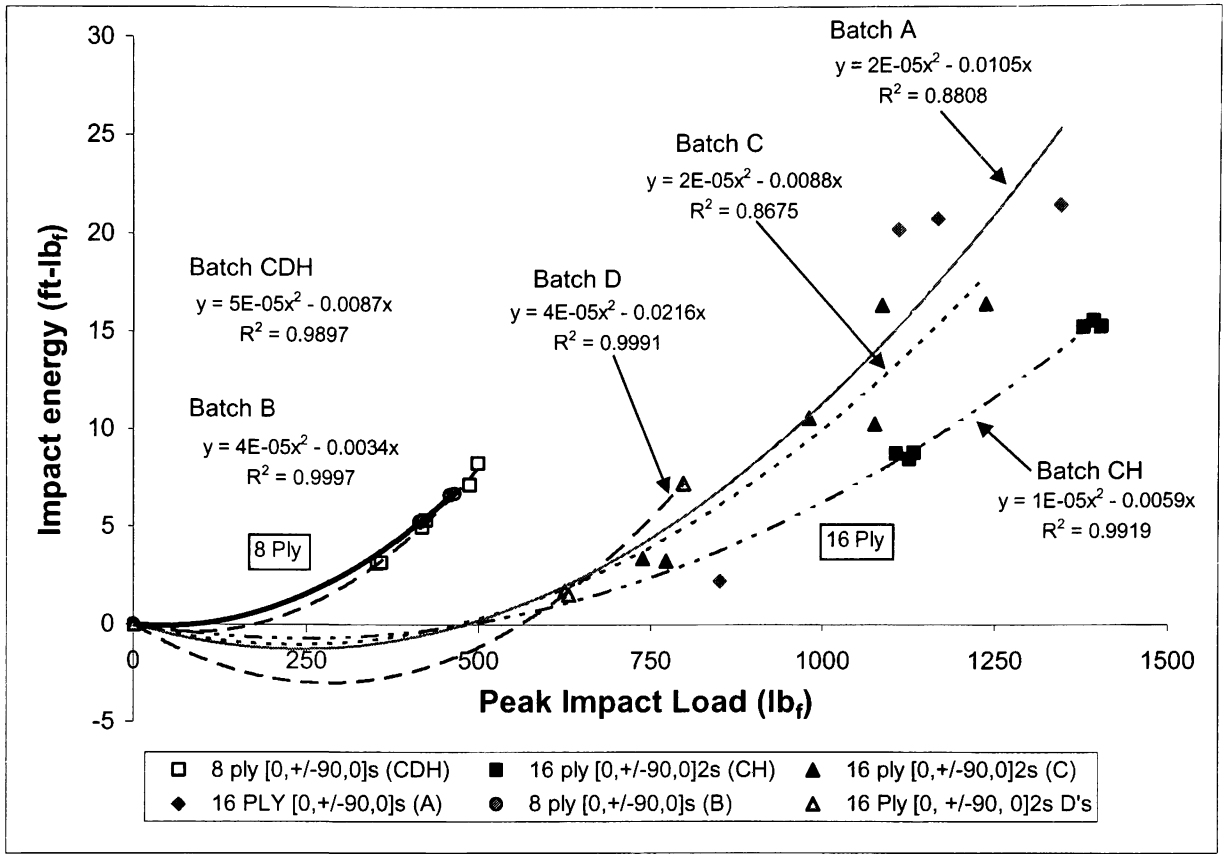


Figure 4.1.1 Impact energy vs. peak impact load according to specimen batch

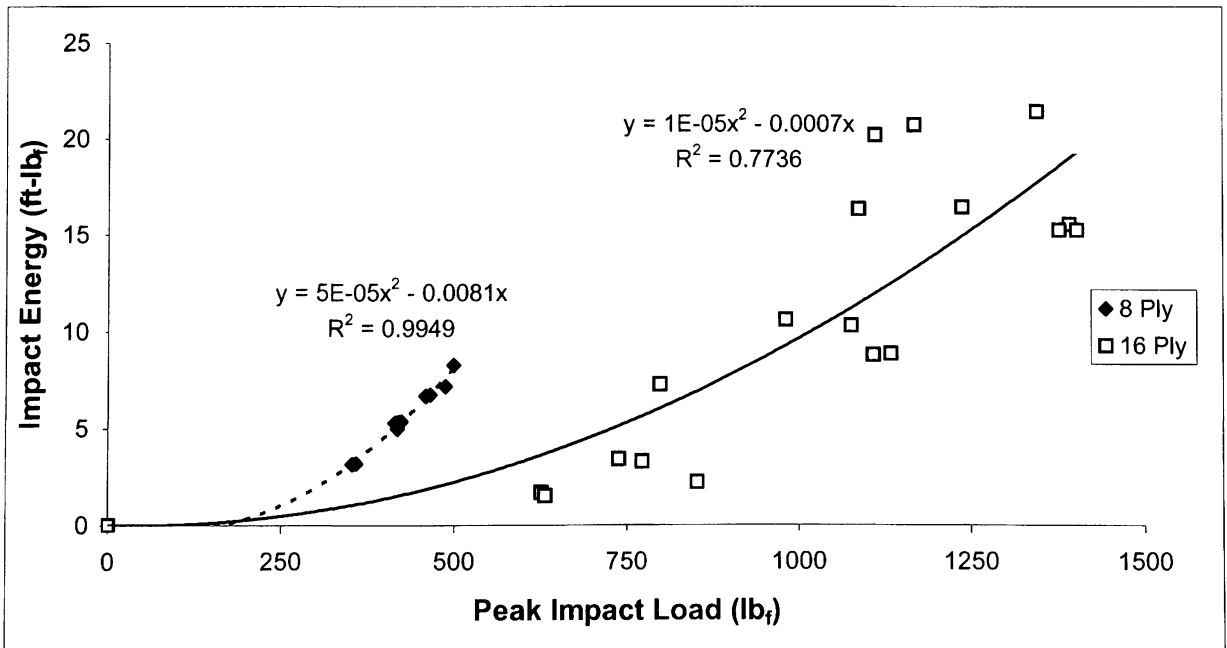


Figure 4.1.2 Impact energy vs. peak impact load according to ply thickness

All the higher energy impacts (~ 20 ft-lb_f) on the 16 ply laminates sustained damage that was readily visible. The front surface had an obvious indentation that was identical in shape to the tup's hemispherical head, while the back surface had subtle separation of fibers, as shown in Figure 4.1.3(a) and Figure 4.1.3(b), respectively. The specimens that were impacted at energies less than 14 ft-lb_f sustained damage that was extremely difficult to detect visually. On these specimens the only visual damage detectable is on the back face where there was ply separation similar but not as obvious to that shown in Figure 4.1.3(b). For the laminates in batch D, with the unsupported impact boundary conditions, the laminates with impact energies of ~ 7 ft-lb_f sustained damage similar to that shown in Figures 4.1.3(a) and 4.1.3(b).

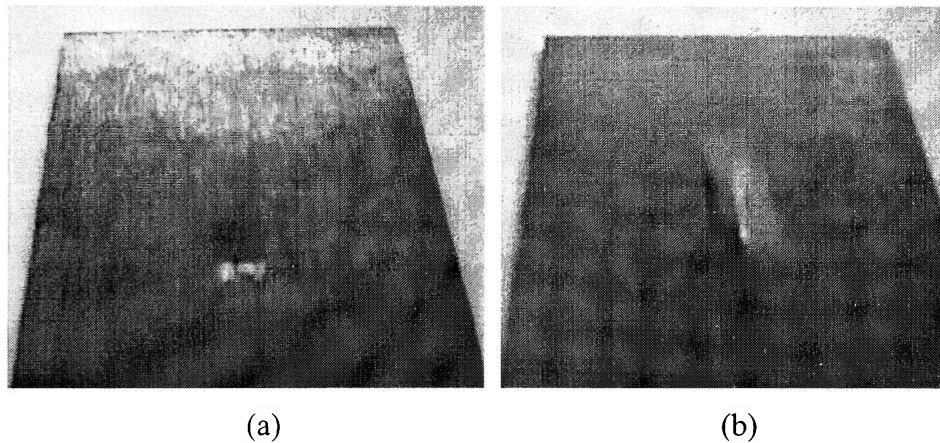


Figure 4.1.3 Front surface (a) and back surface (b) impact damage

During compression testing, the specimens failed by crushing inward due to the interply shear stresses; the resulting failure is shown in Figure 4.1.4. The guides on the compression fixture prevented buckling of the laminates, as previously stated.

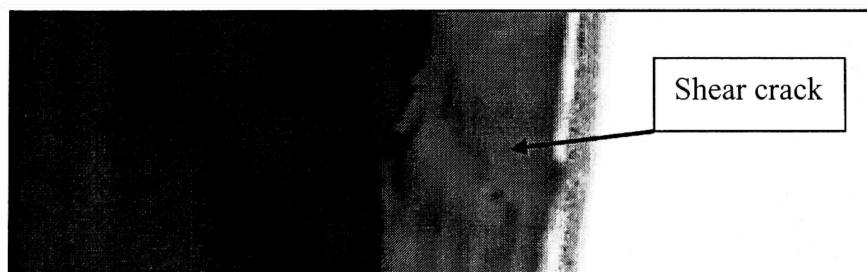


Figure 4.1.4 Specimen failure as a result of compression loading

The results from compression testing of all 36 samples, as shown in Figure 4.1.5, illustrate a wide variance in the data. It should be noted that the specimens in batch D are not included in Figure 4.1.5 due to the difference in impact boundary conditions. Polynomial trendlines were determined for the 8 ply and 16 ply samples. The 16 ply polynomial's best fit coefficient of determination, R^2 , is quite low correlating ~24% of the data and the 8 ply is only 5% of the data.

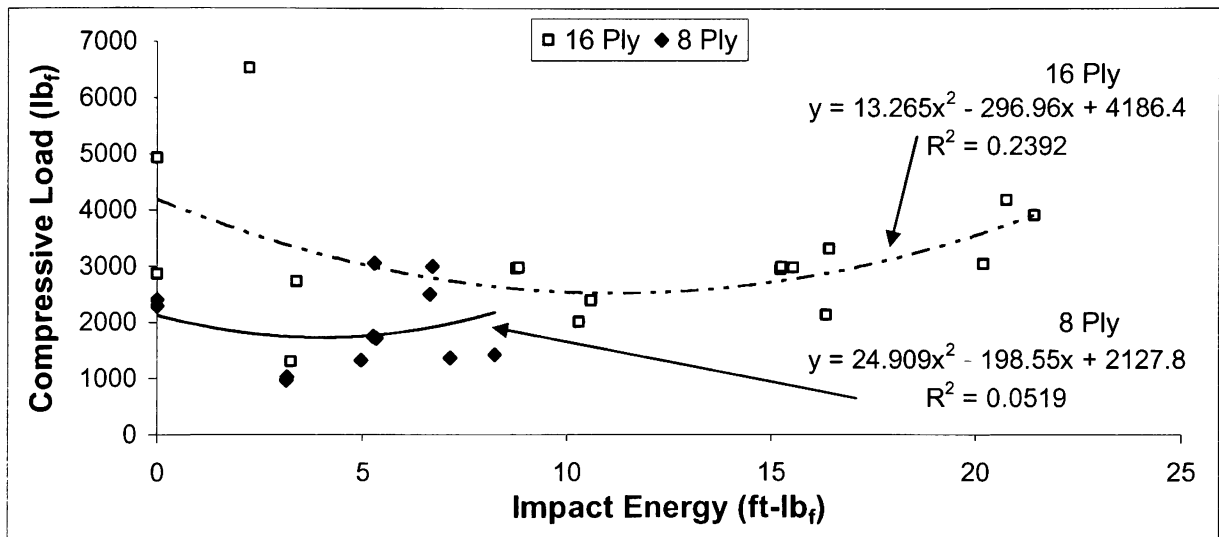


Figure 4.1.5 Compressive load vs. impact energy

The concave upward polynomial is the best fit trend for the data generated as a result of this research (shown in Figures 4.1.5 and 4.1.7). At impact energies greater than 22 ft-lb_f, it is reasonable to assume that the compressive load would drop considerably as a result of more impact energy; however, more research is required to justify this analysis. It would not be feasible to use the current trend for higher impact energies, to do so would result in evaluating a higher compressive load as result of a higher impact energy which is physically impossible. It is possible that the data points which were impacted at greater energy and maintained a higher CAI load is a reaction to a smaller damage size in the fiber and matrix interface. The damage associated with greater impact energies resulted in more surface damage (Figure 4.1.3); however the interply delaminations are smaller in area when compared to the laminates with lower impact

energies. Delaminations and delamination size can directly affect CAI. It is likely that the damage as a result of impact energies greater than 22 ft-lb_f will have large interply delaminations and obvious surface damage or possibly penetrating damage, all of which would severely reduce the CAI load.

Previous experimental research has also shown a concave upward polynomial trend similar to that shown in Figures 4.1.5 and 4.1.7. Prichard and Hogg [14] studied the role of compression after impact (CAI) testing in 16 ply thermosets and thermoplastics with laminate orientation of [-45, 0, +45, 90]_{2S}, which produced a concave upward parabolic trend when compressive stress versus impact energy data is plotted for the thermoset. Dost et al. [13] conducted studies on a wide variety of laminate stacking sequences consisting of 24-32 plies made of IM7/8551-7 material. While the best fit curve was not generated, the same concave upward trend was evident from the data plot.

As a result of CAI, it is noted that almost all of the 8 ply laminates and few of the 16 ply laminates failed at locations other than the impact damaged region. The locations for failure were most often in the corners of the laminate. At these positions, there are no guides on the compression jig to prevent buckling. Shown in Figure 4.1.6(a) is one of four possible locations for this type of free-edge buckling failure to occur. The buckling is an interply failure in which the plies separate in a delamination type fashion as shown in Figure 4.1.6(b). Also, because the specimens were cut by hand using a wet-diamond-blade cutting tool, the edges are not perfectly straight. Therefore, the edges that are facing the bottom or top of the fixture did not fit exactly flush. Stress concentrations developed at these regions where only part of the edge face supported the applied compressive load. Because of this type of failure occurred in almost the entire 8 ply laminates, the difficulty associated with C-scanning these thin specimens, and the poor coefficient of determination (R^2) shown in Figure 4.1.5, the rest of the analysis and results herein will concentrate on the 16 ply laminates only.

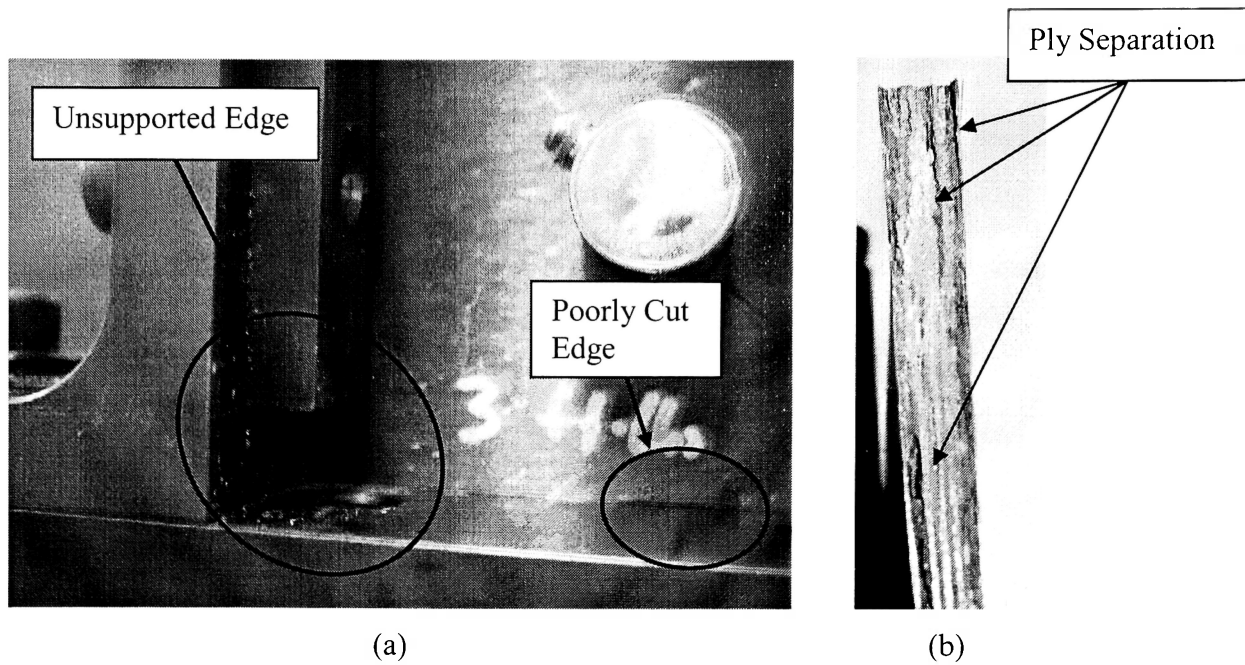


Figure 4.1.6 (a) Free-edge compression failure location (b) ply separation failure

Shown in Figure 4.1.7 is a plot of compressive load versus impact energy that includes the unsupported batch D specimens. A trendline was also added to the entire 16 ply sample set. Although the batch D decreases the variability of the polynomial trendline when compared to Figure 4.1.5, it should be noted that the impact support conditions of this batch are different than the rest of the 16 ply specimens. Performing a statistical analysis of the data, the confidence interval and prediction interval at the 95% confidence level are included in Figure 4.1.7. It can be concluded that 95% of all the given data will fall between the confident intervals, and 95% of all future data will fall between the prediction intervals. As a result of the high variance in the data, the confidence intervals and prediction intervals are extremely broad around the best fit data trend, as can be seen in Figure 4.1.7. For example at an impact energy of 20 ft-lb_f, the difference between the confidence interval and the trend is +/- 40%, and the difference between the trend and the prediction interval is +/-121% at an impact energy of 15 ft-lb_f.

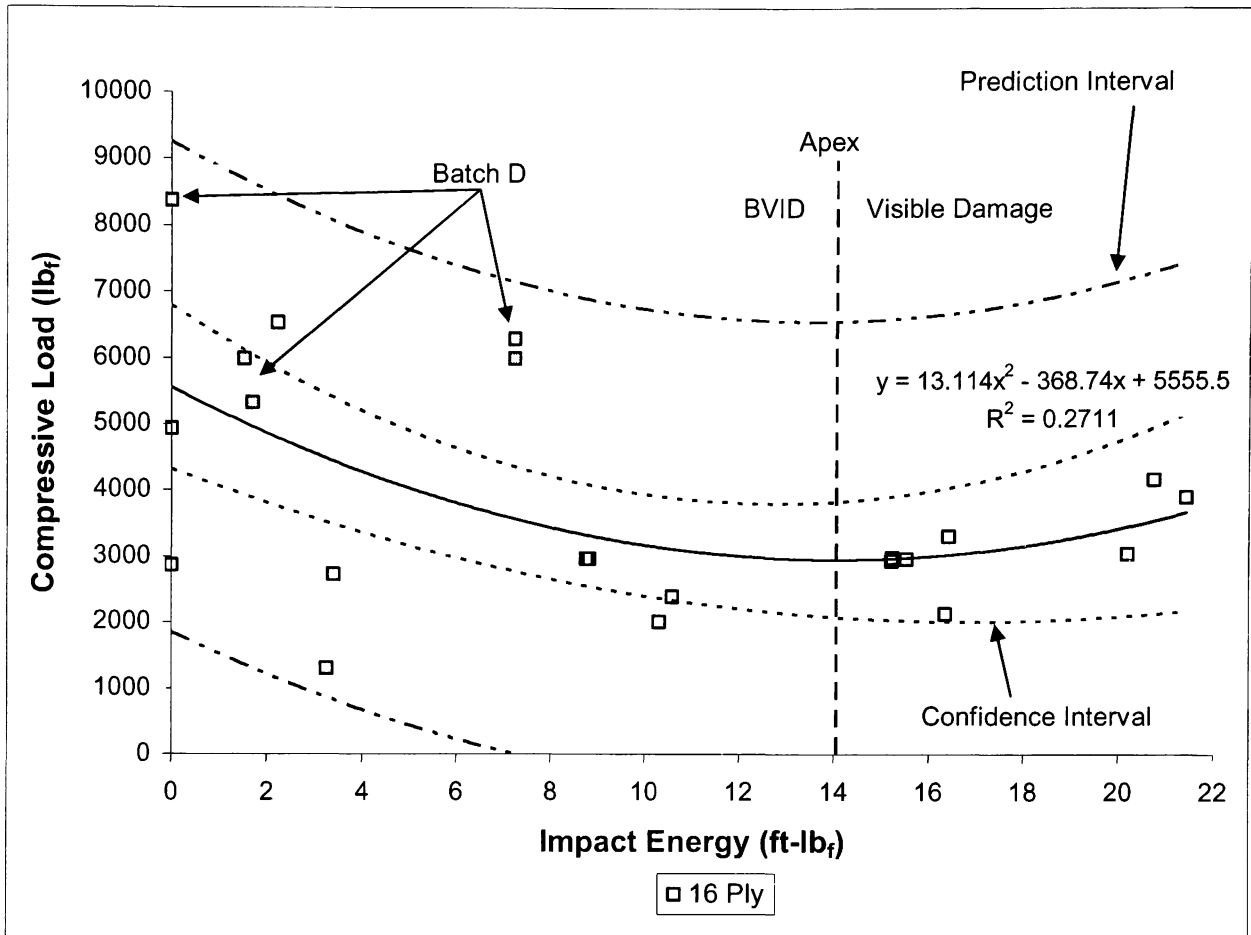


Figure 4.1.7 Compressive load versus impact energy (including batch D)

It is a commonplace, to define data points outside the confidence interval as outliers. Thus, for this analysis, there would be eight outliers in the data shown in Figure 4.1.7. As demonstrated in this research, there is a lot of variability in the data, especially on the lower end of the impact energy realm. In the analysis previously demonstrated in Figure 4.1.7, the 8 data points are not accounted for when plotted on a simple compressive load vs. impact energy plot, thus they are suspected to be outliers. However, as evidenced by the low R^2 value, it is more reasonable to conclude that there are more variables than impact energy that affect compressive load.

Upon reviewing the concave upward polynomial trend shown in Figures 4.1.5 and 4.1.7 and examining the impact specimens, it should be noted that the specimens located to the left of the apex of the trendline (Figure 4.1.7) had barely visible impact damage. The specimens to the right of this apex showed visible damage but without through

penetration. Thus the apex of the parabola indicates approximately where transition between BVID and visible damage occurs for the 16 ply AS4/3501-5A [0, +/-90, 0]_{2S} laminates.

4.2 NEURAL NETWORK APPLICATIONS

As previously stated, the software used for creating and assessing the neural network is Neural Works Professional II/Plus. The network type used was a backpropagation algorithm. Many different network architectures with various parameters were constructed and tested; plus it was concluded that the data from acoustic emission offered no additional information for the network to converge on. Complications arose during compression testing due to data acquisition and the compression test fixture. The laminate sits in the CAI fixture and all four sides are touching the fixture. The rubbing noise associated with loading and the mode conversions and energy loss of the AE signal due to the laminate in contact with the fixture at all times presented a problem. Also, due to the laminate material quality being different for the various batches, the acoustic response was also very different. As can be seen in Appendix C, some laminates were extremely “noisy” while others were “quiet” with less AE hits. The data used herein as the input to the neural networks are strictly limited to UT data only. The output of the neural network is the residual compressive load. The actual data used for the neural networks for batches A, C, CH, and D is given in Appendix E. From every UT image, 50 to 100 data points (depending on network architecture) are taken as the summation of columns or rows. MATLAB performed these summations and transferred the results as a text (.txt) file. These 50 data points surround the damage zone and are associated with peaks in the image plots shown in Appendix B. Discrete values that range from 0 to 1 from the UT image serve as input vectors for each neural network. Some of the more complicated networks also contained binary categorical variables that exist as 1s or 0s. The UT data is followed by the corresponding compressive after impact load. Generally, the training data consisted of the highest, the lowest, and medium values of the CAI loads. The data in the testing set consisted of in-between CAI loads. Neural networks have difficulty predicting on a loads beyond what

they have been trained for. The impact energy associated with each specimen is not included in the input data. Thus these networks were designed to make compressive strength predictions on the information from the UT images alone.

One parameter that was consistently used in every neural network is the SAVEBEST command within the Neuralworks Professional II/Plus software. This feature trains and tests the network alternately, and continues to do so until the network performance begins to degrade. The SAVEBEST command trains the network to the lowest error available for the particular network and prevents the network from overtraining. The neural networks that were designed for each batch, the SAVEBEST options trained down to within 0% error, indicated in Tables 4.2.1-4. However, for the networks that contained all the data, the SAVEBEST command did not train quite as close (Table 4.2.5). Depending on the type of input data, SAVEBEST determines the optimized training and testing network without overtraining. Networks with smaller sets of training data train closer to the actual output as seen in Tables 4.2.1-4.

The first networks constructed were trained and tested for each specimen batch. Listed in Table 4.2.1 are the neural network predictions for the batch CH. Shown in Figure 4.2.1 are the optimized neural network parameters used to generate the results for batch CH. The network consisted of 51 input processing elements (PE) with two hidden layers consisting of 20 PEs apiece. The learning coefficient ratio of 0.002 was set as low as possible to allow the network to iteratively converge on the absolute minimal error. The momentum was set a 0.4 to prevent the network from converging on a point that is a local minima instead of the global minima. The learning rule that produced the most accurate results in all testing in this research was the Delta Rule. This rule calculates the error between the network output and the actual output and is later altered by the derivative of the transfer function and backpropagated into the network layers. This learning rule has an epoch of 1, which means that it calculates weight changes after each iteration. Fast learning was applied and this helped the network converge much faster with less error in the prediction results. This function is only applicable to the Delta rule. In the backpropagation networks generated by Neural Works Professional II/Plus, all layers are connected with a full bias which serves as an offset to the network's output.

Table 4.2.1 Neural network prediction results for batch CH

Data Set	Specimen	Impact Energy (ft-lb _i)	Compressive Load (lb _f)	Predicted Compressive Load	Abs%Diff.
Training	CH2	8.82	2974.1	2974.10	0.00
	CH5	15.23	2941.6	2941.60	0.00
	CH6	15.25	2984.4	2984.40	0.00
Testing	CH1	8.76	2969.7	2968.08	0.05
	CH4	15.54	2974.1	2969.95	0.14

Average error = 0.04

The screenshot shows a neural network configuration dialog box with the following sections:

- # PE's:** Input (51), Hid 1 (20), Hid 2 (20), Hid 3 (0), Output (1). LCoef (0.002) is set for all hidden and output layers.
- Learning Parameters:** Momentum (0.400), Trans. Pt. (10000), LCoef Ratio (0.500), F' Offset (0.100).
- Learn Rule:** Delta-Rule (selected), Norm-Cum-Delta, Ext DBD, QuickProp, MaxProp, Delta-Bar-Delta.
- Transfer:** Linear (selected), TanH, Sigmoid, DNNA, Sine.
- Options:**
 - Connect Prior, Gaussian Init.
 - Auto-Assoc., Minimal Config.
 - Linear Output, MinMax Table
 - SoftMax Output, Bipolar Inputs
 - Fast Learning, Cascade Learn
- I/O Files:**
 - Learn: CH UT train.txt (Browse...)
 - Recall / Test: CH UT test.txt (Browse...)
- Logicon PROJECTION NETWORK (TM)**
- Epoch:** 3 (Set Epoch From File)
- Buttons:** OK, Cancel, Help

Figure 4.2.1 Network input parameters for batch CH

Listed in Table 4.2.2 are best results for the batch A specimens. It should be noted that the batch A laminates were made of very poor quality, yet the network was able to make relatively good predictions. Figure 4.2.2 shows some different parameters incorporated to help the network converge better. Similar to the batch CH specimens, the batch A specimens required a double hidden layer of PE's or neurons to obtain the desired results. Two parameters that were different in this network are the Gaussian initiation and the linear output. Gaussian initiation creates a Gaussian distribution rather than a uniform distribution for noise generation. Neural networks respond very well to "noisy" data. The Gaussian function helps to create artificial noise for the inputs. As a result of this research, it has been determined that this function produces good results when data is somewhat linear. The linear output parameter forces the final output PE to have a linear

transfer function. In this network, all hidden layers had a hyperbolic tangent transfer function with the final layer containing a linear transfer function. It appears that the when a network is predicting similar results using a linear transfer function (TF) or nonlinear TF the linear output option will take advantage of both TF types and produce the best results. A network was also trained using 3 training sets instead of the 4 shown in Table 4.2.2. Here the results were similar with an average data set error of 5.37% with a worst case of 14.7%.

Table 4.2.2 Neural network prediction results for batch A

Data Set	Specimen	Impact Energy (ft-lb _f)	Compressive Load (lb _f)	Predicted Compressive Load	Abs%Diff
Training	A2	0	2865.6	2865.60	0.00
	A3	2.23	6531.9	6531.90	0.00
	A5	21.43	3910.1	3910.10	0.00
	A4	20.2	3042.4	3042.40	0.00
Testing	A6	20.75	4174.8	4492.73	7.62
	A1	0	4936.5	4338.07	12.12

Average error = 3.29

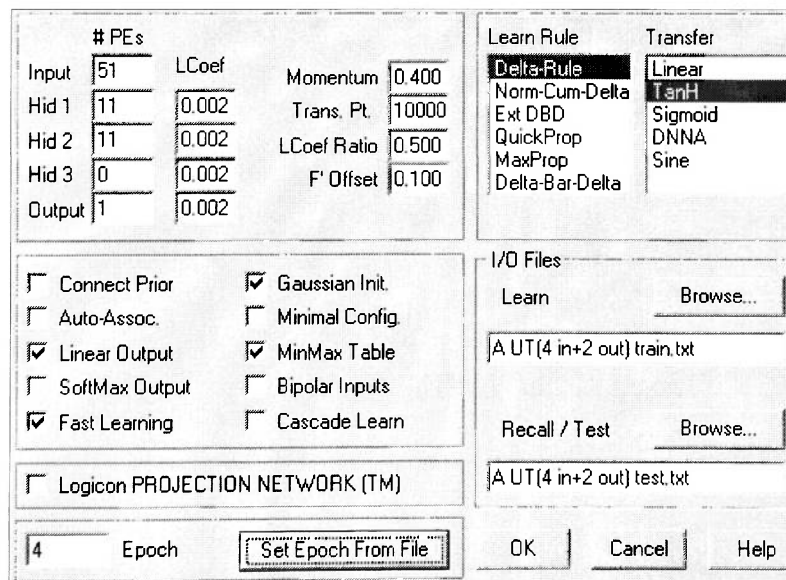


Figure 4.2.2 Network input parameters for batch A

The batch C specimens are similar to the batch A, in that the material construction quality was extremely poor. According to the confidence interval shown in Figure 4.7, there could be 3 outliers in this batch along with 2 outliers in the batch A. Given in Table

4.2.3 are the network results, and shown in Figure 4.2.3 are the input parameters and network architecture. As indicated in Figure 4.2.3, this network consisted of 3 hidden layers with 20 PEs apiece. As can be seen, this network was extremely complicated and was only feasible due to the high clock speed in present day computers.

Table 4.2.3 Neural network prediction results for batch C

Data Set	Specimen	Impact Energy (ft-lb _f)	Compressive Load (lb _f)	Predicted Compressive Load	Abs%Diff
Training	C1	3.26	1298.2	1298.20	0.00
	C3	10.59	2398.2	2398.20	0.00
	C5	16.42	3317.1	3317.10	0.00
	C6	16.35	2132.7	2132.70	0.00
Testing	C2	3.4	2732	2812.41	2.94
	C4	10.3	2007.2	2340.77	16.62
Average error =					3.26

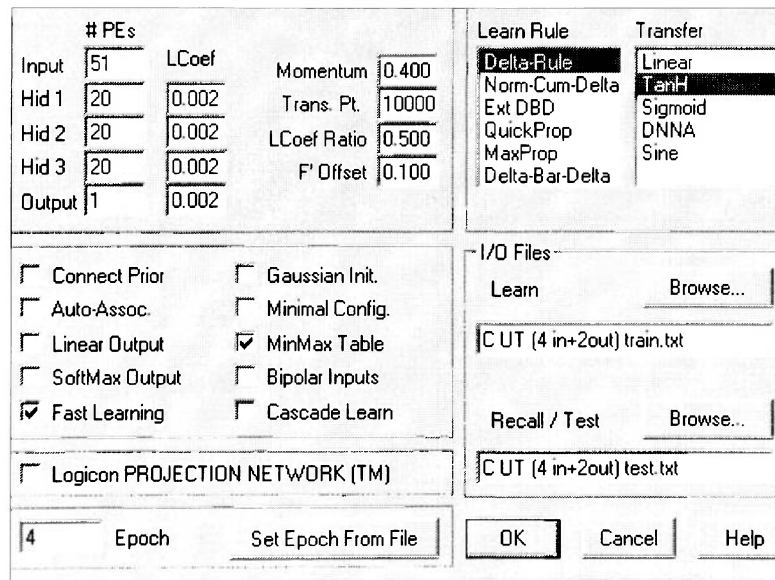


Figure 4.2.3 Network input parameters for batch C

The batch D specimens were the final 16 ply batch created and these laminates had excellent material quality. However, during impact testing, the pneumatic clamped failed; thus, the laminate was simply resting on the clamp head during impact. The damage was much greater as a result of this impact boundary condition. Presented in Table 4.2.4 are the results of the network prediction. Figure 4.2.4 displays the network architecture and the network parameters. The batch D was difficult to train and test with

any great accuracy. Hence the training data consisted of four data sets with testing done on only one.

Table 4.2.4 Neural network prediction results for batch D

Data Set	Specimen	Impact Energy (ft-lb _f)	Compressive Load (lb _f)	Predicted Compressive Load	Abs %Diff
Training	D2	0	8367.5	8367.50	0.00
	D3	1.7	5324.7	5324.70	0.00
	D5	7.24	6023.5	6023.50	0.00
	D4	1.52	5987.2	5987.20	0.00
Testing	D6	7.23	6292	5547.66	11.83
Average error =					2.37

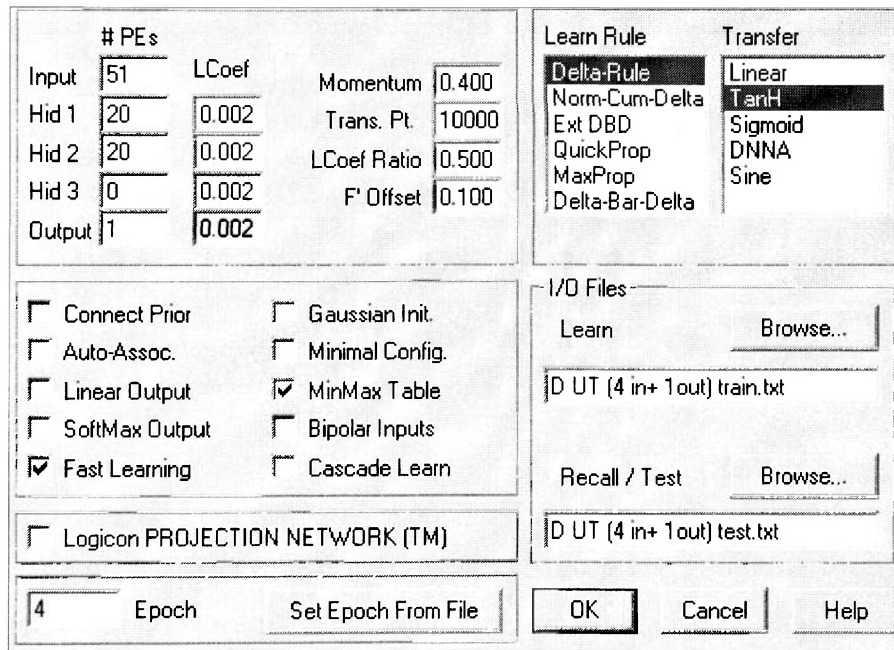


Figure 4.2.4 Network input parameters for batch D

For real world applications, it is be more reasonable to make predictions on composites that are created from multiple material batches; therefore the following networks were trained on all the data from all four batches. Given in Table 4.2.5 are the results from three different networks with variations in input data type and network architecture. The highlighted values are the worst case percent differences. Each of these models used thirteen training sets and tested on nine.

Table 4.2.5 Neural network output from three different networks for all 16 ply data

Data Set	Specimen	Compressive Load	Prediction Model 1	Abs%Diff	Prediction Model 2	Abs%Diff	Prediction Model 3	Abs%Diff
Training	D2	8367.5	8147.97	1.91	8207.63	2.62	8392.17	0.29
	D3	5324.7	5354.31	0.10	5330.21	0.56	5401.99	1.45
	D5	6023.5	6126.12	9.05	5478.65	1.70	6335.95	5.19
	CH2	2974.1	2971.88	0.16	2969.48	0.07	2988.89	0.50
	CH5	2941.6	2950.92	1.33	2980.78	0.32	2998.41	1.93
	C1	1298.2	1474.13	2.09	1325.35	13.55	1604.40	23.59
	C3	2398.2	2354.86	1.88	2353.13	1.81	2270.40	5.33
	A4	3042.4	3038.96	0.68	3021.86	0.11	3042.52	0.00
	C4	2007.2	2010.24	0.04	2006.50	0.15	2104.19	4.83
	C5	3317.1	3329.10	0.98	3284.46	0.36	3234.11	2.50
	A2	2865.6	2873.97	0.17	2870.49	0.29	2893.17	0.96
	A3	6531.9	6582.78	0.23	6517.12	0.78	6553.96	0.34
	A5	3910.1	3906.68	1.59	3972.15	0.09	4049.04	3.55
Testing	CH1	2969.7	2554.67	7.46	3191.22	13.98	3045.20	2.54
	CH4	2974.1	2800.28	27.69	3797.77	5.84	3085.72	3.75
	C2	2732	2802.67	166.88	7291.26	2.59	3302.53	20.88
	CH6	2984.4	1761.55	56.01	1312.96	40.97	3123.53	4.66
	C6	2132.7	2408.62	49.03	3178.42	12.94	2084.57	2.26
	A1	4936.5	5322.09	16.79	5765.50	7.81	5187.63	5.09
	A6	4174.8	2864.08	37.37	2614.78	31.40	3930.74	5.85
	D4	5987.2	6373.27	55.22	2681.20	6.45	7842.18	30.98
	D6	6292	6442.77	44.98	9122.00	2.40	6989.55	11.09
			AVE ERR =	21.89	AVE ERR=	6.67	AVE ERR=	6.25

Prediction Model 1

This neural network consisted of 50 PE's from the columns and 50 PE's from the rows. It was intended to take the data from the UT image and find the normalized sums of rows and columns in an attempt to better represent the input data. The network input parameters are shown in Figure 4.2.5. As indicated in Figure 4.2.5, the architecture for this network is large with three hidden layers consisting of 60, 50, and 40 PE's respectively. This network trained well with low error; however, its prediction capability was less accurate with a worse case of 167% error.

<table border="1"> <tr><td># PEs</td><td></td></tr> <tr><td>Input</td><td>102</td></tr> <tr><td>Hid 1</td><td>60</td></tr> <tr><td>Hid 2</td><td>50</td></tr> <tr><td>Hid 3</td><td>40</td></tr> <tr><td>Output</td><td>1</td></tr> </table>		# PEs		Input	102	Hid 1	60	Hid 2	50	Hid 3	40	Output	1	<table border="1"> <tr><td>LCoeff</td><td></td></tr> <tr><td>Momentum</td><td>0.400</td></tr> <tr><td>Trans. Pt.</td><td>10000</td></tr> <tr><td>LCoeff Ratio</td><td>0.500</td></tr> <tr><td>F' Offset</td><td>0.100</td></tr> </table>		LCoeff		Momentum	0.400	Trans. Pt.	10000	LCoeff Ratio	0.500	F' Offset	0.100	<table border="1"> <tr><td>Learn Rule</td><td></td></tr> <tr><td>Delta-Rule</td><td></td></tr> <tr><td>Norm-Cum-Delta</td><td></td></tr> <tr><td>Ext DBD</td><td></td></tr> <tr><td>QuickProp</td><td></td></tr> <tr><td>MaxProp</td><td></td></tr> <tr><td>Delta-Bar-Delta</td><td></td></tr> </table>	Learn Rule		Delta-Rule		Norm-Cum-Delta		Ext DBD		QuickProp		MaxProp		Delta-Bar-Delta		<table border="1"> <tr><td>Transfer</td><td></td></tr> <tr><td>Linear</td><td></td></tr> <tr><td>TanH</td><td></td></tr> <tr><td>Sigmoid</td><td></td></tr> <tr><td>DNNA</td><td></td></tr> <tr><td>Sine</td><td></td></tr> </table>	Transfer		Linear		TanH		Sigmoid		DNNA		Sine	
# PEs																																																					
Input	102																																																				
Hid 1	60																																																				
Hid 2	50																																																				
Hid 3	40																																																				
Output	1																																																				
LCoeff																																																					
Momentum	0.400																																																				
Trans. Pt.	10000																																																				
LCoeff Ratio	0.500																																																				
F' Offset	0.100																																																				
Learn Rule																																																					
Delta-Rule																																																					
Norm-Cum-Delta																																																					
Ext DBD																																																					
QuickProp																																																					
MaxProp																																																					
Delta-Bar-Delta																																																					
Transfer																																																					
Linear																																																					
TanH																																																					
Sigmoid																																																					
DNNA																																																					
Sine																																																					
<input type="checkbox"/> Connect Prior <input type="checkbox"/> Gaussian Init. <input type="checkbox"/> Auto-Assoc. <input type="checkbox"/> Minimal Config. <input type="checkbox"/> Linear Output <input checked="" type="checkbox"/> MinMax Table <input type="checkbox"/> SoftMax Output <input type="checkbox"/> Bipolar Inputs <input checked="" type="checkbox"/> Fast Learning <input type="checkbox"/> Cascade Learn		I/O Files Learn <input type="button" value="Browse..."/> 16 Ply UT (columns and rows) train Recall / Test <input type="button" value="Browse..."/> 16 Ply UT (columns and rows) test.																																																			
<input type="checkbox"/> Logicon PROJECTION NETWORK (TM)																																																					
13 Epoch <input type="button" value="Set Epoch From File"/>		<input type="button" value="OK"/> <input type="button" value="Cancel"/> <input type="button" value="Help"/>																																																			

Figure 4.2.5 Network parameters for the prediction model 1

Prediction Model 2

This neural network consisted of the summation of rows and columns with 50 PE apiece and 4 categorical variables resulting in 106 input PEs. The four categorical type variables included in the input data set are binary numbers existing as 1s or 0s. The first variables discriminate the different support conditions, i.e. unsupported boundary conditions are represented by 0 and clamped conditions are represented by 1. The second categorical variables are for the failure types. Those laminates that failed by crushing within the damage region are represented by 1 while laminates failing at areas other than the damage region are represented by 0. The final categorical is shown below as variables that discriminate the different batches. This neural network architecture consists of three hidden layers with 10 PEs apiece. Other network parameters are the same as shown in Figure 4.2.5.

- A: 0 0
- C: 0 1
- D: 1 1
- CH: 1 0

Prediction Model 3

This model included only the summation of columns and the same categorical type variables as previously stated for a total of 55 input PEs. The architecture was the same as model 2 with three hidden layers containing 10 PEs apiece.

CHAPTER 5

CONCLUSIONS AND RECOMMENDATIONS

5.1 CONCLUSIONS

Neural Network Analysis

- Through the use of neural computing, it appears that a backpropagation algorithm is capable of predicting ultimate compressive strength using the data from an ultrasonic image of a carbon/epoxy laminate subjected to low velocity impact damage. This analysis is applicable to real world situations where the impact energy is unknown and an image of the damage region is easily attainable.
- Some batches had artificial discontinuities accidentally created during manufacturing, the UT data picks up these flaws while the AE signal is distorted. When the neural network is looking at the UT image and it sees the flaws, it is able to make an accurate prediction. Determining if the flaw is artificial or a result of impact damage is irrelevant; the AE data cannot make the distinction thus causing the networks using this data to make false predictions.
- The data that could possibly be outliers in the statistical analysis are accurately predicted on as a result of neural computing. Thus, from this research, neural computing offered more accurate prediction capability than statistical analysis.

Statistical Analysis

- In the compressive load versus impact energy plot, there is a wide variance in the data, especially in the lower impact energy realm. As a result, the prediction intervals are very broad around the best fit polynomial trend. Future data point prediction is therefore not accurate.
- The polynomial trend is the best fit trend for the data in this research. Using the current trend for determining compressive loads at higher impact energies is not advisable. Due to the concave upward parabola representing the trend in the data, specimens impacted at energies greater than 22 ft-lb_f would result in higher compressive loads; this is physically impossible.

- The specimens in batches A and C were constructed poorly containing manufacturing defects. All of the specimens in batch D were impacted with unsupported boundary conditions resulting in greater damage. Many of the specimens that are made from batches A, C and D were determined as outliers in the statistical analysis yet the neural network is able to make predictions on these same data points

Addendum

- The initial goal was to make predictions to within a +/-5% error. For batch CH this was possible. Other batches and associated neural networks had some promising results, while overcoming the differences in material quality between each batch and in some cases different support conditions during impact, the best network that was trained using all the batches made predictions with an average error of 6.25% and a worse case error of 30%.
- Added categorical type variables helped the neural networks converge with more prediction accuracy. However, this may not be required if the different batches had been constructed with similar material properties. Also, the network built using data from the rows, columns, and categorical variables did not predict quite as well as the network built with just columns and categorical variables. The added data from the rows may present a problem causing the network to converge on a false minima from the added variables. More neural network testing is required to validate this hypothesis.
- Acoustic emission data gathered during compression loading was determined to not be used as inputs to the neural network. This research was more concerned with making predictions using the UT image alone.

5.2 RECOMMENDATIONS

- The 8 ply laminates were too thin for this type of compression testing. The Boeing BSS-7260 CAI fixture was designed for much thicker laminates. The 8 ply laminates failed at regions other than the damage zone. Also, the UT

capabilities for the 8 ply were difficult to establish due to the defect echo being very close to the front or back wall of the A-trace in a C-scan. The 16 ply laminates were close to being too thin as well. Some laminates failed during loading at areas other than the damage region. For future testing, it is recommended that thicker laminates be used.

- Even though, there was a large data set of 16 ply laminates, each batch was different. The larger networks trained on the thirteen samples and tested on nine, but the batches that were trained and tested on had very different material qualities. It is recommended that for future testing, during material creation, special attention should be given to creating all laminate batches exactly the same.
- When building the neural networks, it was found that the network architecture and the organization of the input data had the largest effect on the prediction results. Finding the optimal network is a trial and error process using the Neural Works Professional II/Plus software. It was attempted to use the software Predict by NeuralWare which builds the most optimized network architecture based on the data inputted. Presently, the prediction results from this software are worse than those posed by the Professional II/Plus software. It could be possible to find a more accurate prediction network than the architectures presented in this research using the same data. Future research could use the same data and concentrate on finding optimal network architectures.
- The MATLAB algorithm used in this research is very simple in that it sums the rows or columns and normalizes the data. There are likely better ways of quantifying the UT image. Future research could stress this point and find a better measure of the image for the network to make predictions on.

REFERENCES

1. Abrate, Serge, *Impact on Composite Structures*. Cambridge, United Kingdom, 1998, pp. 135-228.
2. Dobyons, A.L. and Porter, T.R., "A Study of the Structural Integrity of Graphite Composite Structure Subjected to Low Velocity Impact," *Polymer Engineering and Science*, Vol. 21, No. 8, 1981, pp. 493-498.
3. ACEE Composite Structure Technology, NASA Conference Publication (CP) 2321, 1984.
4. Liu, Dahsin, "Impact-Induced Delamination – A View of Bending Stiffness Mismatching," *Journal of Composite Materials*, Vol. 22, 1988, pp. 674-692.
5. Cartz, Louis, *Nondestructive Testing*, ASM International, Materials Park, OH, 1995, pp. 81-125.
6. Pollock, Adrian A., "Acoustic Emission Inspection," *Metals Handbook*, 9th Edition, Vol. 17, ASM International, 1989, pp. 278-294.
7. Shull, Peter, Editor, *Nondestructive Evaluation: Theory, Techniques, and Applications*, 2002, New York, NY. pp. 369-444.
8. Fisher, M.E. and Hill, E. v. K., "Burst Pressure Prediction of Filament Wound Composite Pressure Vessels Using Acoustic Emission," *Materials Evaluation*, Vol. 56, No. 12, 1998, pp.1395-1401.
9. Ely, Thomas M. and Hill, E. v. K., "Failure Mechanism Characterization in Graphite/Epoxy Using Acoustic Emission Data," ASNT 1995 Spring Conference, American Society of Nondestructive Testing, Columbus, OH, 1995, pp. 109-111.
10. Fatzinger, Edward. C. and Hill E. v. K., "Low Proof Load Prediction of Ultimate Strengths of Fiberglass/Epoxy I-Beams Using Acoustic Emission," MSAE Thesis, Embry-Riddle Aeronautical University, 2001, Daytona Beach, FL.
11. Hill, Eric v. K., Walker, J. L., and Rowel, G., "Burst Pressure Prediction in Graphite/Epoxy Pressure Vessels Using Neural Networks and Acoustic Emission Amplitude Data," *Materials Evaluation*, Vol. 54, No. 6, 1996, pp. 748-754.
12. Lansing, M. O., Walker, J. L., and Russell, S. S., "Residual Strength Prediction of Impact-Damaged Composite Structures by Optical and

Acoustical Computer Sensing with Neural Network Techniques,”
Composite Materials: Fatigue and Fracture, Seventh Volume, ASTM STP 1330, R. B. Bucinell (ed), American Society for Testing and Materials, Conshohocken, PA, 1998, pp. 285-297.

13. Dost, E. F., Ilcewicz, L. B, Avery, W. B. and Coxon, B. R., “Effects of Stacking Sequence on Impact Damage Resistance and Residual Strength for Quasi-Isotropic Laminates,” T.K. O’Brien (ed.), *Composite Materials: Fatigue and Fracture, Third Volume, ASTM STP 1110*, American Society for Testing Materials, Philadelphia, PA, 1991, pp. 476-500.
14. Prichard, J. C., and Hogg, P. J., “The Role of Impact Damage in Post Impact Compression Testing,” *Composites*, Vol. 21, No. 6, 1990, pp. 503-511.
15. Standard Tests for Toughened Resin Composites. NASA Reference Publication (RP) 1092. 1982. pp. 1-5.

BIBLIOGRAPHY

1. Physical Acoustics Corporation, ULTRAPAC II Users' Manual, Revision 2, Princeton, NJ, 1992.
2. Physical Acoustics Corporation, DiSP User's Manual, Revision 1, Princeton NJ, 2001.
3. Reic, S. R., and Zhou, G., *Impact Behavior of Fiber-Reinforced Composite Materials and Structures*, Boca Raton, FL, 2000.
4. Hoshin, Brian C., and Baker, Alan A., *Composite Materials for Aircraft Structures*. New York, NY, American Institute of Aeronautics and Astronautics, 1986.
5. Sjoblom, Peter O. and Hartness, J. Timothy. "On Low-Velocity Impact Testing of Composite Materials," *Journal of Composite Materials*, Vol. 22, 1988, pp. 30-52.
6. Chong, Edwin K.P. and Żak, Stanislaw H., *An Introduction to Optimization*, 2nd Edition, New York, N.Y. 2001.
7. Miller, R.K. and McIntire, Paul, Editors, *Nondestructive Testing Handbook, Volume 5 of Acoustic Emission Testing*, Second Edition. American Society for Nondestructive Testing (ASNT), 1987.

APPENDIX A
AS4/3501-5A PRODUCT DATA SHEET

**HERCULES CARBON PREPREG TAPE
AS4/3501-5A**

HERCULES® AS4/3501-5A carbon prepreg tape is an amine-cured epoxy resin reinforced with unidirectional carbon fibers. The reinforcements are Hercules continuous Type AS4 carbon filaments, surface-treated to increase the composite shear and transverse tensile strength. Hercules 3501-5A resin was developed to operate in temperature environments of 350°F (177°C). AS4/3501-5A prepreg is recommended for general-purpose structural applications.

<u>Typical Composite Properties</u>	<u>U.S. Units</u>	<u>SI Units</u>
0° Tensile strength at 77° F (25° C)	310,000 psi	2, 139 MPa
0° Tensile modulus at 77°F	21.5 x 10 ⁶ psi	169 GPa
0° Compression strength at 77°F	240,000 psi	1,656 MPa
0° Flexural strength		
At 77° F	250,000 psi	1,725 MPa
At 350° F (177° C)	175,000 psi	1,208 MPa
0° Flexural modulus		
At 77°F	19.5 x 10 ⁶ psi	135 GPa
At 350°F	18.5 x10 ⁶ psi	128 GPa
Short-beam shear strength		
At 77°F	18,500 psi	128 MPa
At 350° F	9,500 psi	66 MPa
Fiber volume	62%	62%
Cured-ply thickness	5.2 mils	0.13 mm

<u>Typical Prepreg Characteristics</u>		
Fiber area weight	4.4 oz/yd ²	150 g/m ²
Standard width	12 in.	30.5 cm
Approximate yield		
At 42% resin content	18.8 ft/lb	12.6 m/kg
At 35% resin content	21.2 ft/lb	14.2 m/kg
Gel time at 350°F (177°C)	3-7 minutes	3-7 minutes
Volatile content, % by weight	1% max	1% max
Out time at room temperature	10 days min	10 days min
Shelf life at 0°F (-18°C)	12 months	12 months

Suggested Cure Cycle

1. Pull 20-in. (508-mm) minimum vacuum on the part. .
2. Place the part in the autoclave
3. Raise the temperature to 225°F (107.2°C) in 45 to 75 min.
4. Pressurize the autoclave to 85 +/- 5 psi (59.8 +/- 3.5 g/mm²).
5. Hold at 225°F (107.2°C), 85 psi, and vacuum on the part for 50 to 60 min
6. Raise the temperature to 350°F (176.7°C) in 45 to 75 min. Hold for 60 min.
7. Cool the part to 150°F (65.5°C) in not less than 45 min. Maintain the pressure and vacuum.
8. Remove the part from the autoclave
9. Post cure it at 370°F (187.8°C) for 3 hrs. (This is recommended to develop optimum properties at 350°F)

Handling and Storage

Composite properties may be degraded if the prepreg is contaminated by incompatible materials such as grease, dust, and dirt. Prepreg tape can be held at room temperature for short periods of time. Before placing the prepreg in low-temperature storage, put it in a clean polyethylene bag and heat-seal the edges. When removing it from low temperature storage, do not bend or twist it. Allow the bag and prepreg to warm to room temperature before opening them; this prevents fiber breakage and moisture contamination.

APPENDIX B
MATLAB IMAGE ASSESSING M-FILE

```

%-----
% To run this file type: readImage filename.type
% Currently, this file has only been tested on bitmap files
%
%-----
%Revision Date: March 7, 2003
%Revised by: Levavie Indieka
%Revision 2 Date: April 15, 2003
%Revised by: Christopher Hess (added the row summation variable)
%-----
%-----
function readImage(aa)

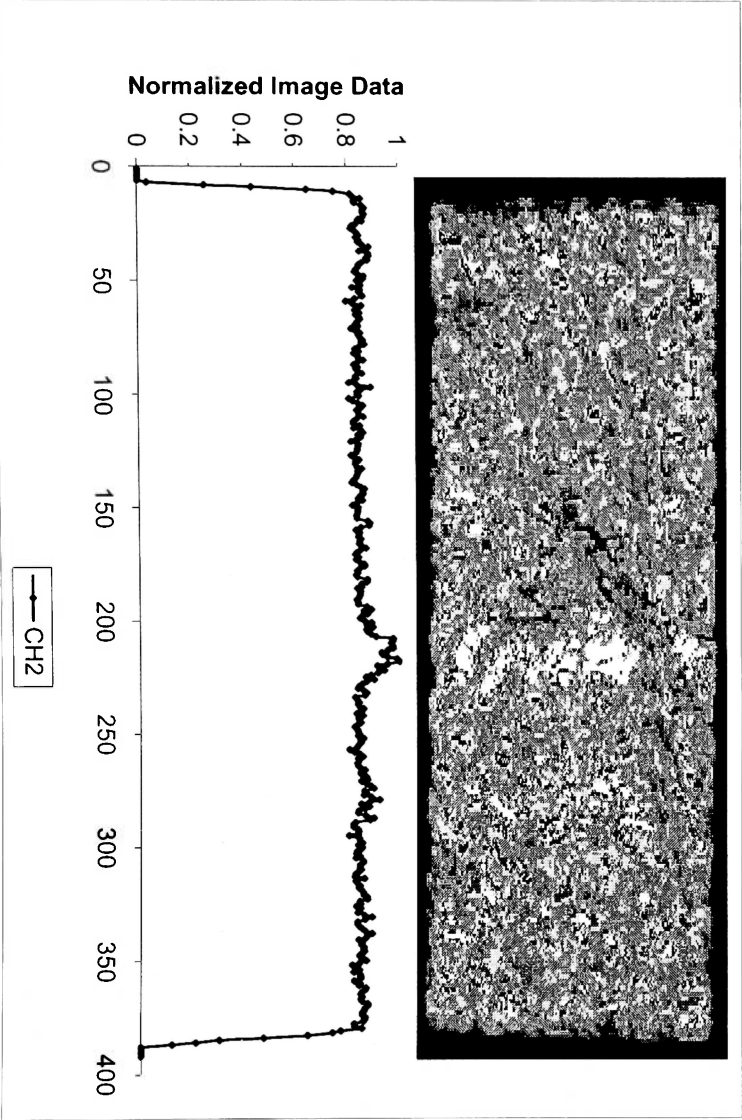
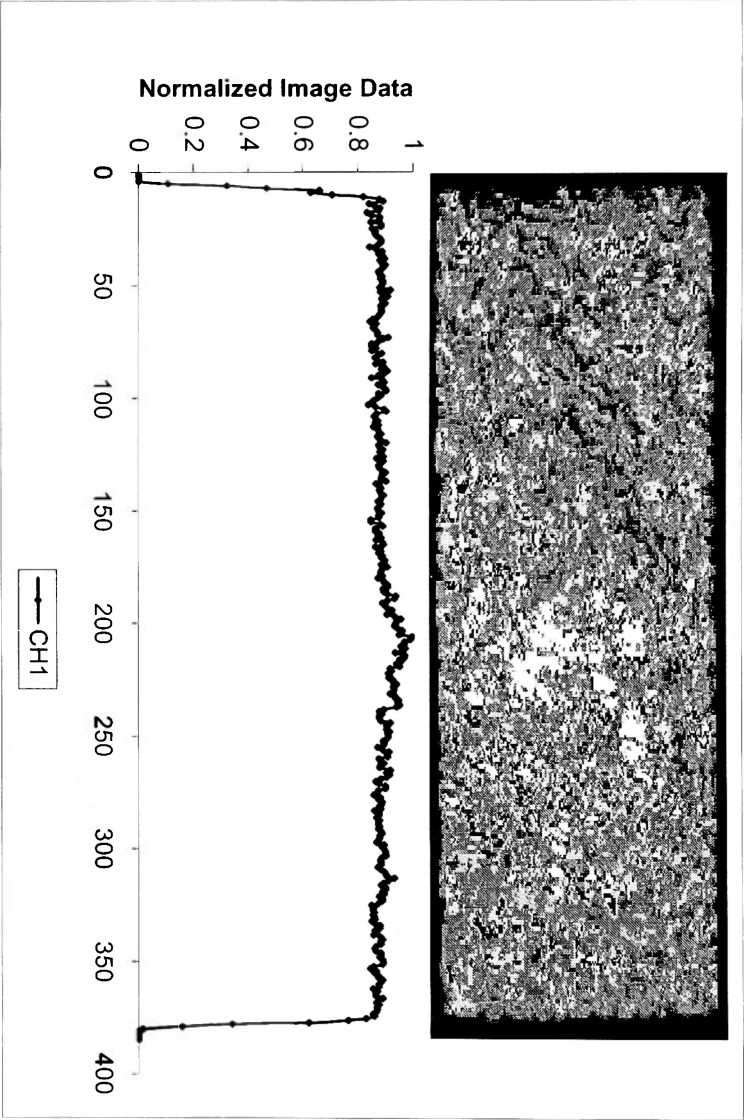
% This reads the image file into the matrix 'B' and stores the associated
% colormap in the matrix 'map_b'
[B,map_b] = imread(aa);

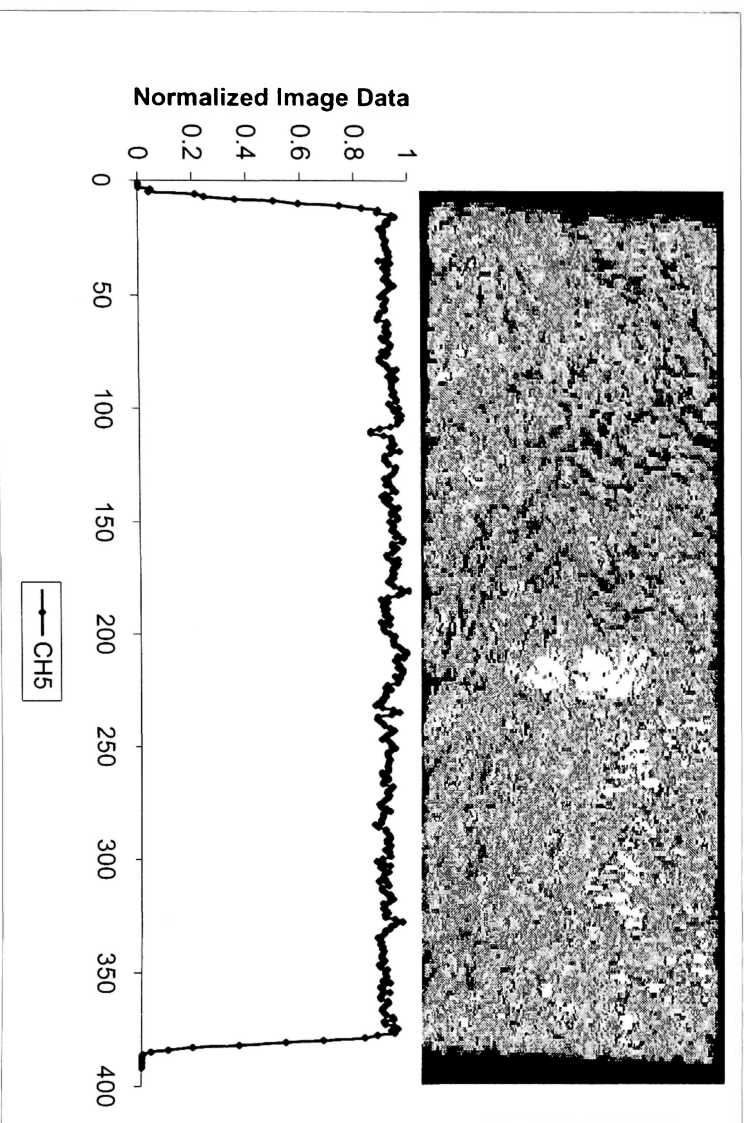
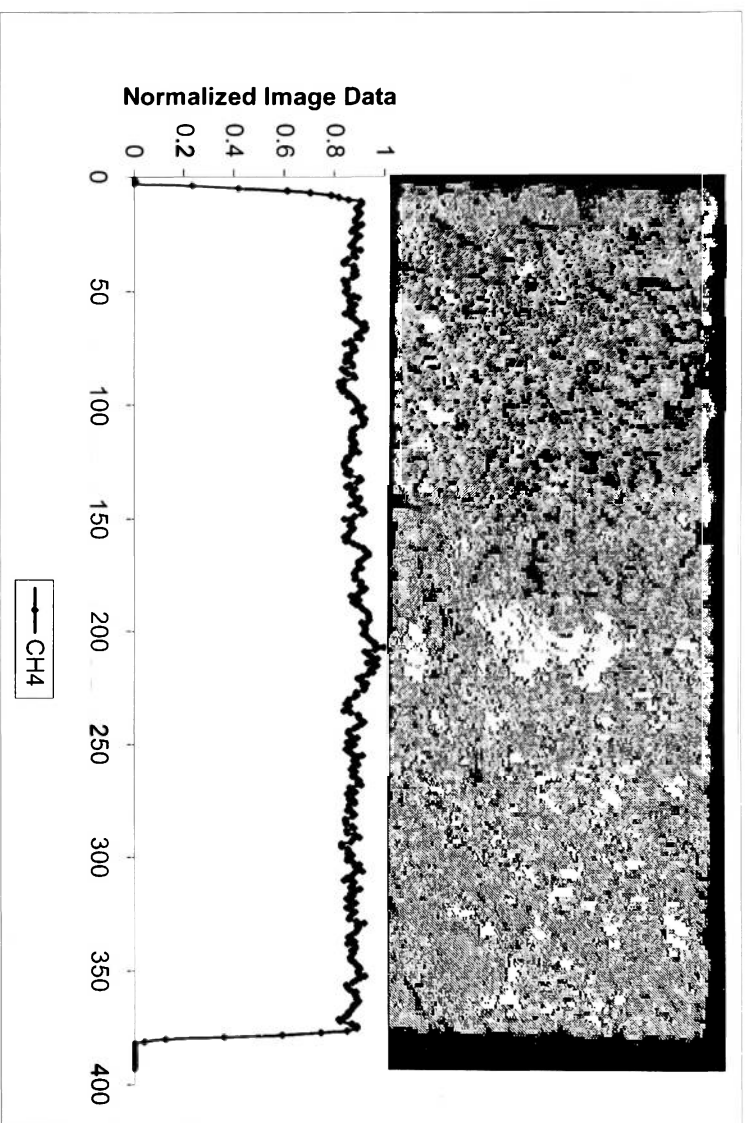
% This sums up the columnar or row elements of the array and then takes the
% transpose
cr = sum(B); %Take away or add (%) to sum the rows or columns accordingly
ccrr = cr';
%scr = sum(B,2); %Take away or add (%) to sum the rows or columns accordingly
%ccrr = cr;
% Gets the number of rows 'm' and columns 'n'
[m,n]=size(ccrr);
% Finds the maximum value in the matrix
g = max(ccrr);
% Normalizes the matrix
gg = ccrr/g;
% Plotting data
% Format
% - first image is the image file
% - second image is a scatter graph of sum of the columns
subplot(2,1,1); image(B)
title('Image of the Test Specimen')
subplot(2,1,2); plot(gg)
title('Scatter Plot of the Sum of Colours in each Column')
xlabel('Columns')
ylabel('Summed and Normalized Columns')

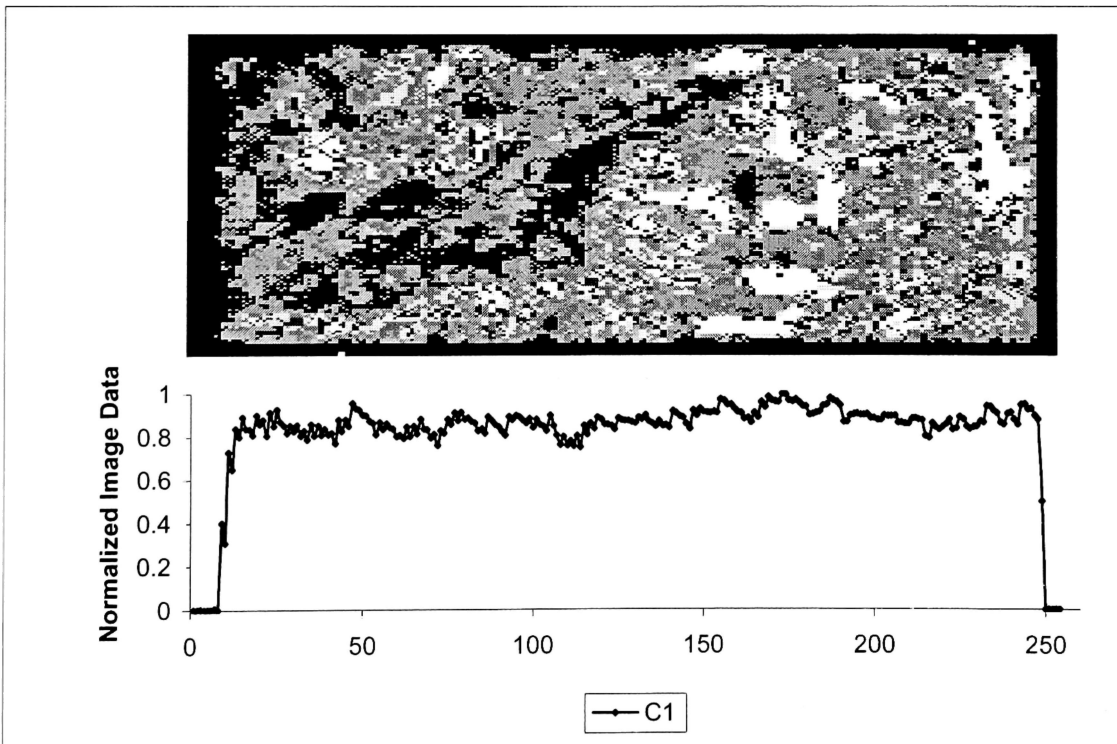
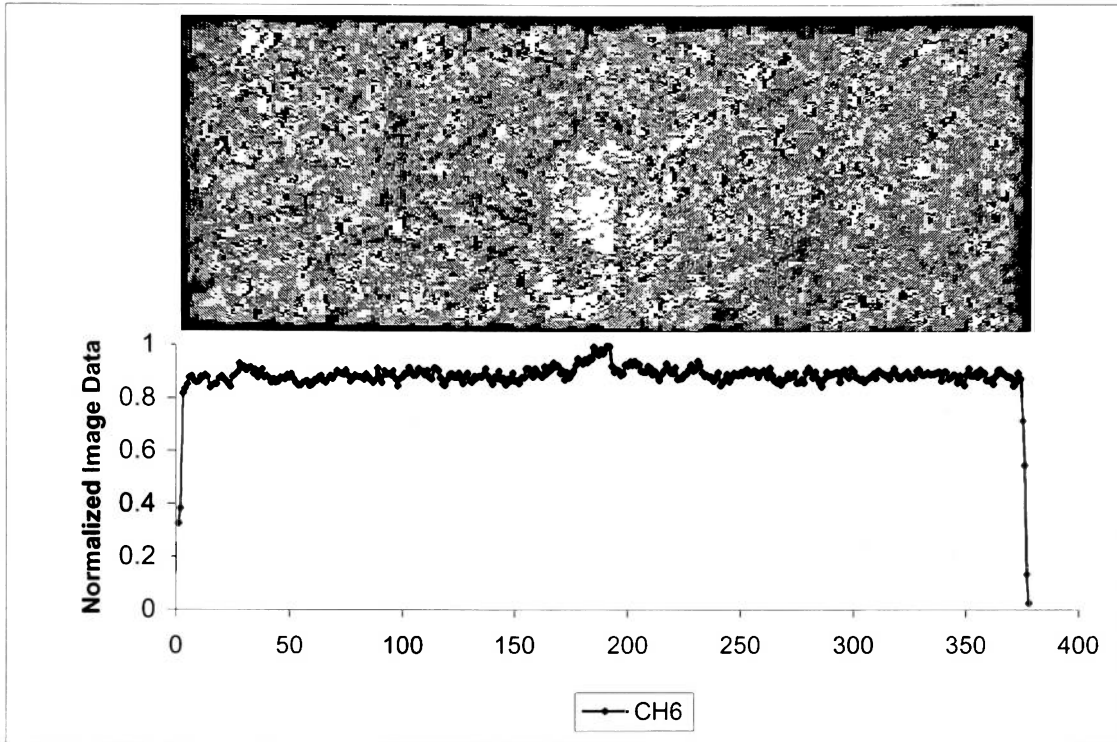
% Writes to a text file
dlmwrite('imageOut.txt', gg , ' ');

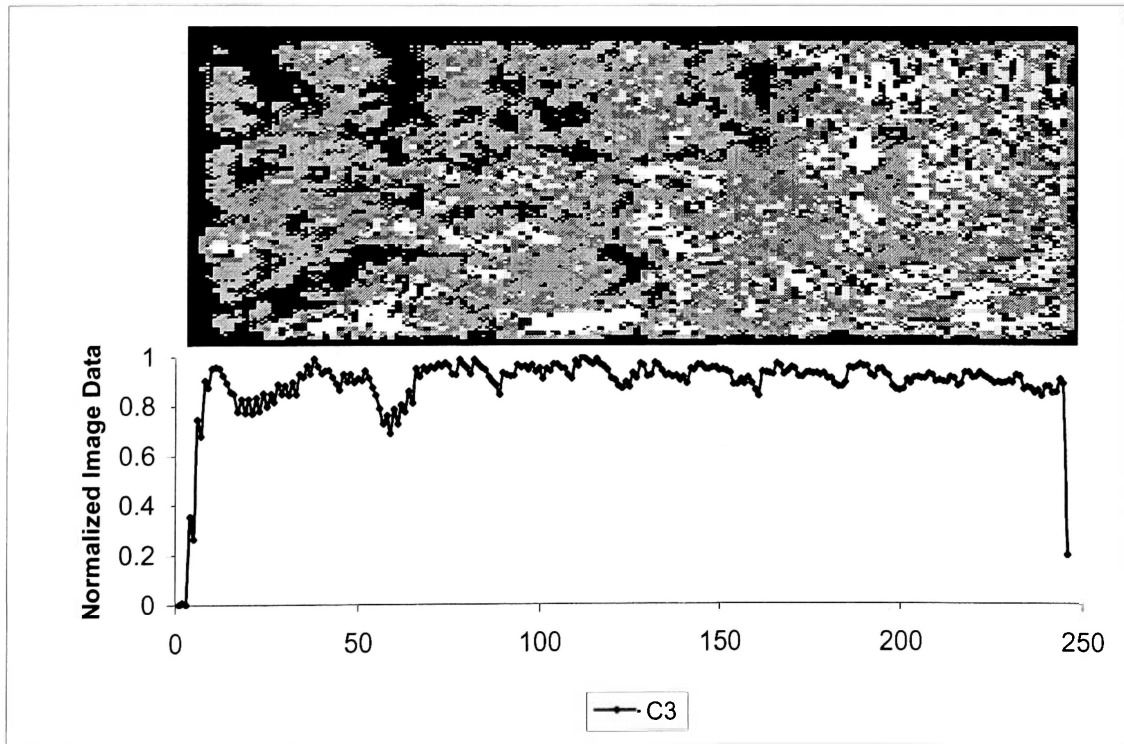
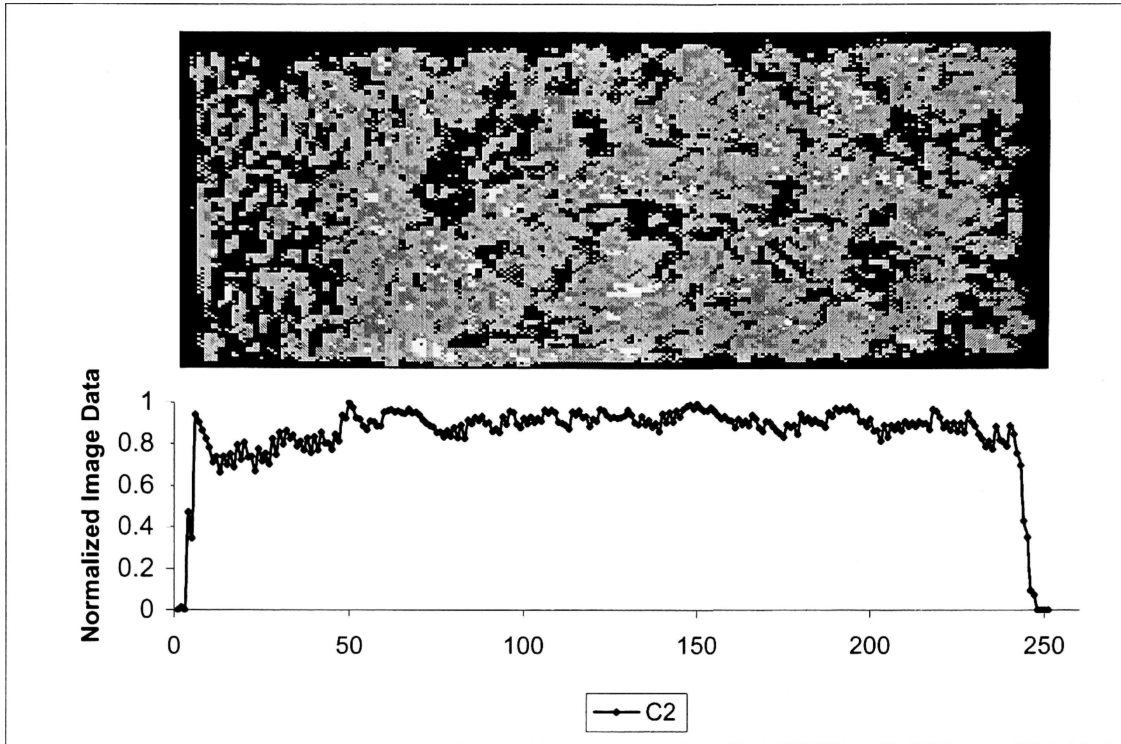
```

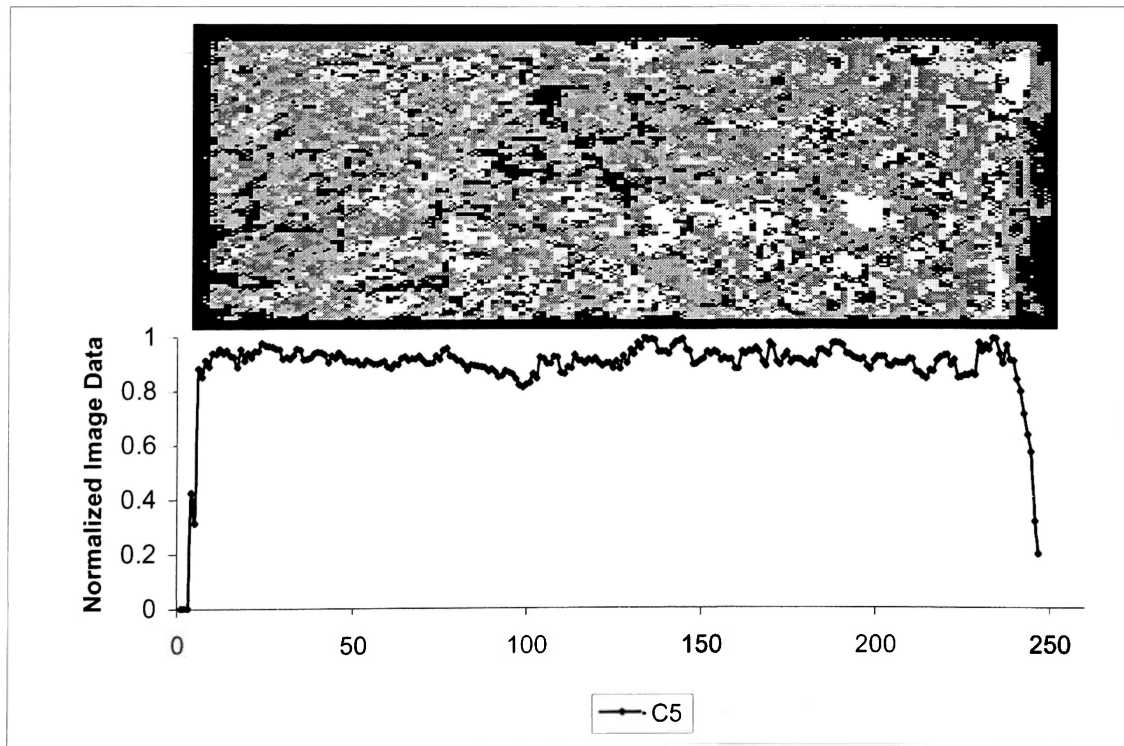
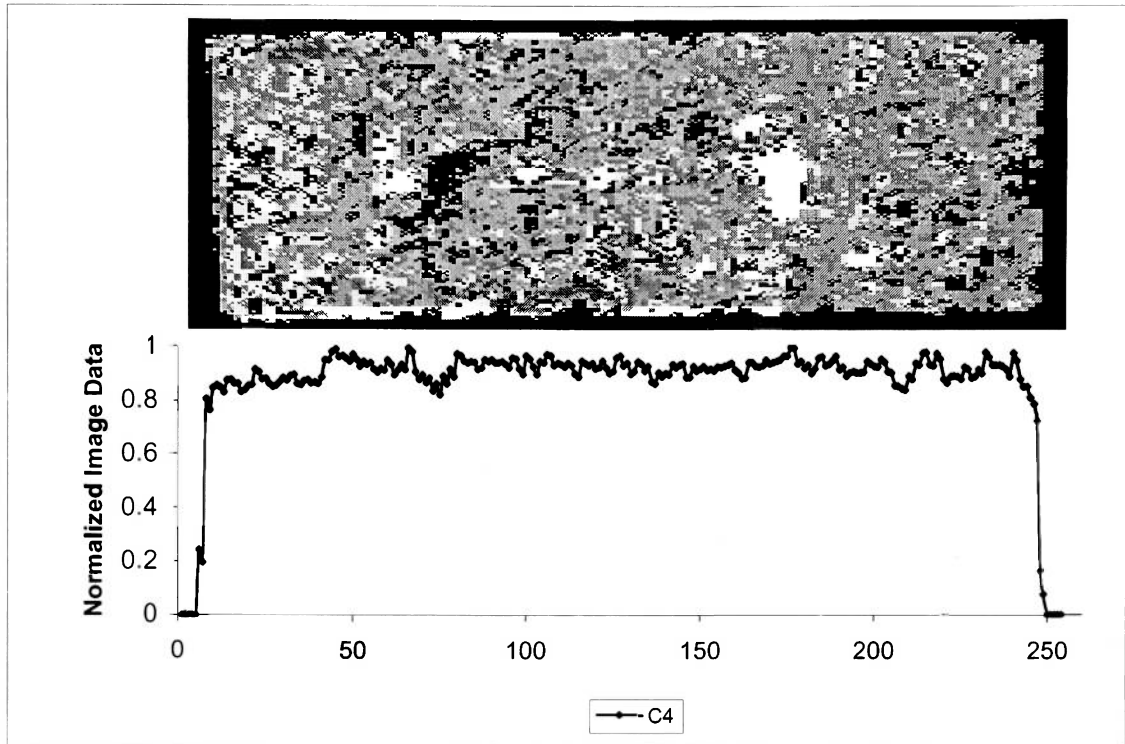
APPENDIX C
MATLAB IMAGE ASSESSMENT

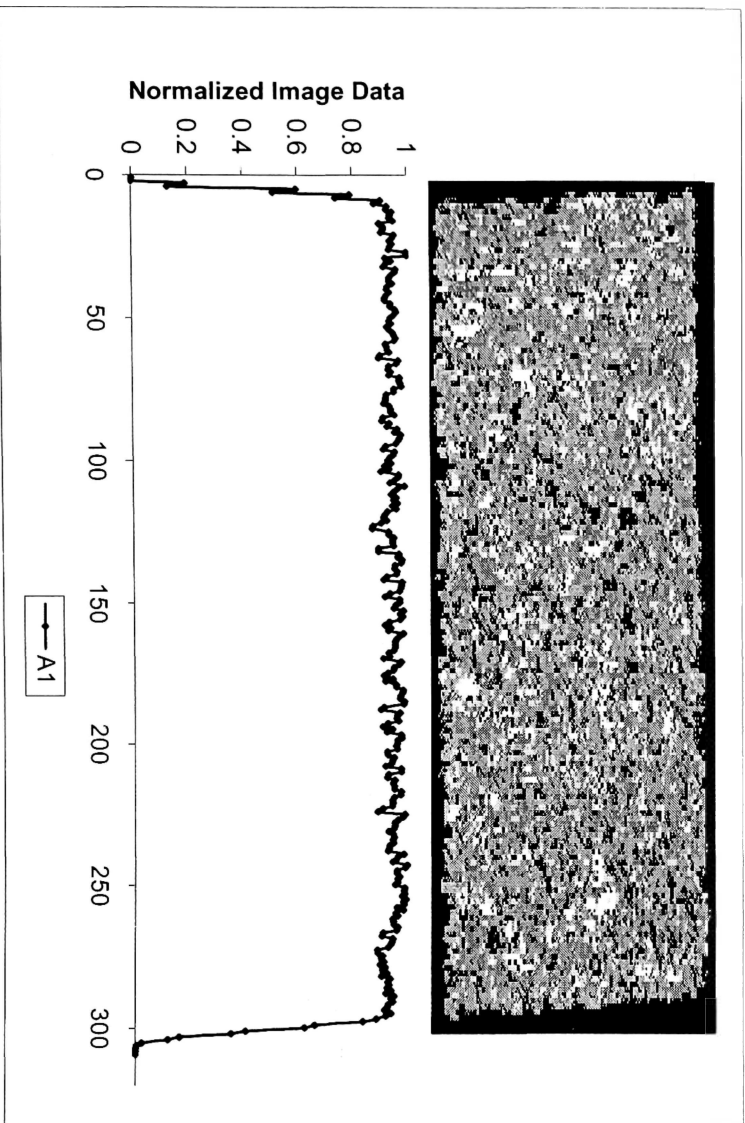
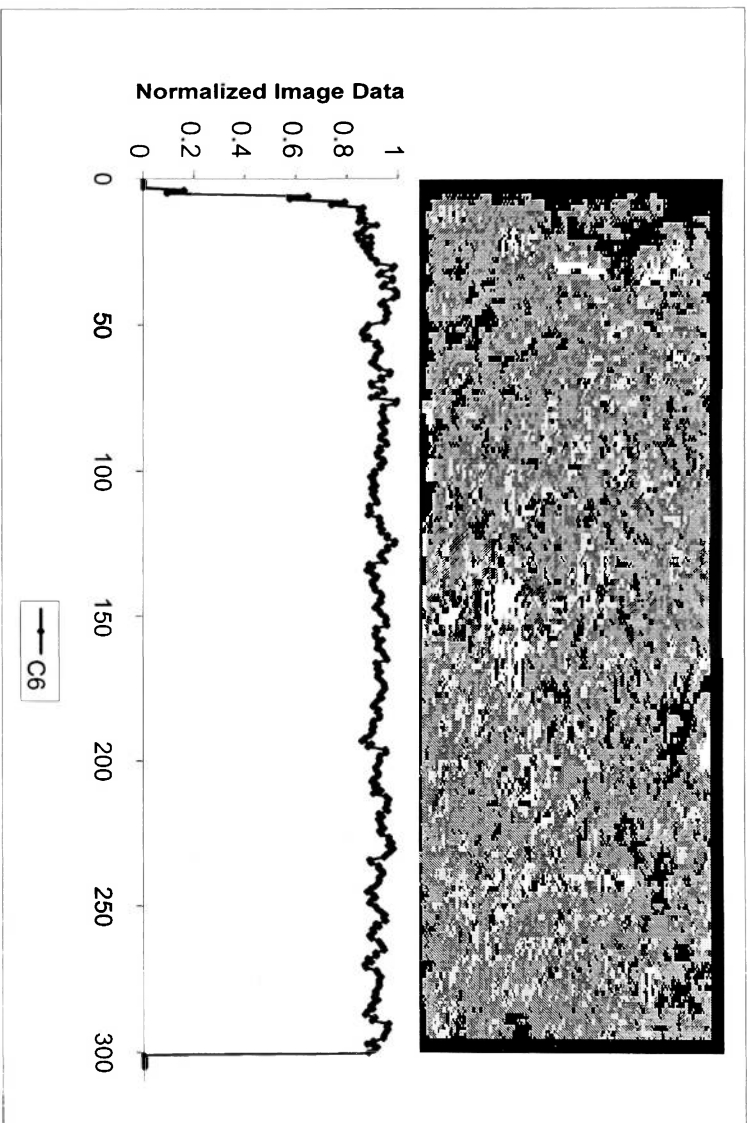


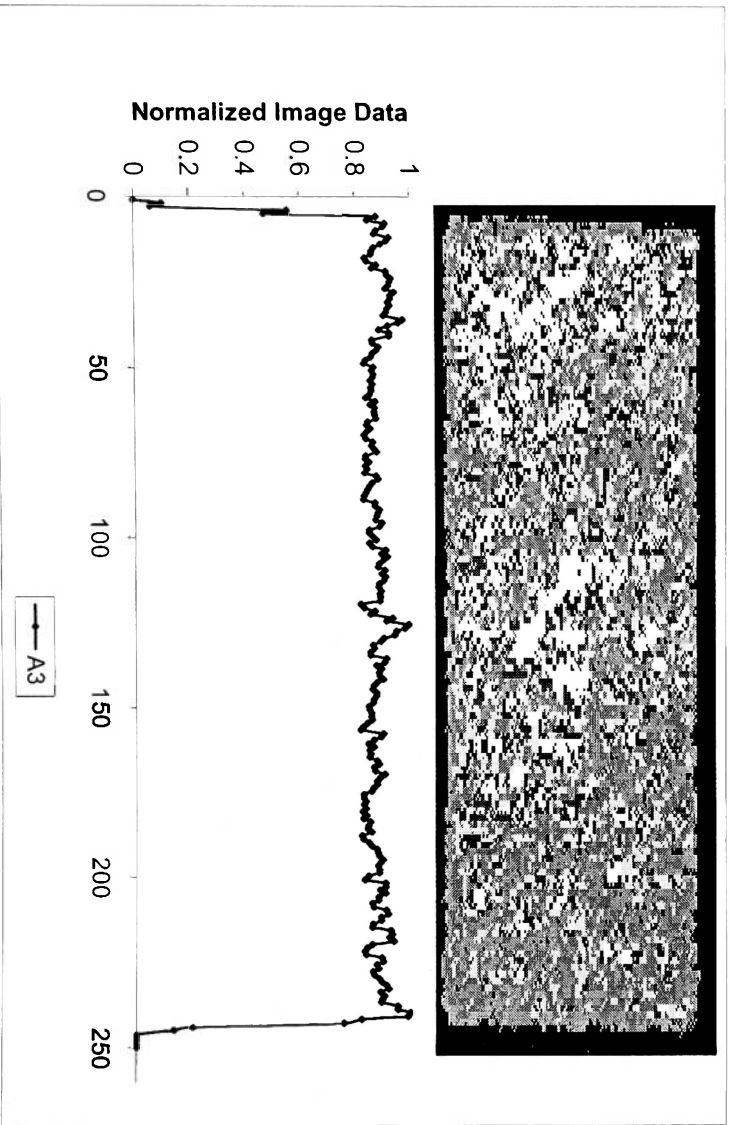
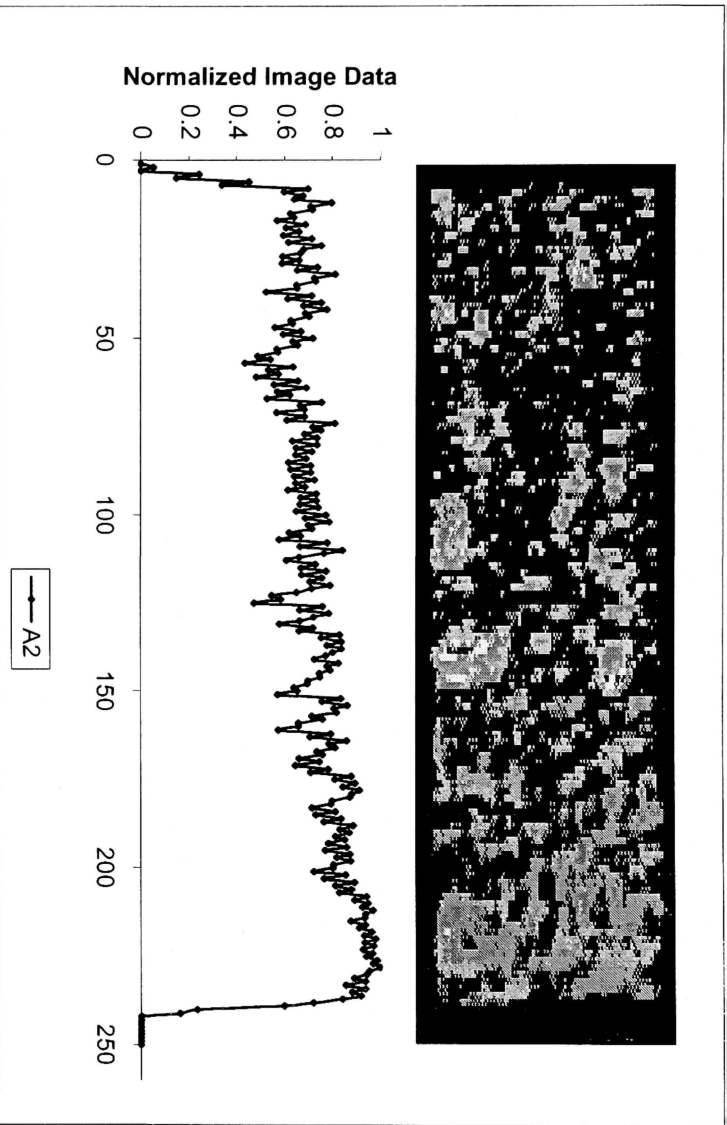


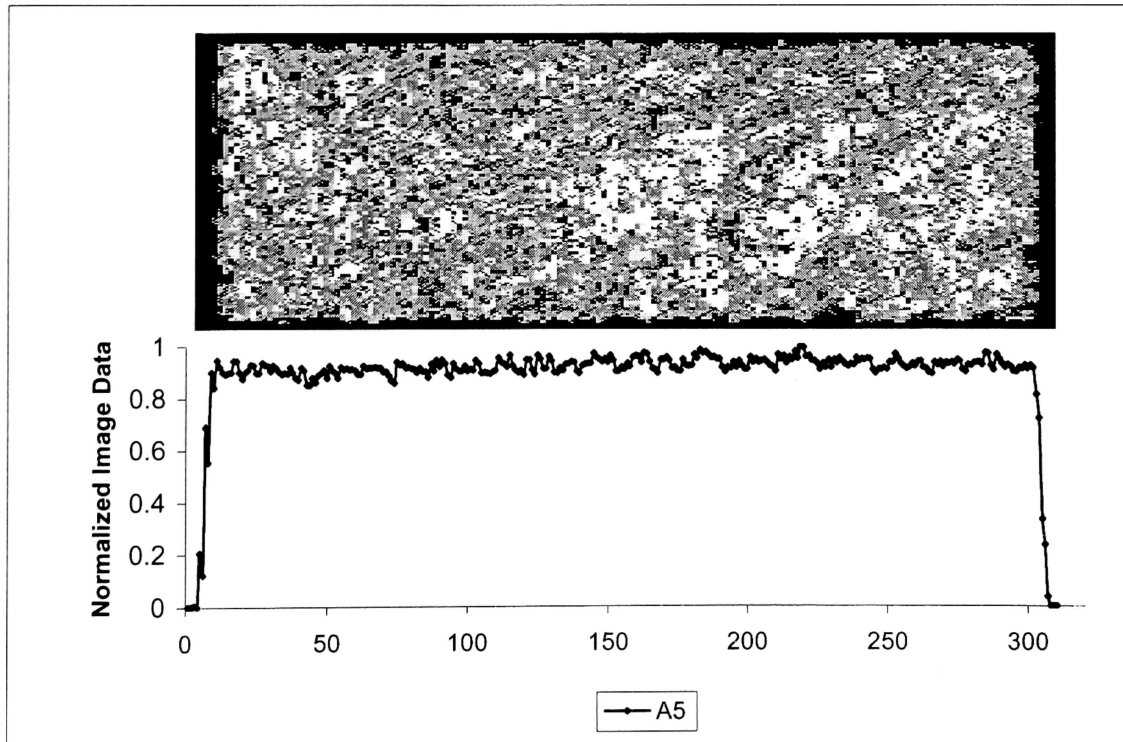
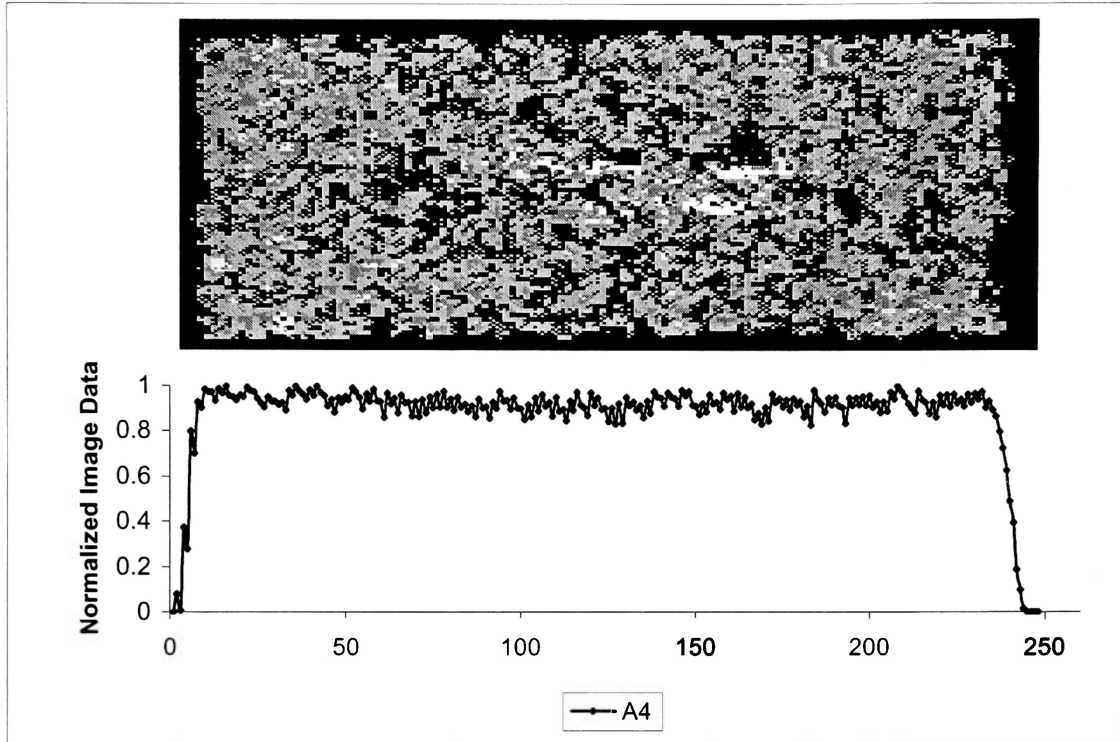


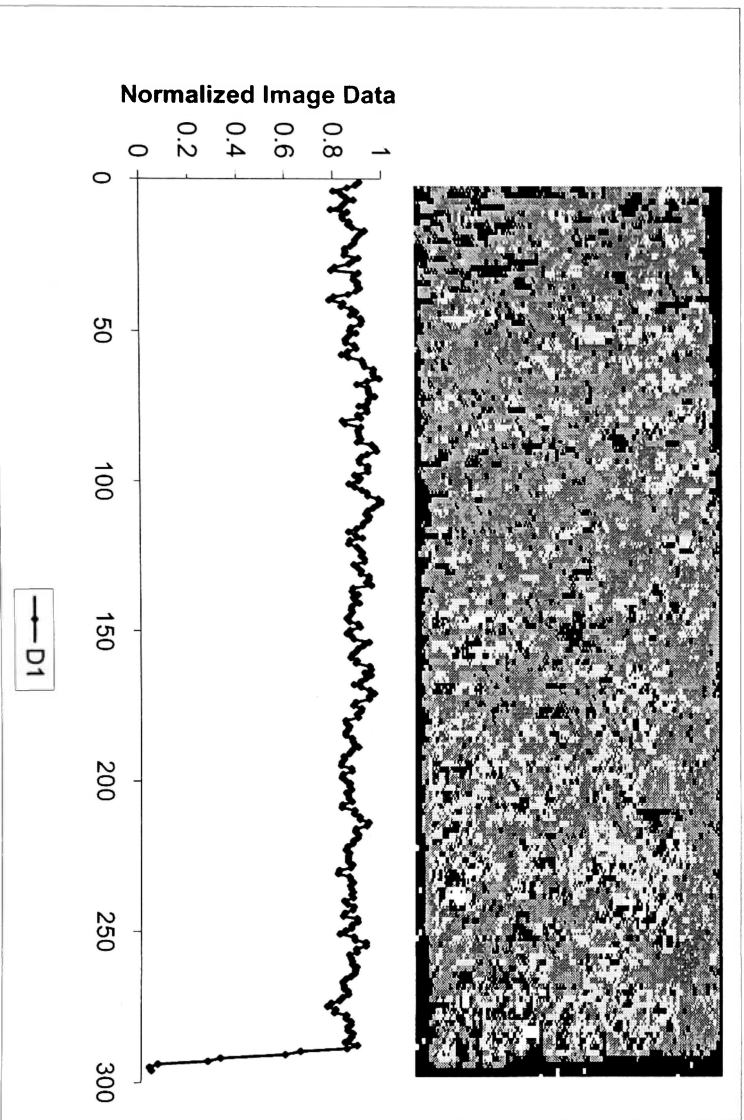
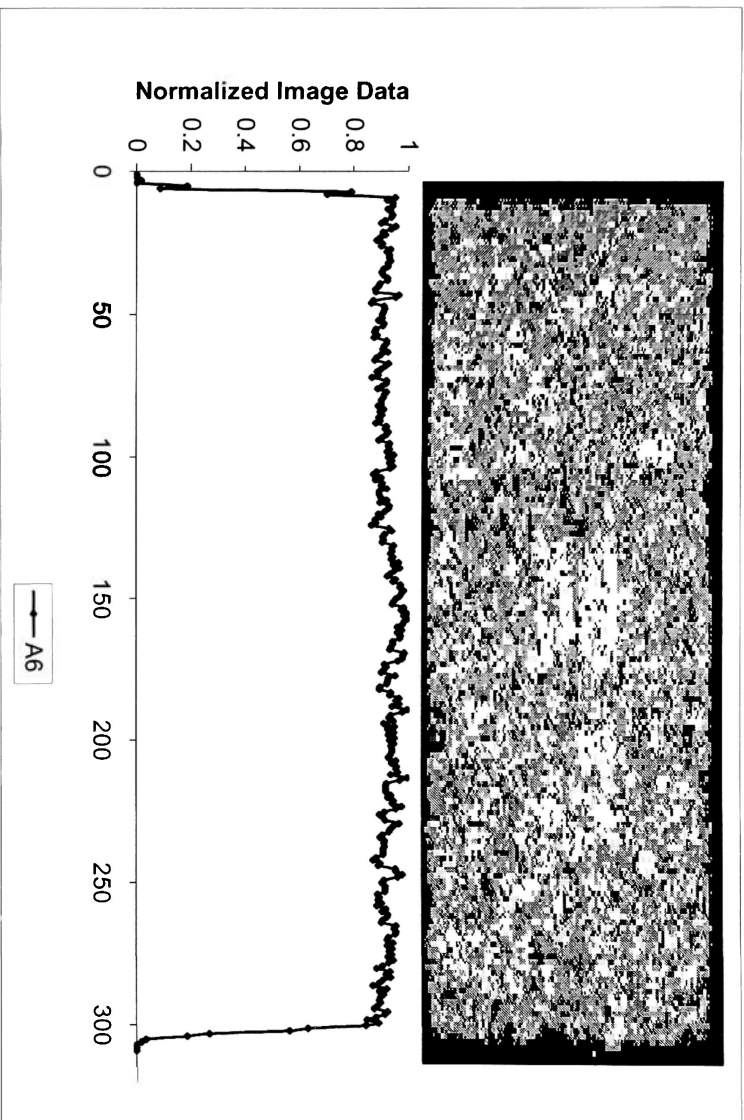


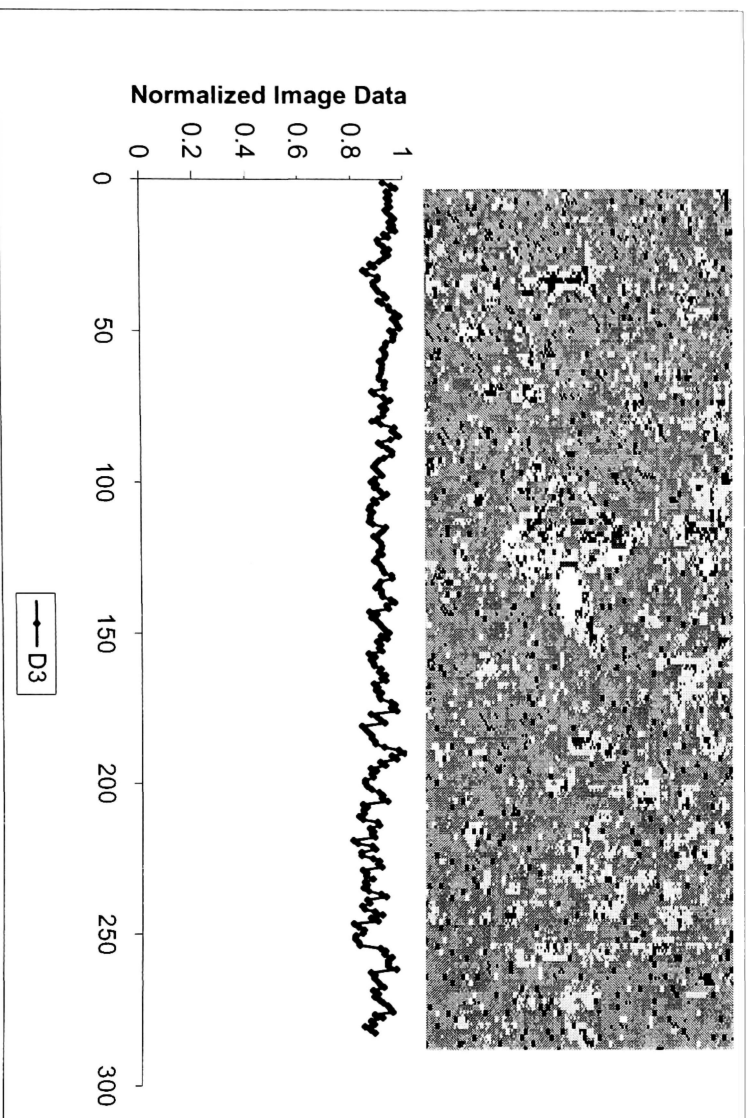
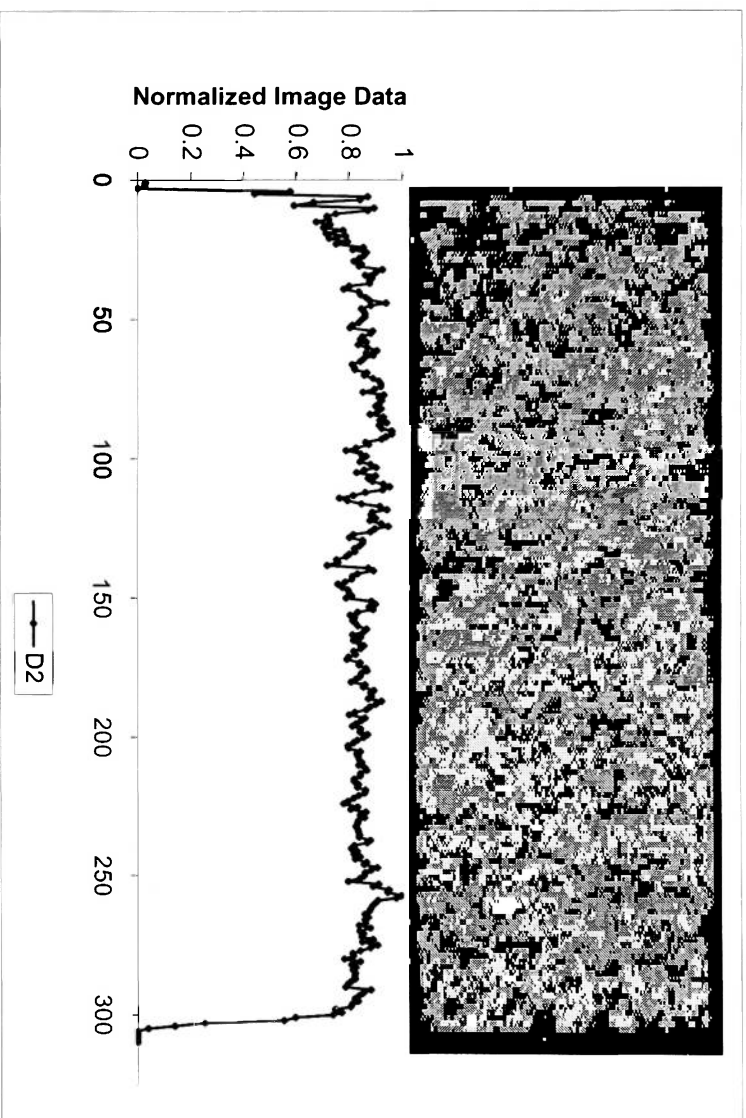


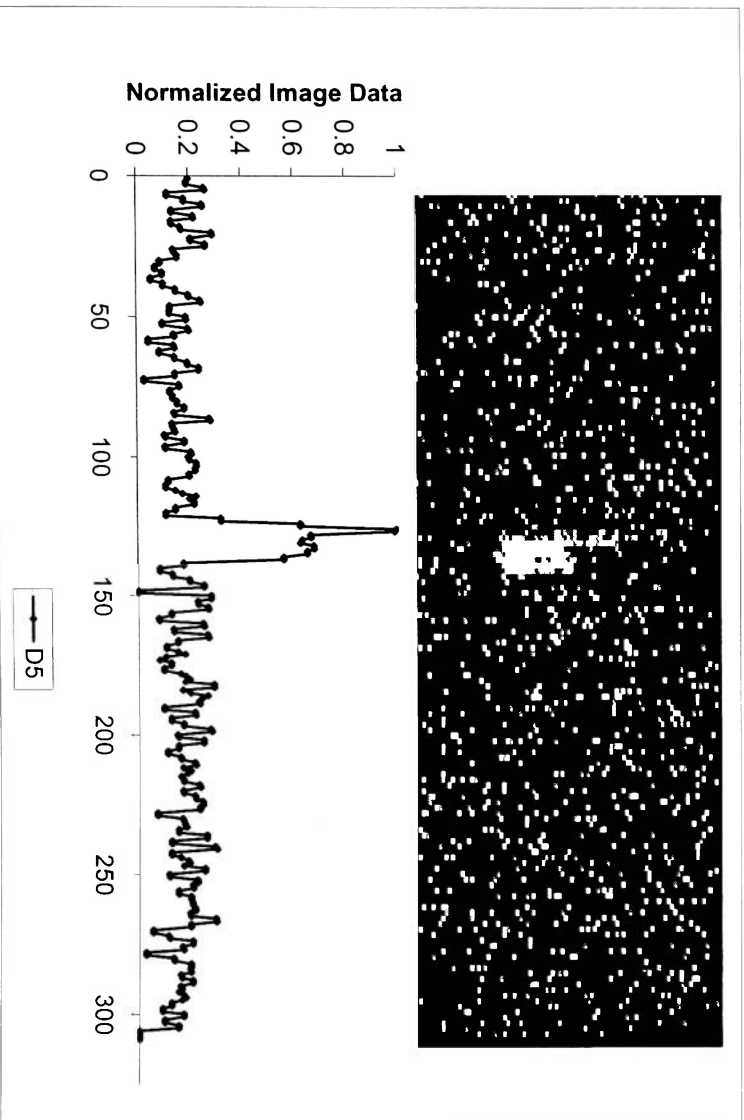
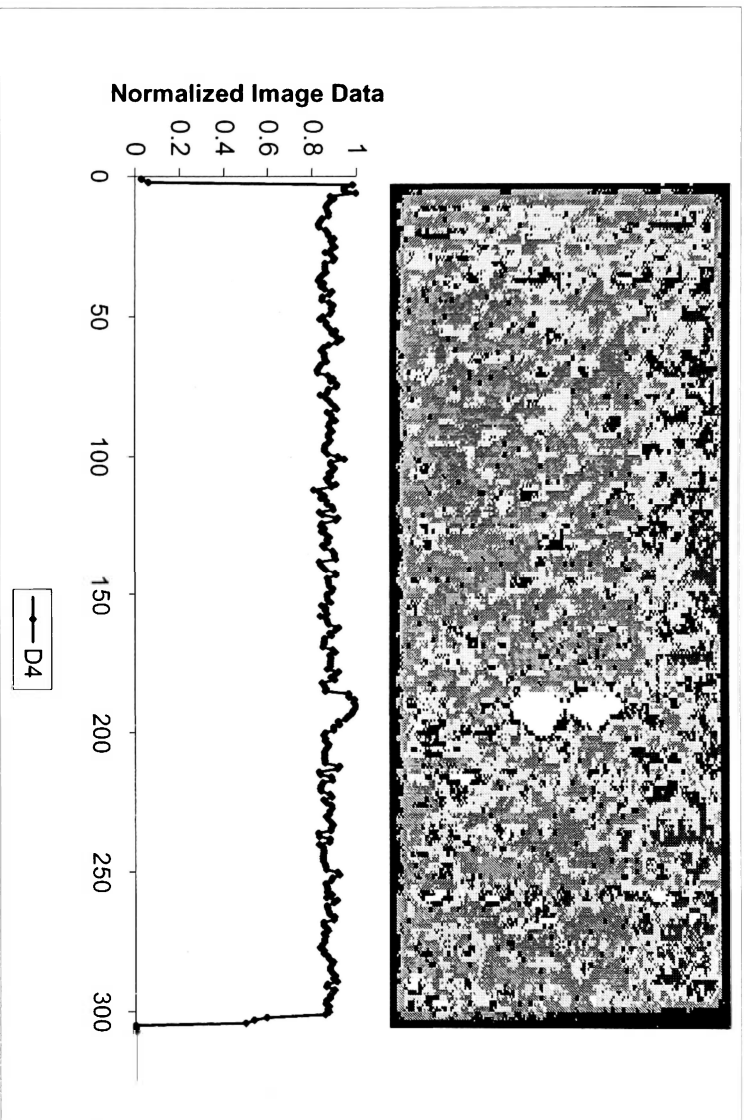


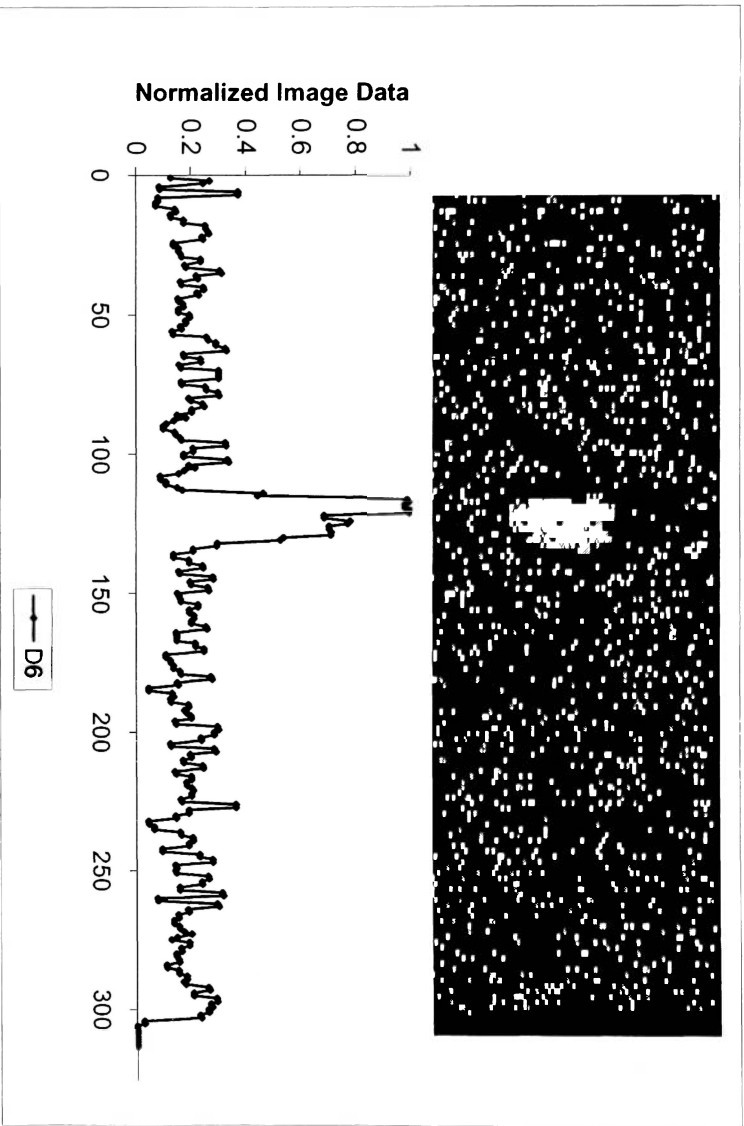




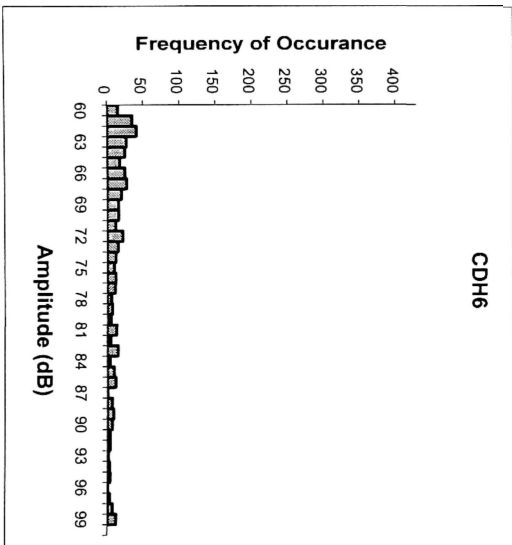
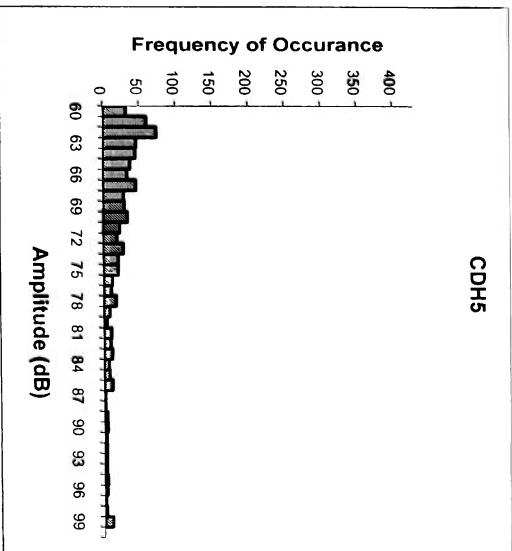
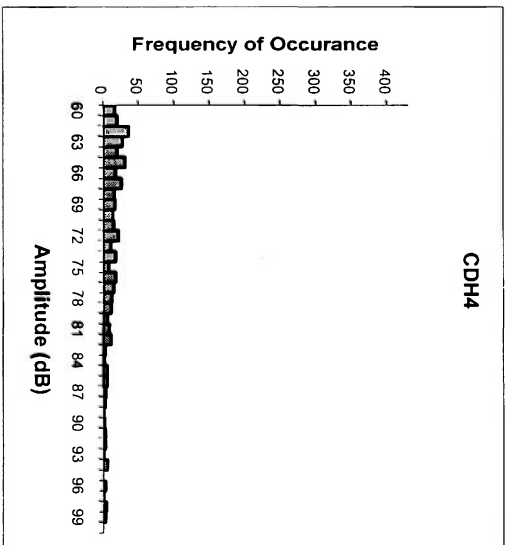
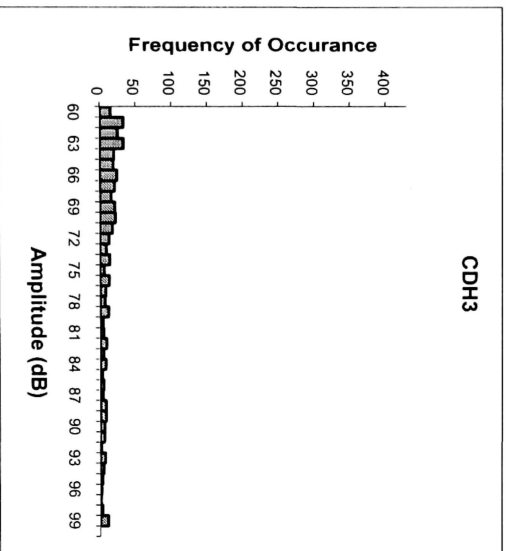
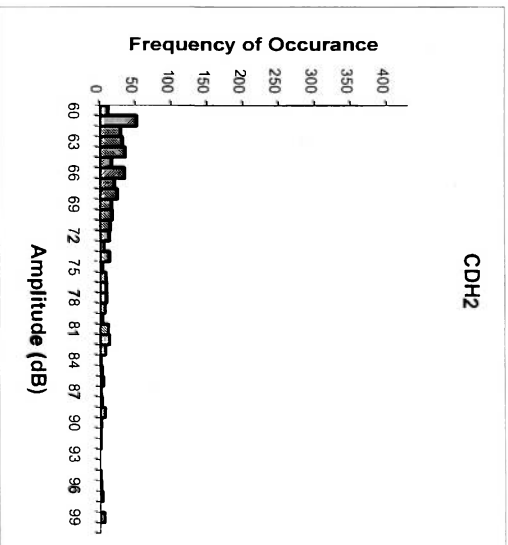
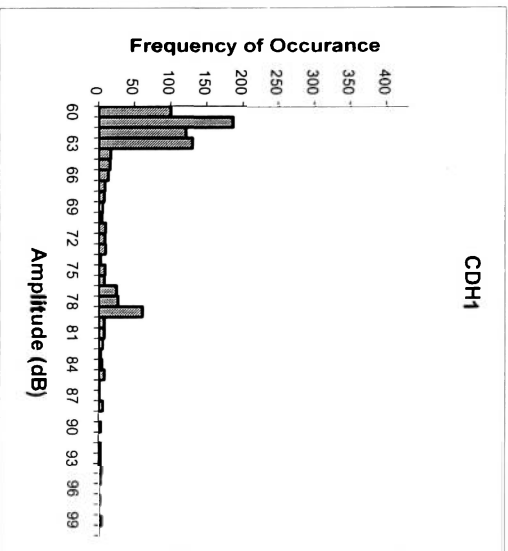


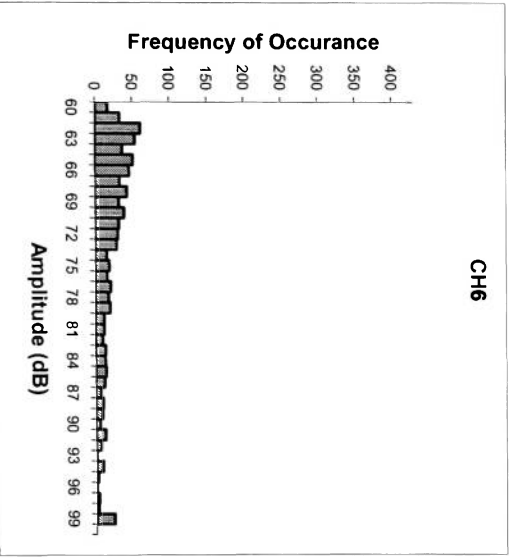
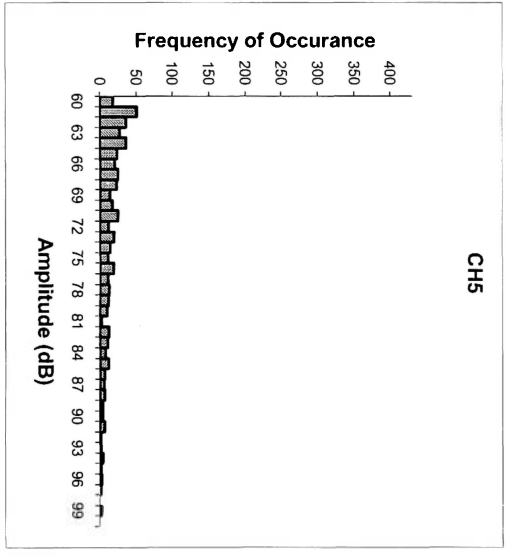
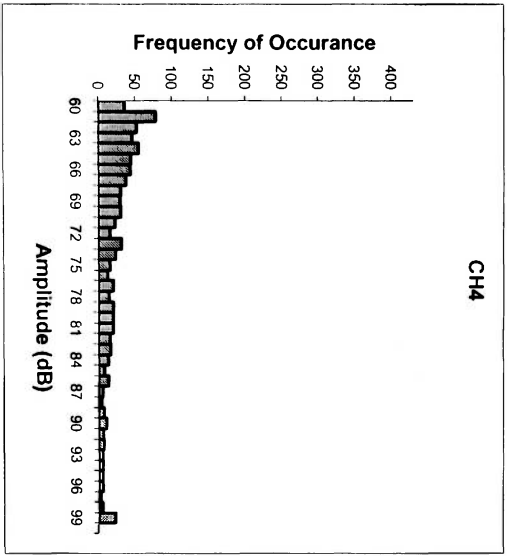
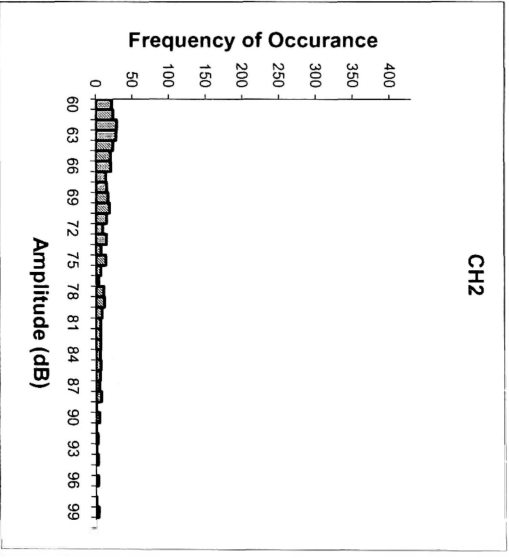
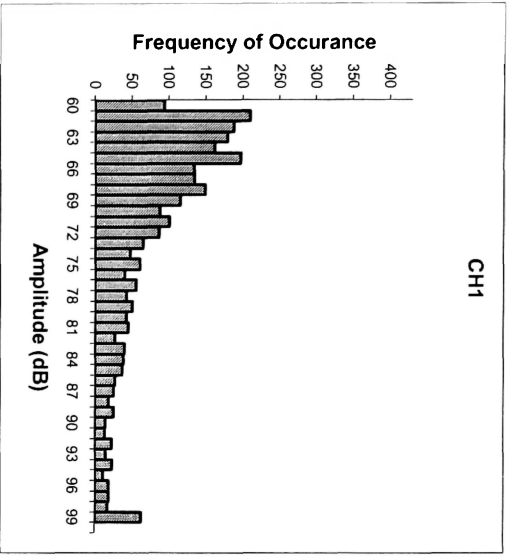


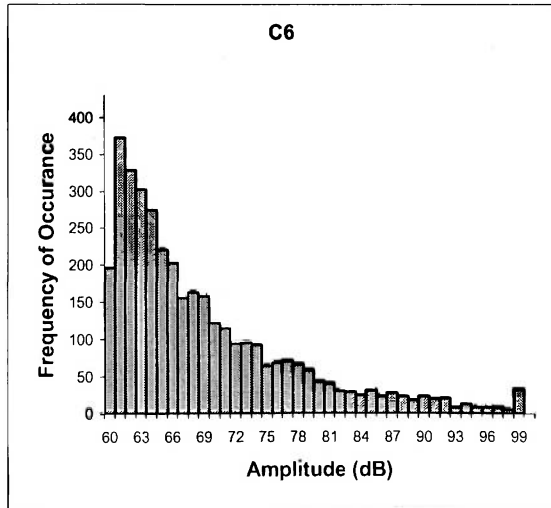
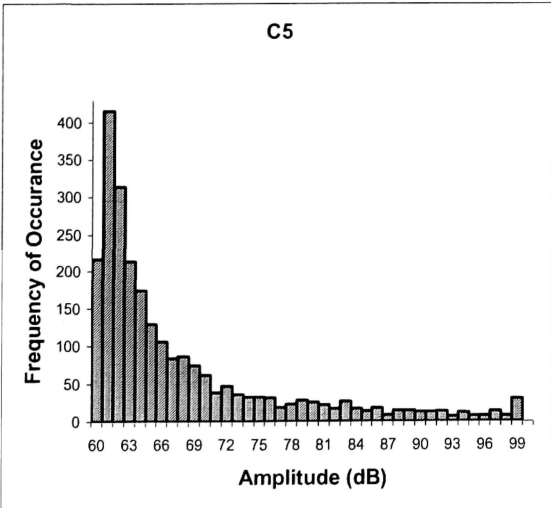
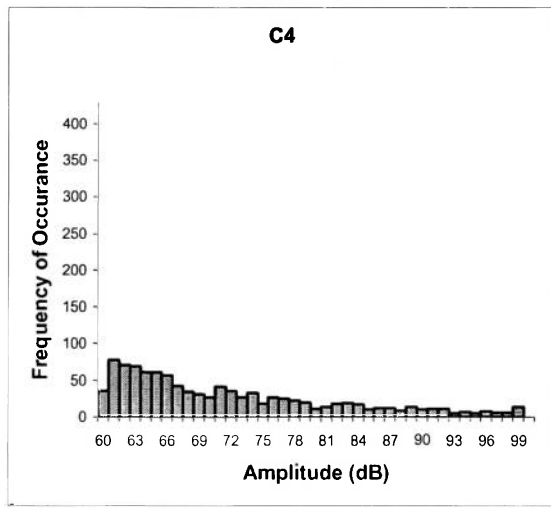
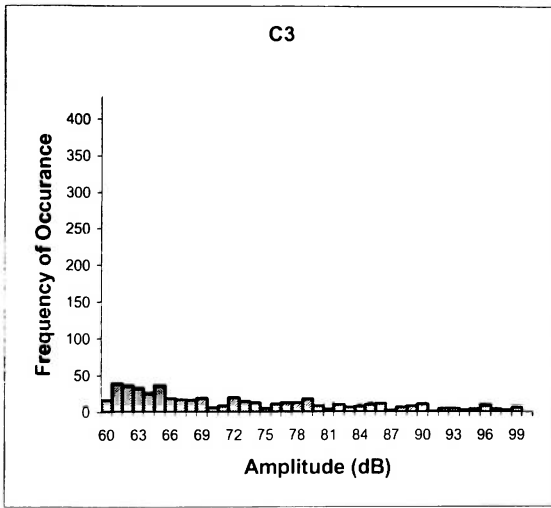
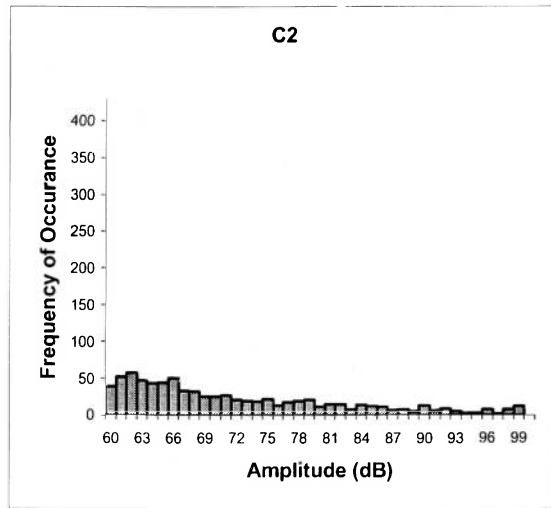
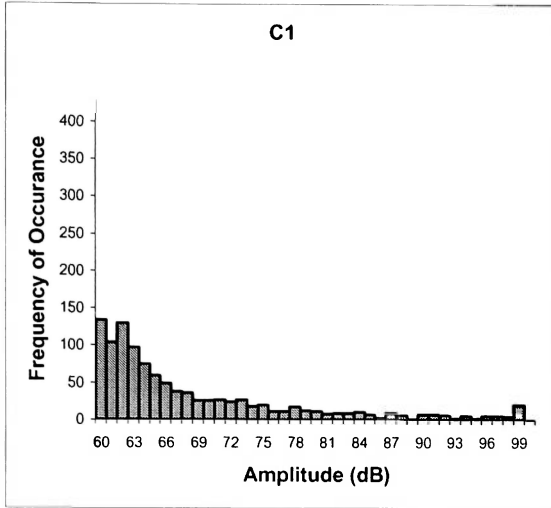


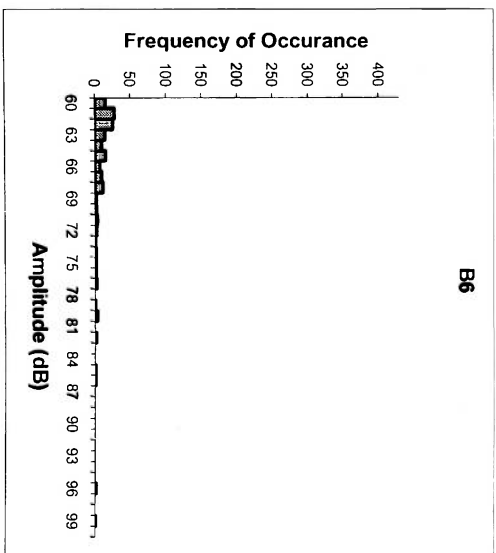
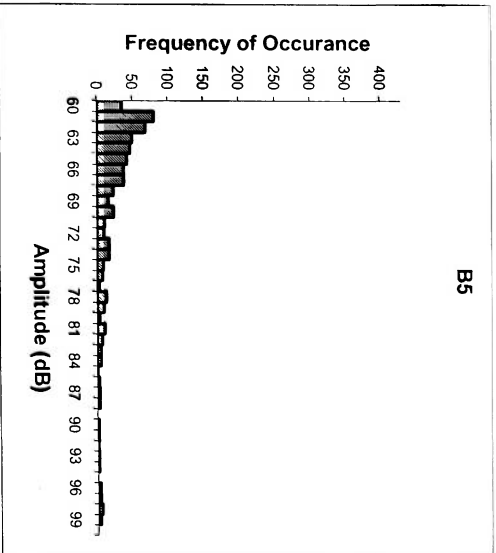
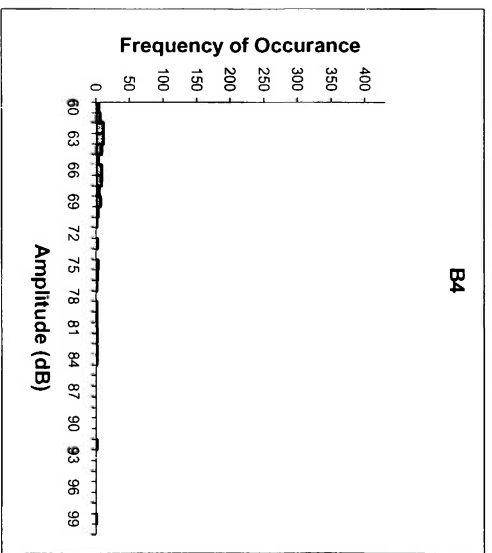
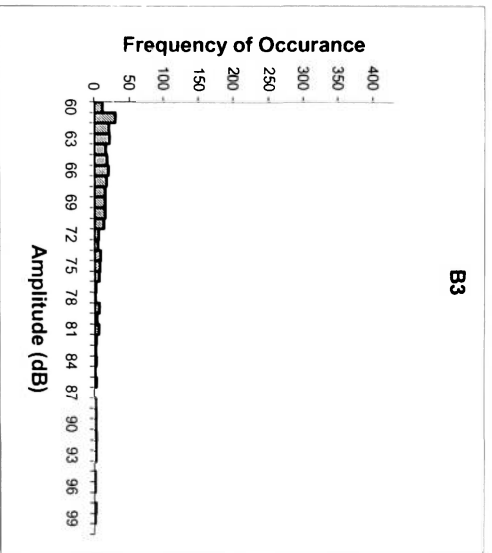
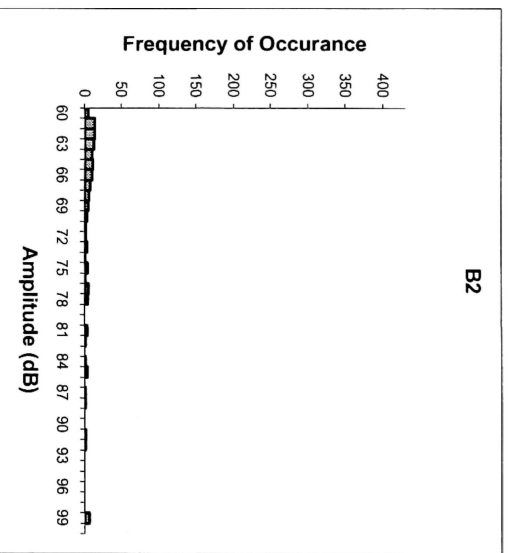
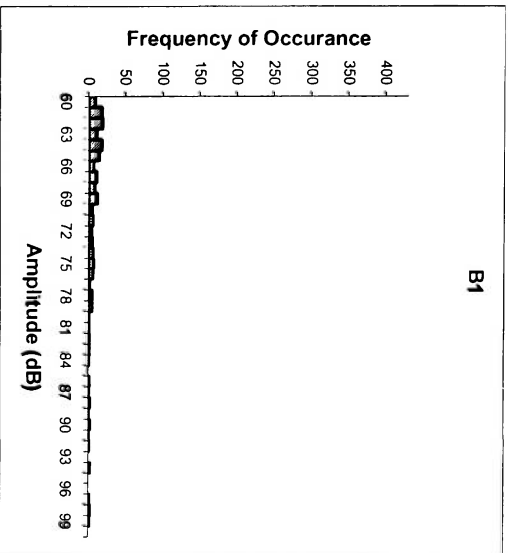


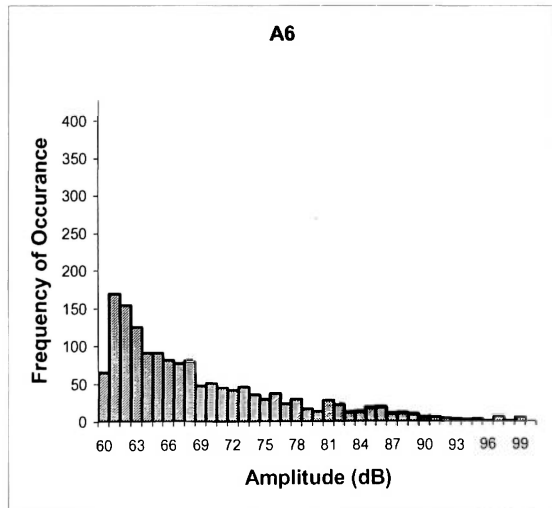
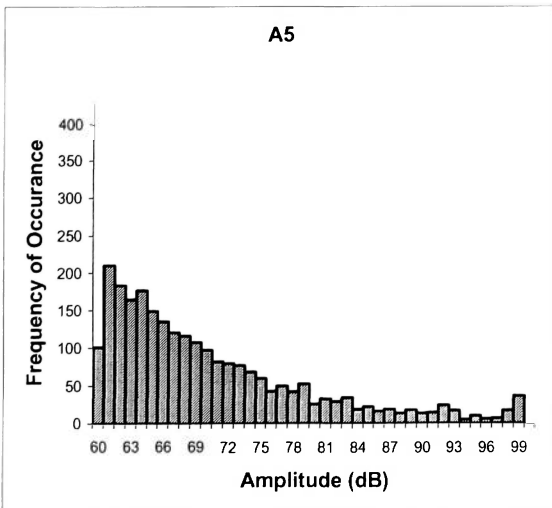
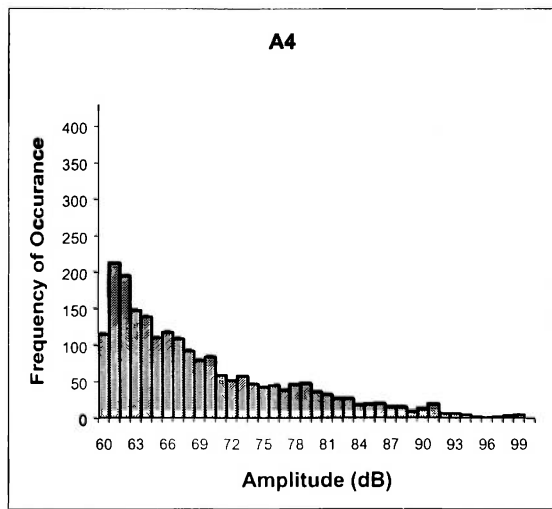
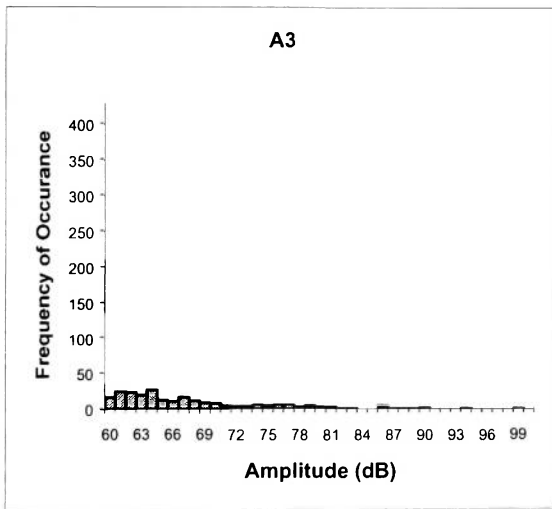
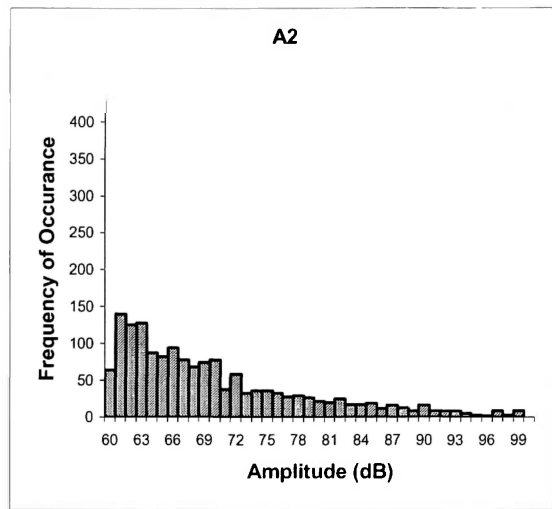
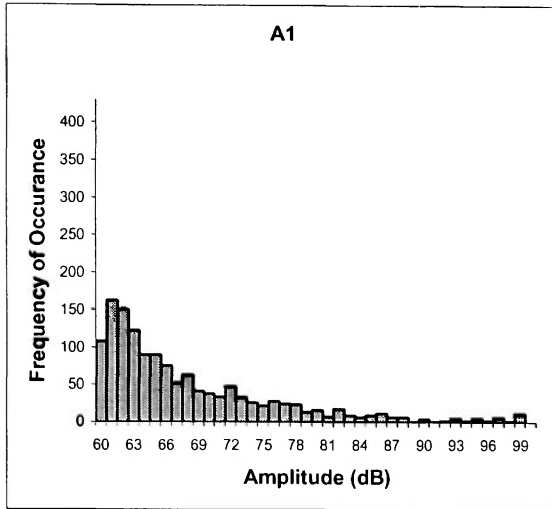
APPENDIX D
ACOUSTIC EMISSION AMPLITUDE DISTRIBUTION

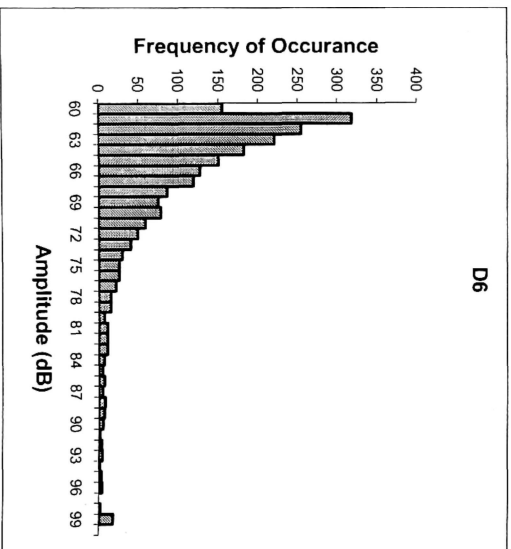
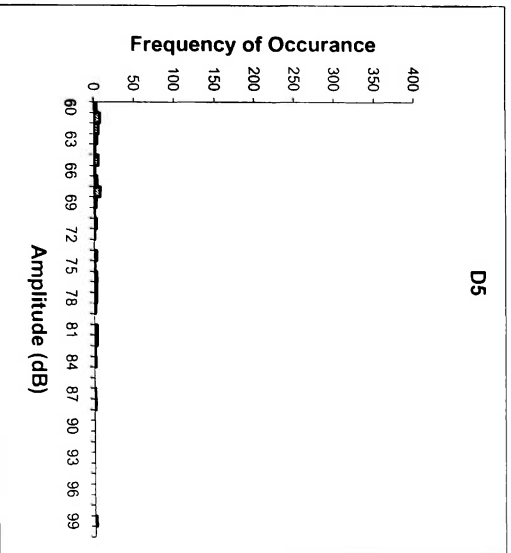
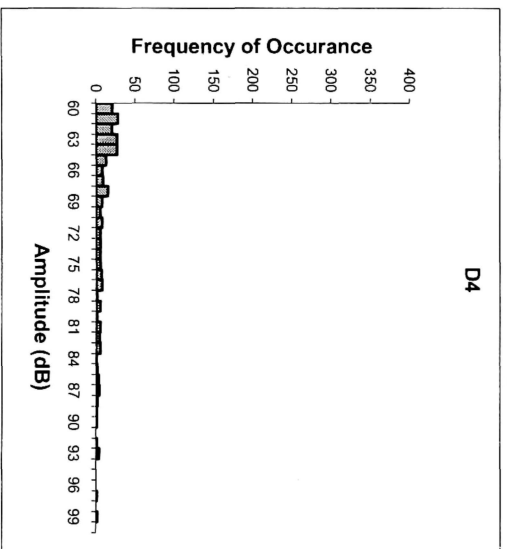
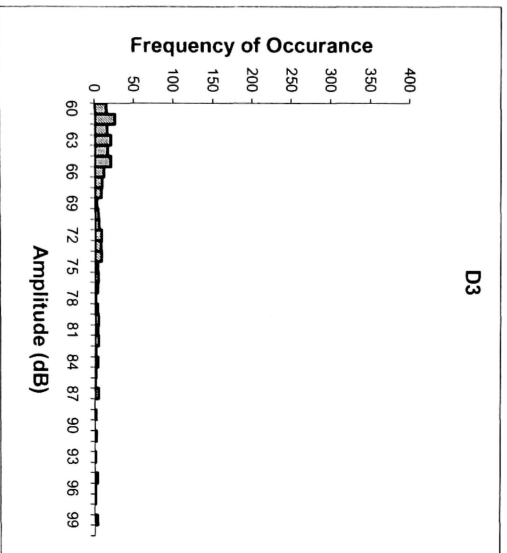
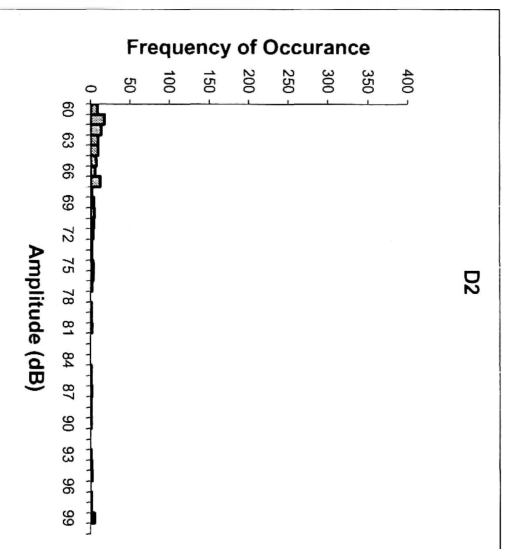
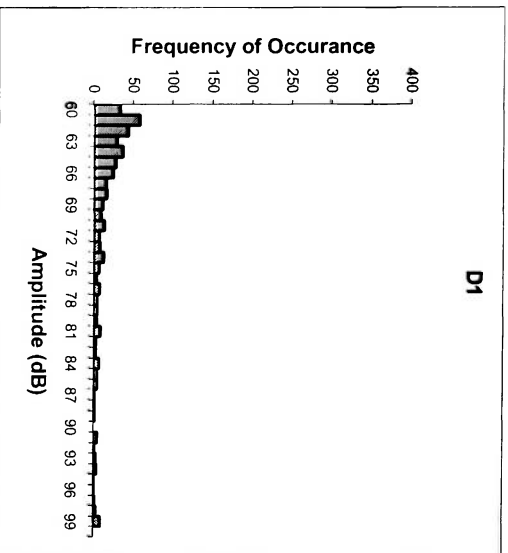












APPENDIX E
NEURAL NETWORK INPUT DATA FOR BATCHES A, C, CH, AND D

Training	A2	0.61202 0.73333 0.67213 0.77814 0.67541 0.75847 0.7082 0.79235 0.71585 0.65355 0.55082 0.58798 0.4765 0.76284 0.66667 0.78907 0.72568 0.66776 0.58251 0.7235 0.66448 0.83279 0.75683 0.84098 0.77923 0.84153 0.80437 0.77486 0.72842 0.82787 0.78033 0.79399 0.74863 0.75082 0.70164 0.69945 0.64317 0.65683 0.57486 0.83934 0.75847 0.86557 0.80984 0.81967 0.71585 0.76284 0.6612 0.6623 0.57596 0.79563 0.70929 2865.6
	A3	0.8527 0.86361 0.91162 0.89525 0.91926 0.90616 0.8898 0.8838 0.91053 0.89798 0.91217 0.90398 0.88925 0.88707 0.8958 0.89034 0.89416 0.89198 0.8227 0.83361 0.87343 0.85543 0.93726 0.91326 0.99564 0.98091 0.95254 0.9449 0.90398 0.89416 0.86579 0.86961 0.85597 0.85597 0.91544 0.90726 0.87834 0.89634 0.88762 0.88816 0.9018 0.88052 0.86907 0.86361 0.87725 0.87834 0.86743 0.8647 0.84888 0.85106 0.85925 6531.9
	A5	0.94865 0.90929 0.89174 0.96662 0.94994 0.91528 0.91314 0.96021 0.9448 0.9003 0.8973 0.91699 0.90757 0.93154 0.93496 0.94138 0.93924 0.90458 0.89816 0.92597 0.93068 0.93282 0.93282 0.97261 0.95721 0.95208 0.94138 0.94994 0.93881 0.96448 0.94566 0.90372 0.90543 0.91955 0.91271 0.9341 0.92041 0.95721 0.96277 0.95978 0.93753 0.97518 0.9709 0.94223 0.91399 0.90929 0.89816 0.94865 0.94737 0.95935 0.94608 3910.1
	A4	0.89506 0.90292 0.84343 0.90123 0.83109 0.92088 0.83446 0.94837 0.9119 0.93098 0.89226 0.91302 0.85859 0.93266 0.87991 0.97363 0.95118 0.94557 0.90909 0.96914 0.95118 0.94388 0.91077 0.9798 0.95791 0.97475 0.9147 0.90965 0.8743 0.92031 0.88608 0.9596 0.92031 0.92705 0.89562 0.96857 0.94052 0.95567 0.88833 0.96745 0.90685 0.94837 0.9046 0.92144 0.85073 0.87991 0.83333 0.90348 0.84624 0.96352 0.92649 3042.4
Testing	A6	0.94138 0.94397 0.93664 0.94741 0.93879 0.96767 0.94612 0.97241 0.95388 0.93664 0.92457 0.95517 0.94655 0.97414 0.97284 0.98534 0.97931 0.97241 0.95862 0.94957 0.94353 0.98664 0.97672 0.99871 0.98664 0.99957 0.98922 0.9806 0.96293 0.97931 0.96164 0.97457 0.97198 0.94526 0.94569 0.93922 0.93491 0.9875 0.98405 0.98147 0.96422 0.91509 0.92284 0.91466 0.90431 0.95474 0.93017 0.92845 0.92414 0.89957 0.89828 4174.8
	A1	0.19363 0.12995 0.59725 0.51291 0.7926 0.74225 0.90361 0.8821 0.92814 0.9247 0.94664 0.94062 0.93718 0.95095 0.89974 0.91394 0.9148 0.9062 0.9531 0.9475 0.93718 0.9475 0.9389 0.93373 0.99828 1 0.92126 0.94191 0.92298 0.9148 0.95869 0.95525 0.94148 0.93503 0.93503 0.94578 0.929 0.92556 0.93589 0.9247 0.9191 0.9191 0.93847 0.93718 0.95697 0.95998 0.95095 0.93976 0.93589 0.94234 0.92599 4936.5

Training	C1	0.90034 0.93113 0.91825 0.91321 0.91097 0.91825 0.91153 0.97256 0.96697 0.95017 0.95073 0.93225 0.91825 0.91041 0.88578 0.88746 0.86786 0.91265 0.89026 0.96081 0.93785 0.98488 0.97088 0.96305 0.96025 1 0.99664 0.97032 0.96529 0.97368 0.95801 0.94513 0.94121 0.9037 0.90482 0.91041 0.91769 0.94513 0.95017 0.97984 0.9692 0.96081 0.94793 0.86954 0.86842 0.89978 0.90538 0.90705 0.90146 0.9009 0.90538 1298.2
	C3	0.97448 0.9637 0.9308 0.94214 0.95973 0.95349 0.92286 0.91889 0.93647 0.93704 0.9325 0.9342 0.92853 0.93647 0.91492 0.91548 0.89166 0.88088 0.88145 0.8962 0.95973 0.95292 0.96143 0.97277 0.96427 0.96256 0.93137 0.91889 0.95179 0.95292 0.9359 0.92456 0.88486 0.87181 0.8667 0.87011 0.90868 0.8928 0.91662 0.91889 0.91548 0.91548 0.93193 0.92683 0.90244 0.90698 0.9013 0.90017 0.92002 0.91548 0.88372 2398.2
	C5	0.92363 0.86734 0.86343 0.88907 0.88462 0.93311 0.91304 0.91193 0.90134 0.9175 0.91137 0.9214 0.90412 0.89409 0.90357 0.90245 0.88462 0.91137 0.88239 0.93032 0.90468 0.95318 0.93757 0.9777 0.95931 1 0.98829 0.99275 0.98941 0.94705 0.94593 0.94537 0.93757 0.96656 0.98161 0.98551 0.99387 0.95318 0.9476 0.89855 0.90078 0.91193 0.92085 0.94649 0.9359 0.94816 0.94147 0.91249 0.9214 0.91583 0.91862 3317.1
	C6	0.93363 0.90942 0.91076 0.89372 0.90314 0.90538 0.9148 0.89731 0.91031 0.90135 0.90942 0.91659 0.92063 0.89013 0.88969 0.89462 0.88475 0.9278 0.9278 0.93408 0.9278 0.93991 0.93498 0.96009 0.95695 0.99058 0.98565 0.95964 0.96188 0.93901 0.93049 0.94126 0.95112 0.88969 0.90269 0.88117 0.90045 0.92063 0.9148 0.90135 0.90314 0.90987 0.91256 0.93363 0.93857 0.93184 0.93587 0.92063 0.913 0.9296 0.93543 2132.7
Testing	C2	0.71879 0.75591 0.70416 0.82621 0.75028 0.85602 0.79753 0.86614 0.82677 0.84364 0.78853 0.8144 0.7694 0.82902 0.75703 0.83352 0.76997 0.85714 0.80427 0.80427 0.77334 0.84814 0.81215 0.93982 0.92407 1 0.97525 0.92688 0.9207 0.88695 0.86839 0.91114 0.9072 0.88808 0.88583 0.95332 0.95894 0.96569 0.95388 0.96007 0.95163 0.94826 0.97075 0.95163 0.95276 0.94151 0.91732 0.90157 0.89089 0.88358 0.85489 2732
	C4	0.93018 0.91498 0.91892 0.9116 0.92736 0.92455 0.92849 0.93412 0.93975 0.91498 0.90541 0.88345 0.88682 0.94369 0.94369 0.92849 0.9268 0.93131 0.95327 0.93863 0.94257 0.9482 0.95158 0.96791 0.96622 1 0.99662 0.93919 0.94707 0.92173 0.93356 0.90259 0.92005 0.9589 0.96509 0.93187 0.93694 0.95045 0.96622 0.91836 0.92736 0.89245 0.90484 0.91047 0.90597 0.90428 0.90822 0.9482 0.9375 0.93018 0.92568 2007.2

Training	CH2	0.83962 0.87433 0.89252 0.86119 0.87702 0.85748 0.84838 0.86557 0.89252 0.87399 0.8969 0.87163 0.8777 0.88949 0.90937 0.97473 0.97305 0.96867 0.97372 0.97642 0.95586 0.9316 0.93464 0.95216 0.98956 1 0.95384 0.91375 0.92655 0.9407 0.91611 0.88848 0.86961 0.90229 0.87197 0.85546 0.84299 0.83794 0.86186 0.8723 0.86489 0.82817 0.83457 0.84164 0.83726 0.84569 0.85883 0.8467 0.83187 0.85647 0.84097 2974.1
	CH5	0.95904 0.94954 0.97837 0.97608 0.93775 0.93873 0.95839 0.9479 0.93742 0.91678 0.91907 0.95937 0.93807 0.9597 0.95511 0.94135 0.93775 0.94463 0.93709 0.94299 0.92955 0.92169 0.93447 0.94397 0.96887 1 0.97444 0.9597 0.92169 0.89581 0.92169 0.90498 0.90301 0.91841 0.90695 0.91612 0.90891 0.93054 0.923 0.89515 0.92923 0.90564 0.90531 0.91022 0.92824 0.94856 0.94364 0.94168 0.94233 0.94266 0.96265 2941.6
	CH6	0.90561 0.93243 0.92024 0.92337 0.89586 0.90456 0.87043 0.89794 0.87739 0.89133 0.90317 0.92651 0.95089 0.94009 0.93173 0.94601 0.93591 0.95158 0.94671 0.99303 0.9683 0.96447 0.98433 0.96865 0.98537 1 0.99408 0.92128 0.90038 0.9063 0.90317 0.88854 0.89202 0.92511 0.92268 0.9373 0.92581 0.94044 0.92616 0.92825 0.90456 0.89969 0.89899 0.92198 0.91501 0.89063 0.90282 0.88784 0.86729 0.89342 0.90456 2984.4
Testing	CH1	0.89492 0.89979 0.90953 0.91058 0.89388 0.89736 0.91023 0.93981 0.93633 0.91023 0.89179 0.8991 0.90779 0.92554 0.91788 0.90745 0.93459 0.95894 0.94433 0.93981 0.93633 0.94468 0.96207 0.96103 0.95164 1 0.99408 0.97251 0.97042 0.95964 0.97495 0.96381 0.93737 0.97356 0.96903 0.95303 0.95616 0.94259 0.95442 0.92067 0.9245 0.91232 0.91823 0.91475 0.92797 0.93076 0.94259 0.93111 0.93424 0.93111 0.91997 2969.7
	CH4	0.91803 0.90196 0.86789 0.88557 0.901 0.87625 0.88846 0.90807 0.91418 0.92832 0.93635 0.94021 0.93989 0.94278 0.91225 0.92639 0.92382 0.928 0.92446 0.91546 0.93282 0.93989 0.94953 0.96496 0.96432 1 0.964 0.92318 0.93796 0.94857 0.97364 0.94825 0.93507 0.97171 0.95886 0.94793 0.95821 0.93668 0.91418 0.89682 0.91257 0.9325 0.91771 0.92478 0.92285 0.89232 0.89489 0.883 0.86178 0.85953 0.84957 2974.1

Training	D2	0.82815 0.83384 0.83823 0.84305 0.84042 0.88163 0.87155 0.82288 0.81105 0.83209 0.81938 0.84349 0.82464 0.86804 0.8584 0.90925 0.88558 0.86409 0.85883 0.84349 0.79965 0.91363 0.89347 0.95309 0.94651 1 0.97983 0.911 0.89917 0.88996 0.88207 0.87681 0.86015 0.87462 0.86234 0.86322 0.83998 0.88207 0.84217 0.85708 0.84831 0.89259 0.8505 0.90925 0.88295 0.84524 0.81499 0.81806 0.78431 0.84349 0.81017 8367.5
	D3	0.89469 0.87049 0.8667 0.87998 0.87097 0.87049 0.86717 0.8814 0.92979 0.91888 0.90607 0.88425 0.89896 0.90987 0.91509 0.91176 0.9037 0.91841 0.89469 0.8871 0.90275 0.91224 0.91698 0.9241 0.95256 0.95398 0.91129 0.90275 0.88994 0.91271 0.91271 0.91746 0.94972 0.963 0.93264 0.93928 0.86765 0.89611 0.87381 0.89421 0.90607 0.91366 0.92362 0.94213 0.91034 0.93359 0.89469 0.91034 0.9018 0.91509 0.86433 5324.7
	D5	0.1991 0.22443 0.22624 0.22172 0.22172 0.19729 0.2009 0.11946 0.11946 0.1086 0.1086 0.1448 0.17376 0.22443 0.1991 0.21719 0.21719 0.14661 0.14661 0.10769 0.1086 0.31946 0.32127 0.62805 0.62715 1 0.99367 0.66787 0.66878 0.63348 0.62805 0.67783 0.68235 0.65339 0.6552 0.56199 0.56199 0.17557 0.17466 0.085068 0.085068 0.13032 0.13575 0.19729 0.1991 0.2552 0.2552 0 0 0.28054 0.28235 6023.5
	D4	0.89098 0.86063 0.85695 0.85649 0.85005 0.8965 0.90754 0.88132 0.88822 0.88638 0.88408 0.88408 0.87029 0.9218 0.9057 0.88868 0.90616 0.84867 0.85649 0.86523 0.86385 0.9678 0.96872 0.99448 0.99034 1 0.99908 0.98942 0.98344 0.96688 0.954 0.91996 0.92502 0.8988 0.90018 0.86109 0.85419 0.86201 0.85833 0.87672 0.87259 0.86661 0.85741 0.85925 0.85649 0.86017 0.85925 0.9264 0.91812 0.83257 0.83855 5987.2
Testing	D6	0.16576 0.32605 0.32969 0.20947 0.20947 0.17304 0.17304 0.33333 0.33698 0.19217 0.21585 0.17486 0.15483 0.087432 0.091075 0.10929 0.10929 0.15027 0.1694 0.46448 0.44536 0.9918 0.99454 0.98179 0.98179 1 0.99818 0.6867 0.6867 0.78233 0.77322 0.70674 0.70674 0.71311 0.71129 0.54007 0.52823 0.29599 0.29326 0.20765 0.20947 0.13661 0.13661 0.19308 0.1949 0.24226 0.2459 0.15574 0.15938 0.28051 0.28233 6292